# Applications of Long-Lived Spin States to High Resolution NMR Studies of Biomolecules

THÈSE N$^O$ 4882 (2010)

ÉCOLE POLYTECHNIQUE FÉDÉRALE DE LAUSANNE

POUR L'OBTENTION DU GRADE DE DOCTEUR ÈS SCIENCES

PAR

## Puneet AHUJA

*EPFL*

ÉCOLE POLYTECHNIQUE
FÉDÉRALE DE LAUSANNE

Suisse
2010

## Soap Bubbles

From years of study and of contemplation
An old man brews a work of clarity,
A gay and convoluted dissertation
Discoursing on sweet wisdom playfully.

An eager student bent on storming heights
Has delved in archives and in libraries,
But adds the touch of genius when he writes
A first book full of deepest subtleties.

A boy, with bowl and straw, sits and blows,
Filling with breath the bubbles from the bowl.
Each praises like a hymn, and each one glows;
Into the filmy beads he blows his soul.

Old man, student, boy, all these three
Out of the Maya-foam of the universe
Create illusions. None is better or worse.
But in each of them the Light of Eternity
Sees its reflection, and burns more joyfully.

**-Hermann Hesse**

**Abstract**

Slow dynamic processes, such as biomolecular folding/unfolding, macromolecular diffusion, etc., can be conveniently monitored by solution-state two-dimensional (2D) NMR spectroscopy, provided the inverse of their rate constants does not exceed the nuclear spin-lattice relaxation time constants ($T_1$). The discovery of long-lived states (LLS) by Malcolm Levitt's group opened a new dimension for the study of slow dynamic phenomena, as magnetization stored in the form of LLS decays with the time constants $T_{LLS}$, where in many cases $T_{LLS} \gg T_1$. In this thesis, various excitation methods and applications of LLS are discussed. Broadband excitation of LLS is suitable to monitor slow processes and has been applied to study the slow ring-flip in tyrosine residues of **BPTI** (Bovine Pancreatic Trypsin Inhibitor), as well as to perform simultaneous measurements of diffusion coefficients in mixtures of molecules with arbitrary $J$-couplings and chemical shifts. The applications of LLS, initially believed to be limited to isolated spin-½ pairs, were extended to larger spin systems, including some common amino acids like **Serine**, **Aspartic Acid**, etc. LLS have been observed in **Glycine** residues of small peptides like **Ala-Gly**, as well as in mobile parts of proteins, e.g., in **Gly** 75 and 76 of **Ubiquitin**. The lifetimes $T_{LLS}$ are more sensitive to dipolar interactions with external spins than longitudinal and transverse relaxation time constants, $T_1$ or $T_2$, and therefore can provide structural information for unfolded proteins. The unfolding of **Ubiquitin** by addition of **Urea** and by varying pH was followed using LLS. The excitation of coherent superpositions across singlet and triplet states, which we call long-lived coherences (LLC's), leads to resolution enhancement in conventional NMR spectroscopy. New methods have been designed to store hyperpolarized ($^{13}C$ or $^{1}H$) magnetization in the form of LLS and have been demonstrated using samples of **Ala-Gly** and **Acrylic Acid**.

**Résumé**

Les phénomènes dynamiques lents, tels que le repliement/dépliement de biomolécules, la diffusion macromoléculaire, etc. peuvent être mesurés par la RMN à deux dimensions (2D) en phase liquide, et ce dans la mesure où les constantes de temps ne sont pas plus longues que la relaxation nucléaires ($T_1$). La découverte d'états de spin à longs temps de vie (Long-lived states - LLS), par le groupe de M. Levitt a ouvert la voie à l'étude de phénomènes lents, car l'aimantation conservée sous la forme de LLS relaxe avec un de temps de vie $T_{LLS}$, tel que dans beaucoup de cas $T_{LLS} >> T_1$. Dans cette thèse de Doctorat, plusieurs méthodes d'excitations, et des applications des LLS sont discutées. L'excitation large bande des LLS peut s'avérer utile pour observer des processus d'échange lents ; cette technique a été appliquée à l'étude de la rotation du cycle aromatique dans la tyrosine de la **BPTI** (Bovine Pancreatic Trypsin Inhibitor), et à la mesure simultanée de coefficients de diffusions dans un mélange de molécules ayant des couplages- $J$ et déplacements chimiques arbitraires. L'application des LLS n'est pas limitée à des paires de spins- ½ isolées mais peut être étendue à des systèmes de spin plus complexes, comme par exemple certains acides aminés tels que la **Sérine**, l'**Acide Aspartique**, etc. Les LLS ont été observés dans des résidus de glycine dans des petit peptides tels que l'**Ala-Gly**, ainsi que dans certaines parties mobiles de protéines telles que l'**Ubiquitine** sur les sites **Gly** 75 et 76. Les temps de vie $T_{LLS}$ sont plus sensibles aux interactions dipolaires avec d'autres spins que les temps de relaxation $T_1$ et $T_2$ : cela peut s'avérer très utile pour extraire des informations structurelles de protéines dépliées. Le dépliement de l'**Ubiquitine** en présence d'**Urée** à pH variable a été mesuré grâce aux LLS. L'excitation de superpositions cohérentes d'états singulets et triplets, appelées cohérences à long temps de vie (Long-lived coherences - LLC's), permet d'augmenter la résolution en spectroscopie RMN. De nouvelles méthodes ont été mises en place pour conserver

l'aimantation de spins hyper-polarisés ($^{13}$C ou $^{1}$H) dans des LLS, et ont été appliquées à l'**Ala-Gly** et l'**Acide Acrylique**.

# Acknowledgements

I would like to express my sincere regards to my thesis director, Prof. Geoffrey Bodenhausen for giving me the opportunity to join his group. I am greatly thankful to him for the freedom he gave to perform research. To me, he is a very eloquent speaker and a great scientist with the wide knowledge of both scientific and non scientific areas.

I would like to thank Prof. Allain, Dr. Brutscher, Prof. Helm and Prof. Zuppiroli for accepting to be a part of my examination committee, reading my thesis, and giving constructive criticism for further improvements in my thesis.

I am thankful to Paul and Riddhiman, with whom I worked substantially during my doctorate. Riddhiman has been like an elder brother to me. He is the person, most responsible, for the foundation I have in the world of NMR. He is an extremely patient scientist with a deep understanding of NMR, specially the theoretical aspects of it. Above all, he is a great human being who has always been very supportive during all kinds of downfalls I had during my stay in Switzerland. I would also like to thank Barnali, the most precious spectrum of Riddhiman.

My sincere regards to Martial Rey as he has been the one to provide the technical assistance for the proper functioning of spectrometers. He is a friendly and approachable person.

I would like to thank Sami, Pascal and all others involved in the dissolution DNP project. Sami and Pascal are very dedicated and enthusiastic scientists, with a feeling of sacred awe for the research. With Sami, I had great fun to work and enjoyed his jokes about yoga. He is also a very good actor and a guitar player. Pascal is a nice and friendly person with a good sense of humor and a broad knowledge of Chemistry, including the details of preparation of wines and other alcohols.

I am grateful to all the present and former members of LRMB for all scientific and non scientific discussions, as well as to bear my philosophical ideas that are completely out of the reality. I had great time with Mariachiara (a very charming and friendly person), Tak (an excellent officemate with whom I had interesting and poetic discussions about music and life, ranging from the mysteries of nuclear spins to the changing moods of nature), Karthik (an excellent theoretician) Nicolas (a symbol of the Swiss army), Marc (a friendly person ready to discuss anything, even apples), Veronika (the sportswoman of our group with a lovely smile

# Table of contents

Table of Contents

Chapter - 1

# **Introduction**

Understanding dynamics of proteins and protein-ligand interactions is of major interest to modern science, because of the strong correlations between the biological activities of proteins and their structural dynamics. These motions occur on broad timescales ranging from picoseconds to several seconds: the backbone and side-chain fluctuations range from pico- to nanoseconds, conformational rearrangements take place on millisecond timescales, and the slow processes like chemical exchange, translational diffusion, etc., occur on the order of several seconds. Any of these motions may be functionally significant and directly related to the interactions of proteins with their environment.

NMR spectroscopy is a powerful analytical tool for the study of macromolecular dynamics because of the wide range of accessible timescales ($10^{-12}$ s to $10^5$ s)[1] with minimal interference to the sample. On the NMR timescale, motions ranging from picoseconds to nanoseconds are regarded as fast, whereas the motions ranging from microseconds to seconds are regarded as slow.

Various methods have been developed to study fast dynamics by NMR. Backbone and side-chain fluctuations, occuring on picosecond to nanosecond timescales, can be studied by measuring three relaxation rates: the longitudinal relaxation rate ($R_1$), the transverse relaxation rate ($R_2$), and the steady state hetronuclear NOE.[2-3] These relaxation rates are influenced by fast motions via modulations of dipolar and chemical shift anisotropy (CSA) interactions of nuclei caused by molecular reorientations. The 'model-free' analysis of these relaxation rates, proposed by Lipari and Szabo,[4] provides order parameters and internal correlation times of motions of bond vectors.

Conformational exchange, taking place on microsecond to millisecond time scale, can be probed by $R_{1\rho}$ or $R_2$ relaxation measurements. The transverse relaxation rate $R_2$ can be measured by Carr-Purcell-Meiboom-Gill (CPMG) experiments[5-6] which rely upon the application of a train of refocusing $\pi$-pulses, while in $R_{1\rho}$ experiments,[7] transverse relaxation rates are measured in the presence of an RF field. In these experiments, the exchange contribution to the relaxation rates is partially or fully suppressed. Then, plotting the relaxation rate constants as a function of the strength of the RF field yields dispersion curves that can provide exchange rates.[8]

Slow dynamic processes such as translational diffusion,[9] chemical exchange, protein ligand interactions, folding/unfolding of biomolecules,[10] proline isomerization,[11] etc., occur on timescales of seconds and play an important role in biology. For the study of these processes methods like ZZ exchange spectroscopy (ZZ-EXSY)[12] are available, where longitudinal two-spin order is excited in scalar coupled spins. The upper limit of accessible timescales of these processes is determined by the spin-lattice relaxation time constant ($T_1$), which is often regarded as the maximum lifetime of nuclear spin memory.

There are two ways of broadening the range of accessible timescales of slow dynamic processes: *i)* to use the nuclei with low gyromagnetic ratios. *ii)* to use the magnetization with longer lifetimes.

Various methods have been established to exploit the long $T_1$'s of $^{15}$N-nuclei, which are due to their smaller gyromagnetic ratio compared to protons ($|\gamma(^1\mathrm{H})/\gamma(^{15}\mathrm{N})| = 10$). For instance, translational diffusion coefficients in macromolecules (with molecular mass ~ 45kDa) have been measured by storing the magnetization on $^{15}$N during the diffusion period.[13] Proton-detected $^{15}$N exchange spectroscopy (EXSY) has been designed to measure the exchange rates between two coexisting folds of a 34mer RNA exchanging on a timescale of a few seconds ($\tau_{obs} \sim T_1(^{15}\mathrm{N}) < 5\mathrm{s}$).[10]

Another way of increasing the range of accessible timescales could be based on finding ways to sustain magnetization (coherences or populations) for longer times. In the group of M. Levitt, it has been discovered that the lifetimes of spin memory can be extended by more than an order of magnitude when the magnetization is stored in the form of particular spin distributions, known as long-lived states (LLS).[14-15] For instance, in a partially-deuterated saccharide the lifetimes of LLS ($T_{LLS}$) can be 37 times longer than conventional spin-lattice relaxation times ($T_1$).[16] LLS in $^{15}N_2O$ last for several minutes ($T_{LLS}$ = 26 min and $T_{LLS}/T_1$= 8) which is the longest lifetime recorded so far.[17] For two-spin scalar-coupled systems, LLS rely on the populations of Singlet States (SS). The very long memory of LLS stems from the fact that the major source of relaxation, i.e., dipolar interactions between the involved spins, is inactive. If other relaxation mechanisms such as chemical shift anisotropy (CSA), interactions with paramagnetic substances, etc., are absent, LLS should have infinite lifetimes, provided they are well isolated from other faster-relaxing states. However, in practice, LLS have finite relaxation rates because of other relaxing mechanisms and non-ideal 'spin-locking'.[18-21]

In this thesis, various improvements in LLS spectroscopy are discussed. Applications to small molecules of biological interest, as well as to proteins like Ubiquitin, are demonstrated. The concept of long-lived coherences (LLC's), which leads to resolution enhancement in NMR spectroscopy, is described. Methods to store hyperpolarized magnetization in the form of LLS and applications thereof are presented.

# Chapter - 2

# Coherent evolution: pulse sequences for excitation and sustaining long-lived states

Long-lived states (LLS) have very slow relaxation rates because once populated and isolated properly from other fast-relaxing states, they remain unaffected by the dipolar interaction between the involved spins, the main relaxation mechanism in liquid state NMR.[21] Therefore, efficient excitation and sustaining of LLS (minimizing coherent leakage) in favorable conditions is crucial. This is the main concern of the present chapter. In this chapter, important features of LLS for a system comprising scalar-coupled spins $I$ and $S$ = 1/2 under the coherent part of Hamiltonian are described, as well as the evolution of the density operator under various pulse sequences for efficient excitation of LLS.

## 2.1 Theory

In a rotating frame of reference, the spin Hamiltonian for a pair of scalar-coupled spins- ½ is given by:

$$H^{Rot} = \nu_I I_z + \nu_S S_z + J_{IS}\vec{I}\cdot\vec{S} \tag{2.1.1}$$

where $\nu_I$ and $\nu_S$ are the offset frequencies of the two spins and $J_{IS}$ is the scalar coupling constant.

For a weakly-coupled $IS$ system $\left(\left|J_{IS}\right| << \left|\nu_I - \nu_S\right| = \Delta\nu_{IS}\right)$, the Hamiltonian can be truncated to the following form:

$$H^{Rot} = \nu_I I_z + \nu_S S_z + J_{IS} I_Z S_Z \tag{2.1.2}$$

which is diagonal in the Zeeman product basis (PB), so that the eigenbasis is the product base (PB):

$$\Phi_{PB} = \left\{ |\alpha\alpha\rangle, |\alpha\beta\rangle, |\beta\alpha\rangle, |\beta\beta\rangle \right\} \tag{2.1.3}$$

However, the spin system behaves like an $I_2$ system in the absence of chemical shifts and evolves under the following isotropic Hamiltonian:

$$H = J_{IS} \vec{I} \cdot \vec{S} \tag{2.1.4}$$

which has the following singlet-triplet (ST) eigenbasis:

$$\Phi_{ST} = \left\{ |T_{+1}\rangle, |T_0\rangle, |S_0\rangle, |T_{-1}\rangle \right\} \tag{2.1.5}$$

where:

$$T_{+1} = |\alpha\alpha\rangle; \quad T_0 = \frac{1}{\sqrt{2}}\left( |\alpha\beta\rangle + |\beta\alpha\rangle \right); \quad S_0 = \frac{1}{\sqrt{2}}\left( |\alpha\beta\rangle - |\beta\alpha\rangle \right); \quad T_{-1} = |\beta\beta\rangle$$

The matrix for the basis conversion between the PB and the ST basis is the following:

$$V = \begin{pmatrix} 1 & 0 & 0 & 0 \\ 0 & \frac{1}{\sqrt{2}} & \frac{1}{\sqrt{2}} & 0 \\ 0 & \frac{1}{\sqrt{2}} & -\frac{1}{\sqrt{2}} & 0 \\ 0 & 0 & 0 & 1 \end{pmatrix}, \text{ with the property } V = V^{-1} \tag{2.1.6}$$

$$\Phi_{PB} = V \cdot \Phi_{ST} \tag{2.1.7}$$

So, the Cartesian product operators in the PB can be transformed into the symmetry-related ST by the following transformation:

$$O_{PB} = V^{-1} O_{ST} V \tag{2.1.8}$$

A weakly-coupled *IS* system can be converted into an $I_2$ system by removing the chemical shift difference between the two spins involved. In practice, it can be achieved in two ways: *i) the zero-field method:* [14] this requires one to take the sample out of the magnetic field, where the chemical shifts vanish; and *ii) the high-field method:* [15-16] this requires the application of a suitable RF pulse sequence to suppress the chemical shift difference between the two spins and is described below.

If a continuous-wave (CW) radio frequency (RF) with an amplitude $\left| v_1 \right| = \left| -\gamma B_1 /(2\pi) \right| \gg \Delta v_{IS}$

is applied and the RF carrier $v_{RF}$ is placed half-way between the two chemical shifts,

$$v_{RF} = v_{av} = (v_I + v_S)/2 \qquad (2.1.9)$$

Then the Hamiltonian in a frame rotating at $v_{av}$ is given by:

$$H = v_1(I_x + S_x) + J_{IS}\vec{I}\cdot\vec{S} + \frac{\Delta v_{IS}}{2}(I_z - S_z) \qquad (2.1.10)$$

The last term $(I_z - S_z)$ does not commute with $(I_x + S_x)$ but can be neglected when $v_1 \gg \Delta v_{IS}$:

$$H = v_1(I_x + S_x) + J_{IS}\vec{I}\cdot\vec{S} \qquad (2.1.11)$$

This Hamiltonian is symmetric under a permutation of the spins $I$ and $S$. Its ST basis is given

by Eq. (2.1.5).

The effective fields experienced by the spins $I$ and $S$ are tilted through angles $\theta_{I,S}$ with respect

to the $z$-axis:

$$\tan\theta_{I,S} = \frac{\left| v_1 \right|}{v_{I,S}} \qquad (2.1.12)$$

with $0 < \theta_{I,S} < \pi$. If $v_1 \gg \Delta v_{IS}$, $\theta_{I,S} \sim \pi/2$, hence $\sin\theta_{I,S} \approx 1$ and $\cos\theta_{I,S} \approx 0$.

In the presence of an RF field, the operators of spins $K = \{I, S\}$ need to be transformed into

the tilted interaction frame which can be achieved by the following transformation:

$$\begin{pmatrix} K_x' \\ K_y' \\ K_z' \end{pmatrix} = \begin{pmatrix} \cos\theta_K & 0 & -\sin\theta_K \\ 0 & 1 & 0 \\ \sin\theta_K & 0 & \cos\theta_K \end{pmatrix} \begin{pmatrix} K_x \\ K_y \\ K_z \end{pmatrix} \qquad (2.1.13)$$

where $K' = \{I, S\}$ are the corresponding operators in the tilted frame.

When $\theta_{I,S} \sim \pi/2$, this simply amounts to relabeling $K_z' \rightarrow K_x$, as suggested by Eq. (2.1.13).

In the tilted frame, the following combinations of Cartesian operator terms can contribute to

the populations of singlet or triplet states:

$\{E, (I_z' + S_z'), 2I_z'S_z', ZQ_x'\}_{PB}$

Where $ZQ_x{'} = 1/2(2I_x{'}S_x{'} + 2I_y{'}S_y{'})$

The conversion matrix in the tilted frame of reference can be written as follows:

$$
\begin{pmatrix} |S_0\rangle\langle S_0| \\ |T_0\rangle\langle T_0| \\ |T_1\rangle\langle T_1| \\ |T_{-1}\rangle\langle T_{-1}| \end{pmatrix} = \begin{pmatrix} \frac{1}{4} & 0 & -\frac{1}{2} & -1 \\ \frac{1}{4} & 0 & -\frac{1}{2} & 1 \\ \frac{1}{4} & \frac{1}{2} & \frac{1}{2} & 0 \\ \frac{1}{4} & -\frac{1}{2} & \frac{1}{2} & 0 \end{pmatrix} \cdot \begin{pmatrix} E \\ I_z{'} + S_z{'} \\ 2I_z{'}S_z{'} \\ ZQ_x{'} \end{pmatrix}
\tag{2.1.14}
$$

It can be transformed into the rotating frame by using Eq. (2.1.13):

$$
\begin{pmatrix} |S_0\rangle\langle S_0| \\ |T_0\rangle\langle T_0| \\ |T_1\rangle\langle T_1| \\ |T_{-1}\rangle\langle T_{-1}| \end{pmatrix} = \begin{pmatrix} \frac{1}{4} & 0 & -\frac{1}{2} & -1 \\ \frac{1}{4} & 0 & -\frac{1}{2} & 1 \\ \frac{1}{4} & \frac{1}{2} & \frac{1}{2} & 0 \\ \frac{1}{4} & -\frac{1}{2} & \frac{1}{2} & 0 \end{pmatrix} \cdot \begin{pmatrix} E \\ I_x + S_x \\ 2I_xS_x \\ \frac{1}{2}\left(I_zS_z + I_yS_y\right) \end{pmatrix}
\tag{2.1.15}
$$

According to Eq. (2.1.15), the LLS, in the rotating frame, can be expressed as follows:

$$
|S_0\rangle\langle S_0| = \frac{1}{4}E - \frac{1}{2}(2I_zS_z) - ZQ_x
\tag{2.1.16}
$$

Therefore, LLS can be excited via $2I_zS_z$, $ZQ_x$ or by the sum of these components.

The experiments described in this thesis have been performed by the high field method.[16] The high-field method for sustaining LLS, where LLS are populated via $ZQ_x$ excitation, was first demonstrated by M. Carravetta and M. Levitt.[15] Their designed pulse sequence suffers from several drawbacks: i) the RF carrier $\nu_{RF}$ must be positioned at the mean chemical shift of the two spins, i.e., $\nu_{RF} = (\nu_1 + \nu_2)/2$. ii) the efficiency of the excitation depends on the difference $\Delta\nu_{IS} = (\nu_I - \nu_S)$ between the chemical shifts and iii) the efficiency also depends on the scalar coupling constant $J_{IS}$, between the relevant spins.

Often, slow dynamic processes A ↔ B, such as folding of biomolecules, lead to different

chemical shifts in the two sites, i.e., $\nu_I^A \neq \nu_I^B$ and $\nu_S^A \neq \nu_S^B$. Also, the chemical shift difference between the two sites may be affected by different chemical environments, i.e., $\Delta\nu_{IS}^A \neq \Delta\nu_{IS}^B$. Furthermore, the scalar couplings can also be different in the two sites, i.e, ($J_{IS}^A \neq J_{IS}^B$). All these limitations make it impractical to use the original method for studying slow dynamic processes. In our group, new methods were developed to alleviate these various limitations which make slow exchange phenomenon amenable by long-lived state NMR spectroscopy and are discussed in the next sections.

## 2.2 LLS excitation *via* constructive addition of *ZQ$_x$* and *ZZ* order

It can be seen from Eq. (2.1.16) that the LLS can be populated by exciting the sum of $2I_zS_z$ and *ZQ$_x$* which can be achieved by the following pulse sequence (Sequence I):[16]
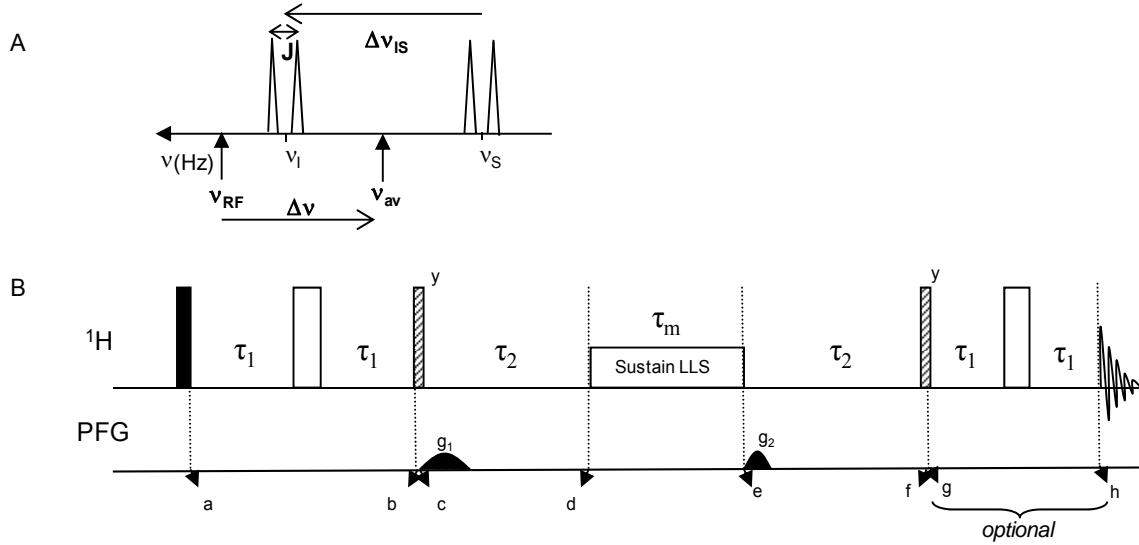


Figure 2.2.1: (A) Sketch of an NMR spectrum of a weakly coupled two-spin ½ system with relevant parameters. (B) A pulse sequence (sequence I) designed to populate LLS via the sum of longitudinal two-spin order, $I_ZS_Z$ and real part of zero-quantum, *ZQ$_x$*. Pulses of π, π/2 and π/4 are indicated by open, filled and hatched rectangles, respectively. The phases of the pulses are along x-axis unless otherwise specified.

The density operator in the rotating frame of reference at time point 'a' of the pulse sequence in Fig. 2.2.1(B) is:

$$\sigma(a) = -I_y - S_y \tag{2.2.1}$$

This is converted by a spin-echo to antiphase terms at time point 'b', provided $\tau_1 = 1/(4J_{IS})$:

$$\sigma(b) = 2\left(I_x S_z + I_z S_x\right) \tag{2.2.2}$$

After the $\pi/4$ pulse, at time point 'c',

$$\sigma(c) = \left(2I_x S_x - 2I_z S_z\right) = ZQ_x + DQ_x - 2I_z S_z \tag{2.2.3}$$

The term $DQ_x$ is destroyed by the pulsed field gradient (PFG) $g_1$.

At this point, $ZQ_x$ term and $I_Z S_Z$ have opposite signs. So, a delay $\tau_2 = 1/(2\Delta v_{IS})$ is inserted between points 'c' and 'd' to reverse the sign of the zero-quantum coherences ($ZQ_x \rightarrow -ZQ_x$), under the effect of the difference between the chemical shifts $\Delta v_{IS} = (v_I - v_S)$. This 'zero-quantum reversal' is necessary to prevent the mutual cancelation of $ZQ$ and $ZZ$ contributions to the LLS. The density operator at time point 'd' is given by:

$$\sigma(d) = -ZQ_x - 2I_z S_z = |S_0\rangle\langle S_0| - \left(\frac{1}{2}\right)\left(|T_{-1}\rangle\langle T_{-1}| + |T_1\rangle\langle T_1|\right) \tag{2.2.4}$$

A suitable RF irradiation is applied during the time period 'd-e' to suppress the chemical shift difference between the two spins. This makes the spin system behave similar to an $I_2$ system. During this period, the spin system is best described in terms of eigenstates of the total spin angular momentum, i.e., singlet and triplet states. The application of RF irradiation converts the sum of $ZQ_x$ coherence and $ZZ$ spin-order into population differences between singlet and triplet states (as shown in Eq. 2.1.11). Populations of triplet states equilibrate after a short time, while the singlet state population, being isolated from the three triplet states, decays with a time constant $T_{LLS}$, which can be more than an order of magnitude higher than $T_1$. After a mixing time $\tau_m$, the RF irradiation is switched off which is sufficient to convert the $I_2$ spin-system back to an $IS$ spin system. As the RF field is switched off, the system evolves under the weak-coupling Hamiltonian as shown in Eq. 2.1.2 and the population of the LLS converts back to the sum of $ZQ_x$ and $I_Z S_Z$.

The density operator at time point 'e' is given by:

$\sigma(e) = a|S_0\rangle\langle S_0| = a[E/4 - I_zS_z - ZQ_x]$ with $a = \exp(-\tau_m/T_{LLS})$     (2.2.5)

None of the terms $ZQ_x$ and $I_ZS_Z$ can be observed directly by NMR. So, the density operator has to be converted to an observable, which is done during the 'e-f' and 'f-g' parts of the pulse sequence of Fig. 2.2.1 (B). The density operator at point 'g' is given by:

$\sigma(g) = a\ I_yS_y + (a/2)\ [2I_xS_z + 2I_zS_x]$     (2.2.6)

where $I_yS_y$ is a multiple-quantum coherence that remains undetected.

We can see from Eq. (2.2.6) that the signal detected here will be an antiphase doublet which can be converted to an in-phase signal by inserting a spin-echo (part 'g-h') in the pulse sequence. This can be expressed as:

$\sigma(h) = -(a/2)\ [I_y + S_y]$     (2.2.7)

It is worth mentioning here that losses due to transverse relaxation during the pulse sequence are neglected. These losses can be significant in the case of macromolecules. Though the above pulse sequence relieves the requirement of placing the carrier position at the mean chemical shift $\nu_{RF} = (\nu_1 + \nu_2)/2$, it still requires the precise knowledge of the delays $\tau_1$ and $\tau_2$ which are dependent on the $J$-coupling constant ($J_{IS}$) and on the chemical shift difference ($\Delta\nu_{IS}$), respectively. In the next section, a pulse sequence that removes the dependence on the chemical-shift difference is described.


## 2.3 LLS excitation via longitudinal two-spin order (*ZZ*)

The pulse sequence (sequence I) described in the previous section (Section 2.2) features a dependence on the values of the $J$-coupling $J_{IS}$ and the chemical shift difference $\Delta\nu_{IS}$, which are often unknown. For instance, in a two-site chemical exchange (A$\longleftrightarrow$B) the chemical shift differences between the relevant spins in the two conformations A and B, can vary, i.e., $\Delta\nu_{IS}^{A}$ $\neq \Delta\nu_{IS}^{B}$. In Sequence I, the delay $\tau_2$, which depends on $\Delta\nu_{IS}$, is necessary for carrying out the inversion of $ZQ_x \rightarrow -ZQ_x$. Therefore, the excitation of LLS without $ZQ_x$, i.e., only by using

*ZZ*, would make the pulse sequence independent of $\Delta\nu_{IS}$. For exciting LLS by *ZZ*, it is required to suppress zero-quantum coherences so as to avoid the mutual cancelation of $ZQ_x$ and *ZZ* because of their opposite signs at time point 'c' (Eq. 2.2.3). Dephasing of zero-quantum coherences (ZQC's) can be achieved by a Thrippleton-Keeler filter (T.K. filter)[22] which is an ingenious method using a combination of a pulsed field gradients (PFG's) and a frequency-modulated CHIRP pulse to filter out ZQC's independently of the chemical shifts. Below is the pulse sequence (sequence II) which can be used for excitation of LLS via *ZZ* order:[16]
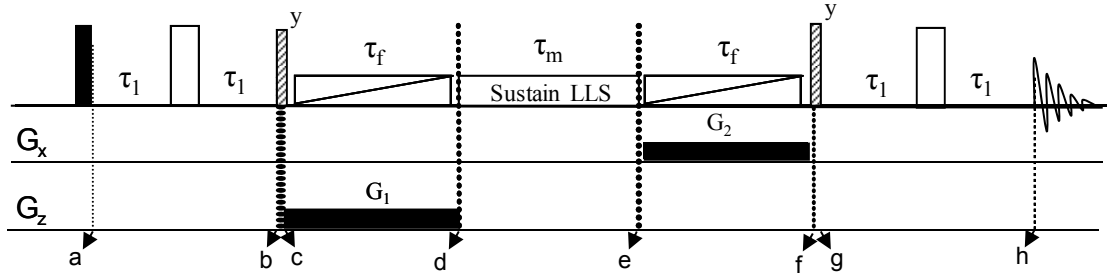


Figure 2.3.1. A pulse sequence (sequence II) designed to populate LLS via longitudinal two-spin order, $I_ZS_Z$. Here, ZQC's are dephased by a T.K. filter. Pulses with $\pi$, $\pi/2$ and $\pi/4$ are indicated by open, filled and hatched rectangles, respectively. The phases of the pulses are along the x-axis unless otherwise specified.

It has been explained in detail (Section 2.2) that at time point 'c', the density operator has following form:

$$\sigma(c) = (2I_xS_x - 2I_zS_z) = ZQ_x + DQ_x - 2I_zS_z \tag{2.3.1}$$

Here, between points 'c' and 'd' instead of the delay $\tau_2$, a T.K. filter is applied which causes dephasing of zero-quantum coherences. At point 'd' only *ZZ* order survives:

$$\sigma(d) = -2I_zS_z \tag{2.3.2}$$

This is then converted to the population of LLS by the application of a suitable RF-irradiation between points 'd' and 'e':

$\sigma(e) = (a/2).|S_0><S_0| = (a/2). [E/4 - I_zS_z - ZQ_x]$ with $a = \exp(-\tau_m/T_{LLS})$ (2.3.3)

Between points 'e' and 'f' another T.K. filter is applied to dephase zero-quantum coherences,

yielding the following density operator at time point 'f':

$$\sigma(f) = (-a/2).I_zS_z \tag{2.3.4}$$

This is converted to detectable antiphase terms by application of a $\pi/4$ pulse at 'g':

$$\sigma(g) = (-a/4).(I_xS_z + I_zS_x) \tag{2.3.5}$$

that can be converted to in-phase terms by a spin-echo, leading to the following density operator at time point 'h':

$$\sigma(h) = (-a/4).(I_y + S_y) \tag{2.3.6}$$

The sequence II can excite LLS independently of not only $\Delta\nu_{IS}$, but also independently of the offsets $\nu_I$ or $\nu_S$, but this extension comes at a cost of 50% of the signal intensity for each interval, the rest being lost as dephased $ZQ_x$. Therefore, the efficiency of this sequence is 25% in comparison to the pulse sequence I.

## 2.4 Two-dimensional LLS Exchange Spectroscopy (2D LLS-EXSY)

Pulse sequence II can excite LLS, independently of $\Delta\nu_{IS}$ but still has a dependence on $J_{IS}$ and cannot be applied to the spin systems having different $J_{IS}$ in two sites A and B undergoing a chemical exchange, i.e., $J_{IS}{}^A \neq J_{IS}{}^B$. One of the possible ways to remove the dependence on $\tau_1$ or $J_{IS}$ is by 2D spectroscopy. In pulse sequences I and II, after the first $\pi/2$ pulse, the system evolves for the delay $2\tau_1 = 1/(2\,J_{IS})$ with a $\pi$-pulse inserted in the middle so that the density operator at the point 'b' is:

$$\sigma(b) = 2\left(I_xS_z + I_zS_x\right) \tag{2.4.1}$$

The fixed delays $\tau_1$ can be replaced by a variable time $t_I$, in the fashion of 2D spectroscopy which makes the sequence broadband with respect to $J_{IS}$. The delay $\tau_2$ between 'c' and 'd' can be replaced by a T.K. filter which dephases $ZQ_x$, consequently, removing the dependence upon $\Delta\nu_{IS}$ (Section 2.3). So, the following broadband 2D pulse sequence (sequence III) [16] which is broadband with respect to $J_{IS}$, $\Delta\nu_{IS}$ or individual offsets, $\nu_I$ and $\nu_S$; is referred as 2D

LLS-EXSY[16] and can be useful for monitoring slow timescale processes (A ⟷ B) using LLS even when $\Delta v_{IS}^A \neq \Delta v_{IS}^B$ and/or $J_{IS}^A \neq J_{IS}^B$:
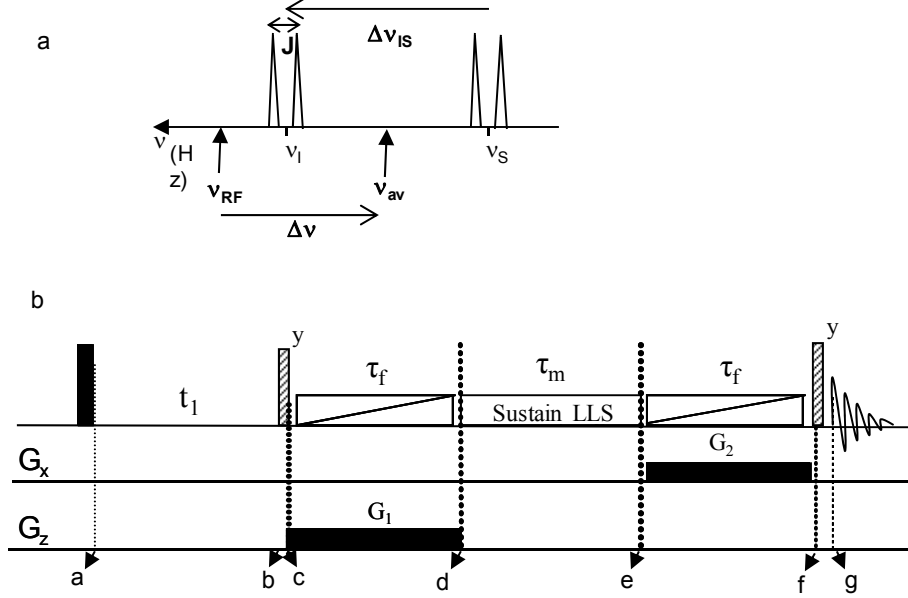


Figure 2.4.1: (A) Sketch of an NMR spectrum of a weakly coupled two-spin ½ system with relevant parameters. (B) A pulse sequence (sequence III) designed to carry out broadband excitation of LLS in 2D spectroscopy via longitudinal two-spin order, $I_Z S_Z$. The pulses with $\pi/2$ and $\pi/4$ are indicated by filled and hatched rectangles, respectively. The phases of the pulses are along the x-axis unless otherwise specified.

This 2D experiment can excite LLS simultaneously in different environments, for example, in two distinct sites A and B where the spins $I$ and $S$ have chemical shifts and couplings $v_I^A$, $v_S^A$, $J_{IS}^A$ and $v_I^B$, $v_S^B$, $J_{IS}^B$, respectively. The chemical shifts labeled during the evolution interval, $t_1$, lead to the coherences modulated at the frequencies, $v_I^A$, $v_S^A$, $v_I^B$ and $v_S^B$ at point 'b'. LLS$^A$ and LLS$^B$ are then excited at point 'd' and sustained in the interval 'd-e' where exchange may occur between the two sites, A and B. At point 'g', LLS populations are transformed back into antiphase single–quantum coherences, resuming precession at the four chemical shifts in the $t_2$ dimension. Two types of non-diagonal peaks are expected for $I$ spin (and for the S spin): *i)* from magnetization labeled at $v_I^A$ during $t_1$ being detected at $v_S^A$, the so-called LLS-blending peaks. These peaks arise because of magnetization mixing in LLS. *ii)* Arising from

magnetization labeled at $\nu_I^A$ during $t_1$ and detected at $\nu_I^B$ and $\nu_S^B$, which are the exchange peaks arising from the chemical exchange between the two sites as shown schematically in Fig. 2.4.2.
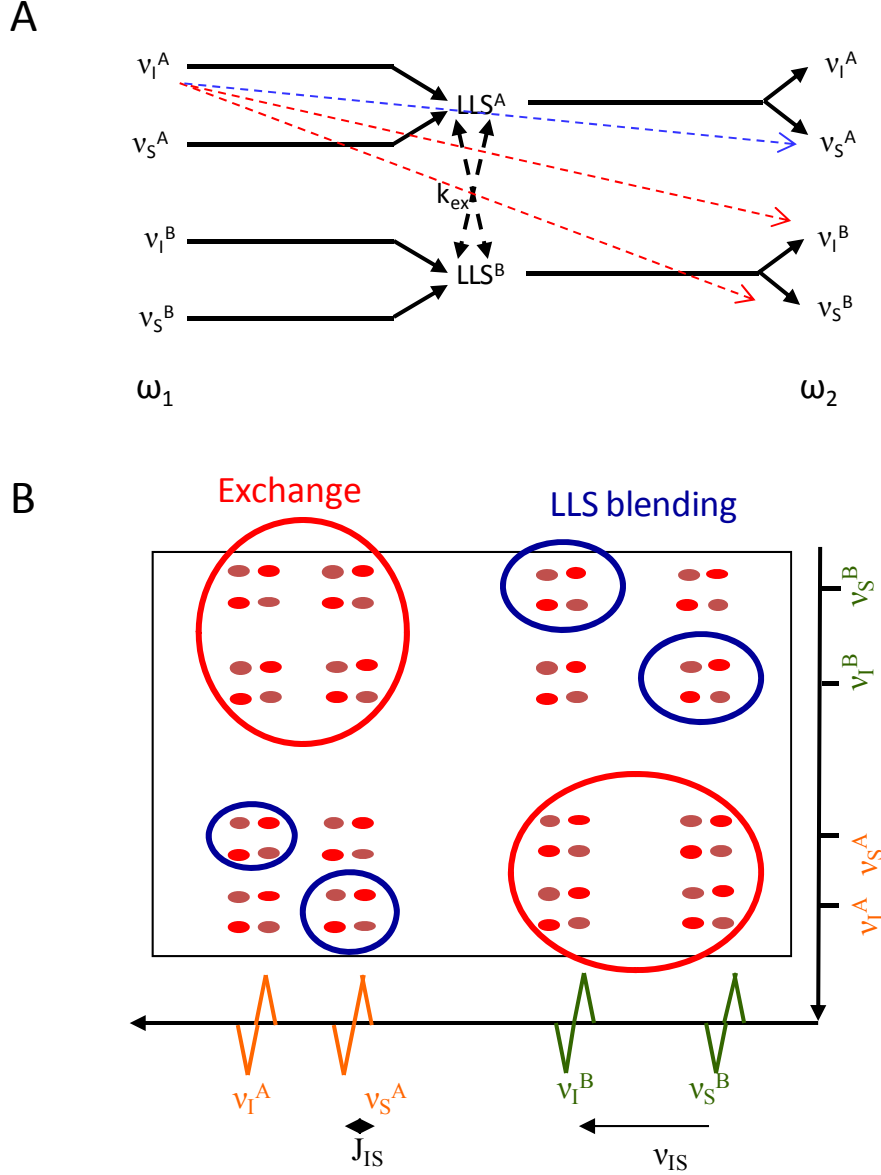


Figure 2.4.2: (A) Chemical shift correlations that can be observed in the 2D spectrum obtained from 2D LLS-EXSY. (B) Sketch of a 2D LLS-EXSY spectrum that can be expected for a two site exchange between the sites A and B, where two kinds of cross peaks are expected: LLS-blending and the exchange peaks.

The pulse sequence III is capable of broadband excitation of LLS without any knowledge of $\Delta\nu_{IS}$ or $J_{IS}$ but the lifetimes $T_{LLS}$ tend to decrease rapidly if the carrier position, $\nu_{RF}$ is moved away from the mean chemical shift $((\nu_I + \nu_S)/2)$ of the two spins, i.e., by increasing $\Delta\nu$ (Fig.

2.4.1(A)) if CW irradiation is used during sustaining period. This limitation can be overcome by using other RF schemes such as WALTZ-16 which can sustain LLS efficiently even at $\Delta\nu = 1$ kHz at 400 MHz proton frequency, thus making the sequence III broadband with respect to $\Delta\nu$.[16] It turns out that amplitude and frequency modulated pulses perform even better for sustaining LLS, as will be discussed in detail in the next section.

## 2.4.1 Application to BPTI

The side chain of the Tyrosine-35 residue in Basic Pancreatic Trypsin Inhibitor (BPTI) undergoes slow exchange ($\sim 30$ s$^{-1}$ at 309 K)[12] due to slow rotation of the Tyr ring and the H$^{\delta1}$ resonance is exchanged with that of H$^{\delta2}$ and H$^{\varepsilon1}$ with H$^{\varepsilon2}$ as shown in Fig. 2.4.1.1.
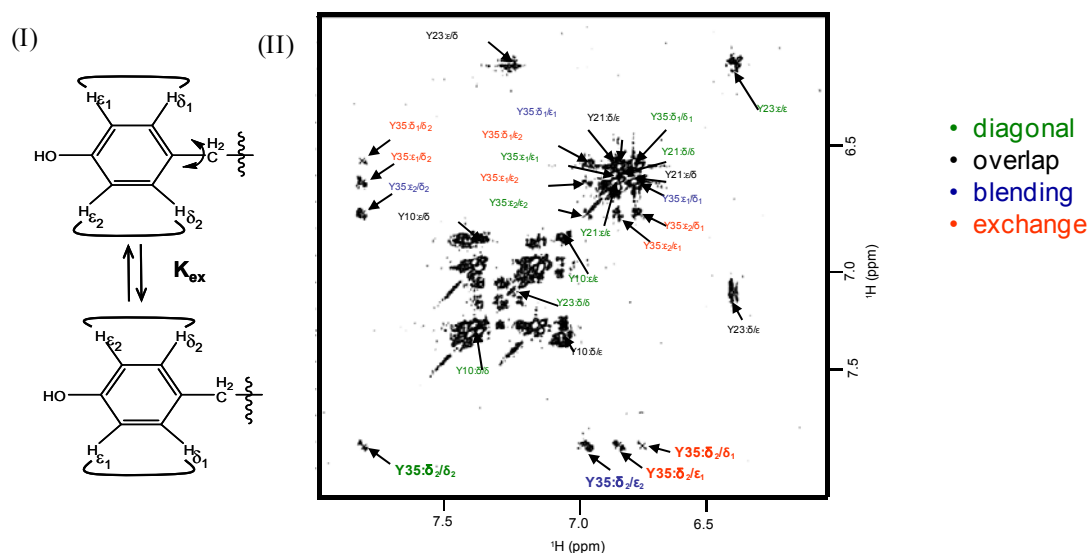


Figure 2.4.1.1. (I) The Tyrosine residue 35 undergoes a slow rotation around the C$^\beta$-C$^\gamma$ axis (30 s$^{-1}$ at 309K).[12] (II) 2D LLS-EXSY spectrum of aromatic protons in BPTI, recorded with a sequence in Fig. 2.4.1. at 310K and 400MHz. The sample was not deuterated. A matrix of 4k×256 points was acquired and transformed to 8k×512 points. The spectral widths in the $t_2$ and $t_1$ dimensions were 5.6 and 2.2 ppm. The carrier frequency $\nu_{RF}$ was set at 7.3 ppm. The peak amplitudes of the $G_1$ and $G_2$ PFG s were 28.5% and 65% of the maximum intensity (50G/cm) along the z and y axes, respectively. A Chirp inversion pulse of length $\tau_f = 12$ ms with a sweep width of 80 kHz and a maximum amplitude of 2348 Hz, was used simultaneously with the gradients to eliminate the $ZQ_x$ coherences. The assignments of diagonal signals are labeled in green; those of cross peaks originating from the exchange are labeled in red, while peaks originating from mixing of magnetization (LLS-blending) in the LLS are labeled in blue. Whenever two types of cross peaks are overlapped due to the positions of the resonances, black labels are used. A mixing time $\tau_m = 300$ ms with contiguous Sinc pulses of 400 μs and peak amplitudes of 7.3 kHz was used.

19

LLS can be excited for the *J*-coupled proton pairs, $H^{\delta 1}$- $H^{\varepsilon 1}$ and $H^{\delta 2}$ - $H^{\varepsilon 2}$ using the above mentioned 2D method. The LLS-EXSY spectrum of the aromatic region of BPTI is shown in Fig. 2.4.1.1 (II). It has been observed by ZZ-exchange spectroscopy[12] that the four cross peak multiplets of Y35 (Tyr) at the chemical shift position of $H^{\delta 2}$ in the $t_1$ dimension, are centered at the chemical shifts of the following protons in the $t_2$ dimension: $H^{\delta 2}$ (diagonal peak labeled in green), $H^{\varepsilon 2}$ (due to LLS blending, in blue), $H^{\varepsilon 1}$ and $H^{\delta 1}$ (both labeled in red).While for residues Y10, Y21 and Y23 in BPTI, the exchange cross peaks coincide with the LLS blending peaks, due to the fact that the chemical shifts of the $H^{\delta 1}$ and $H^{\delta 2}$ protons, on the one hand, and those of the $H^{\varepsilon 1}$ and $H^{\varepsilon 2}$ protons, on the other hand, are averaged out by fast exchange on the NMR time scale.

We measured the exchange of the Tyr-35 flip by using ZZ-EXSY and LLS-EXSY at 600 MHz. For the ZZ-EXSY experiment, the pulse sequence shown in Fig. 2.4.1 (similar to LLS-EXSY) was used without the RF irradiation during the time period 'd-e'. Fig.2.4.1.2 shows the decay of the diagonal peak $H^{\delta 2}$- $H^{\delta 2}$ and exchange cross peak $H^{\delta 2}$- $H^{\delta 1}$ obtained by both methods.
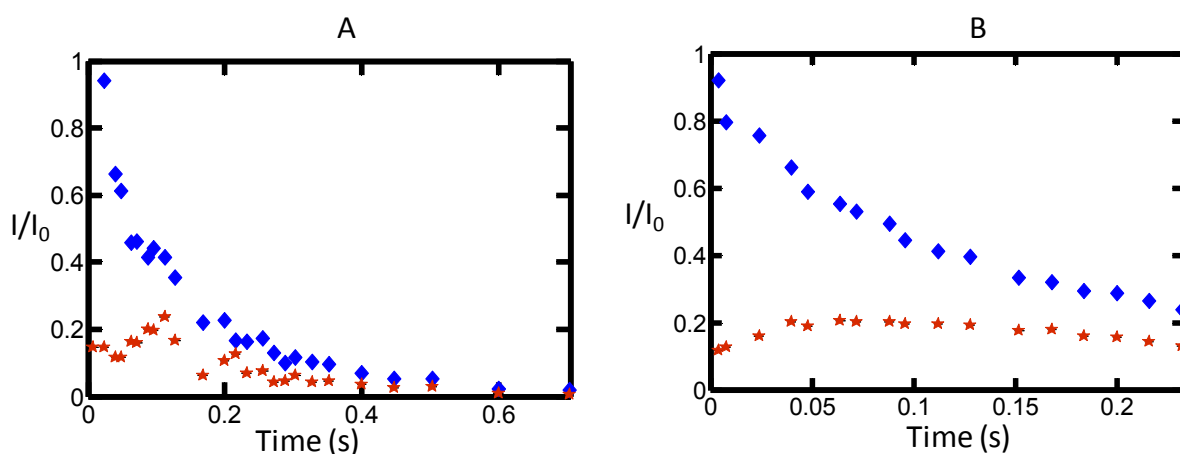


Figure 2.4.1.2. Decay of the diagonal peak $H^{\delta 2}$- $H^{\delta 2}$ (Blue diamonds) and exchange cross peak $H^{\delta 2}$- $H^{\delta 1}$ (Red stars) of Y35 in BPTI, obtained from LLS-EXSY (A) and ZZ-EXSY (B). The experiments were performed at 600 MHz spectrometer.

**2.5 Increased bandwidth for sustaining LLS**

Various ways for efficient excitation of LLS have been discussed in the previous sections but still the dependence on the carrier position for sustaining LLS prevails. After excitation, LLS is subjected to an RF irradiation, the amplitude of which should be as high as possible for suppressing the chemical shift differences. However, the amplitude is limited by the highest power that can be afforded without causing any harm to the electronics of the spectrometer or causing any significant sample heating. In practice, If the condition $\Delta \nu_{IS} \ll \nu_{RF}$ (Fig. 2.4.1 (A)) is satisfied, LLS is sustained efficiently. Otherwise, LLS is poorly isolated from other fast-relaxing spin states and therefore decays fast. Also, the efficiency of sustaining LLS decreases as the RF carrier position $\nu_{RF}$ is moved away from the exact middle ($\nu_{av} = (\nu_I + \nu_S)/2$) of the two spins, i.e., with increasing $\Delta \nu = \nu_{RF} - \nu_{av}$.

We have addressed these aspects experimentally and found out that the use of amplitude- and frequency-modulated "shaped" pulses can sustain LLS with better lifetimes for larger values of $\Delta \nu_{IS}$ and $\Delta \nu$.[23] This opens the way to applications to molecules containing pairs of coupled spins $I$ and $S$ that feature either (i) a wide range of offsets $\Delta \nu = \nu_{av} - \nu_{RF}$ between the average chemical shift of the spins, $\nu_{av} = (\nu_I + \nu_S)/2$, and the carrier frequency $\nu_{RF}$ or (ii) large differences in chemical shifts $\Delta \nu_{IS} = \nu_I - \nu_S$. The ability of the RF scheme to sustain LLS depends critically on these two parameters. In studies of exchange processes involving several molecular conformations, where each conformation is associated with a characteristic set of chemical shifts, it is quite likely to have wide ranges of offsets. Spreads in chemical shifts are even more likely to occur when the two coupled spins belong to nuclear species such as $^{13}$C.

*2.5.1 Results*

Various shaped and composite pulses have been tested in the view of achieving the longest possible lifetimes of LLS over the widest possible bandwidths, i.e., ranges of $\Delta \nu_{IS}$ and $\Delta \nu$. A

partially-deuterated saccharide with two diastereotopic protons attached to the same carbon with a shift difference of 0.19 ppm (75 Hz at 400 MHz), was used as a test system to measure the efficiency of various pulses. Different decoupling schemes were tested as a function of the offset $\Delta v$. It was observed that in the offset range where the decoupling sequence remained effective, $R_{LLS}$ remained close to the value obtained for $\Delta v = 0$. Outside this range it increased abruptly. Each decoupling sequence was tested with a mixing time $\tau_m = 30$ s and a relaxation delay of 1 s between scans, so as to establish the maximum amplitude ($v_1^{max}$) that can be applied without causing any significant heating. The amplitudes $v_1^{max}$ that were considered to be safe, correspond to an attenuation of 1dB below the amplitude that causes detectable change in the level of the lock signal. A sequence of contiguous Gaussian $\pi$ pulses with peak RF amplitudes $v_1^{max} = 7$ kHz truncated at 1% of their maximum value and pulse lengths $\tau_p = 175$ $\mu$s was found to give a profile of $R_{LLS}$ that is very similar to the WALTZ-16 sequence[24] with a constant RF amplitude $v_1^{max} = 3.9$ kHz (Fig. 2.5.1.1 A (a)-(b)). A sequence of contiguous Refocusing Broadband Universal Rotation Pulses (RE-BURP), with peak RF amplitudes $v_1^{max} = 15.7$ kHz, pulse lengths $\tau_p = 400$ $\mu$s, and shapes defined by the summation of 15 sine and cosine modulated pulses was found to cover a bandwidth of $\pm$ 7 kHz (Fig. 2.5.1.1 A (c)). It was verified experimentally that, as the pulse length of the RE-BURP shape is decreased by a factor of 2 and $v_1^{max}$ increased by the same factor, a twofold improvement of the bandwidth is observed. Different pulses from the BURP family (I-BURP, U-BURP) were also tested, but gave less satisfactory results. The profile of an RF sequence using contiguous Sinc-shaped pulses[25] was found to be even wider than that of the RE-BURP sequence (Fig. 2.5.1.1 A (d)). Frequency-modulated CHIRP[26] or TanhTan[27] pulses afforded offset profiles of the rate constants $R_{LLS}$ ($\Delta v$) that were remarkably wide, though not as regular as for amplitude-modulated pulses (Fig. 2.5.1.1 B). The maximum apparent lifetimes of the LLS sustained during $\tau_m$ using frequency-modulated pulses, at a given offset $\Delta v$, correlate with the

maximum amplitudes of the pulses, i.e., frequency-modulated pulses with low amplitudes afford large bandwidths for sustaining, but with higher $R_{LLS}$ values. The bandwidth of the $R_{LLS}$ ($\Delta \nu$) profile increased as the frequency sweep range of the pulses increased. The possibility of sustaining LLS using frequency-modulated pulses is encouraging in the view of using LLS in Magnetic Resonance Imaging (MRI).
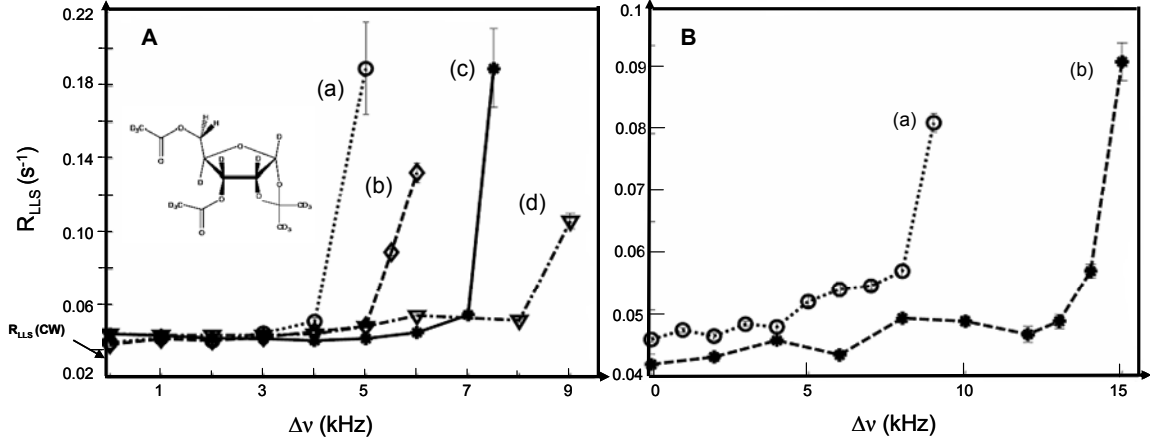


Figure 2.5.1.1. A. Comparison of experimental relaxation rate constants $R_{LLS} = 1/T_{LLS}$ of LLS in a partially deuterated saccharide (see insert), as a function of the offset $\Delta \nu$, observed for different RF schemes applied during the interval $\tau_m$: (a) (open circles) sequence of contiguous Gaussian $\pi$ pulses of length $\tau_p = 175$ µs and peak RF amplitudes $\nu_1^{max} = 7$ kHz, truncated at 1 % of their maximum; (b) (open diamonds) WALTZ-16 scheme using 'hard' pulses with a constant RF amplitude $\nu_1^{max} = 3.9$ kHz (i.e., the length of each $\pi/2$ pulse was $\tau_p = 64$ µs); (c) (asterisks) sequence of contiguous RE-BURP pulses of length $\tau_p = 400$ µs with peak RF amplitudes $\nu_1^{max} = 15.7$ kHz; (d) (open triangles) sequence of contiguous Sinc-shaped $\pi$ pulses (truncated at the 2$^{nd}$ nul-passage on either side of the peaks) of duration $\tau_p = 340$ µs and peak RF amplitudes $\nu_1^{max} = 12.4$ kHz. The 'true' relaxation rate constant $R_{LLS}$ (CW), indicated by an arrow on the left, was measured experimentally using continuous-wave (CW) decoupling with $\Delta \nu = 0$ and a constant RF amplitude $\nu_1^{max} = 1.3$ kHz. B. Experimental relaxation rate constants $R_{LLS}$ as a function of the offset $\Delta \nu$ using an RF sequence consisting of: (a) contiguous CHIRP pulses each of duration $\tau_p = 1$ ms with a frequency sweep of the RF carrier over a range of 22 kHz and a maximum amplitude $\nu_1^{max} = 4.4$ kHz, apodized [26] by quarter sinc-waves in the first and last 10 % of the sweeps and (b) TanhTan pulses of duration $\tau_p = 1$ ms, maximum amplitude $\nu_1^{max} = 4.4$ kHz, frequency sweep range of 44 kHz. All RF sequences except for WALTZ-16, which is composed of pulses along x and –x [24], were formed of blocks of 20 shaped pulses phased according to the five-step cycle of Tycko and al. [28], nested within an MLEV-4 supercycle.[29]

23

*2.5.2 Application to uracil*

The protons $H^5$ and $H^6$ in uracil dissolved in $D_2O$ (Fig. 2.5.2.1) provide an example of a coupled two-spin system with a modest scalar coupling constant, $J_{IS} = 7.7$ Hz and a large chemical shift difference, $\Delta\nu_{IS} = 1.7$ ppm, i.e., 693 or 1040 Hz at 400 or 600 MHz respectively ($B_0 = 9.4$ or 14.1 T). This is a challenging test for RF sequences intended to sustain LLS. Indeed, in a static field of 9.4 T, an attempt to preserve LLS in this pair of coupled protons using WALTZ-16 scheme with moderate amplitude ($\nu_1^{max} = 1.3$ kHz) resulted in scattered signal intensities as a function of time, with an approximate relaxation rate constant $R_{LLS} = 0.18 \pm 0.01$ s$^{-1}$, when fitted to an exponential decay function. When the amplitude was increased to $\nu_1^{max} = 3.9$ kHz, the signal intensities featured a mono-exponential decay as a function of $\tau_m$, which could be fitted with an exponential function with a decay rate $R_{LLS} = 0.12 \pm 0.05$ s$^{-1}$. Increasing the RF amplitude for the WALTZ scheme also resulted in increase of bandwidth.
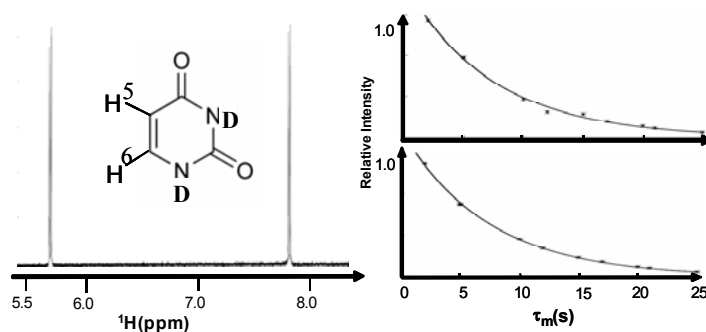


Figure 2.5.2.1. Left: signals of the $H^5$ and $H^6$ protons in a sample of uracil (shown in the inset) dissolved in $D_2O$ recorded with a cryoprobe at 14.1 T (600 MHz proton frequency) with the pulse sequence I of Fig. 2.2.1, using $\tau_m = 12$ s and WALTZ-16. Right: fits of the decays of the summed intensities of the four peaks shown on the left, to the function $\exp(-\tau_m/T_{LLS}) = \exp(-\tau_m R_{LLS})$, using WALTZ-16 with a constant RF amplitude $\tau_1 = 2.6$ kHz (top) and contiguous Sinc pulses with a peak RF amplitude $\tau_1^{max} = 5.6$ kHz and a pulse length of 500 $\mu$s (bottom). The small error bars (of the size of the symbols) reflect the difference in intensities of two identical experiments recorded with the same delay $\tau_m$.

Also, we compared a sequence consisting of contiguous Sinc pulses with WALTZ at 600 MHz. Using a WALTZ-16 sequence, the experimental signal intensities in Fig. 2.5.2.1 are slightly scattered around an ideal exponential decay. We have attributed this behaviour to the fact that the necessary condition for sustaining LLS is not quite fulfilled, since the RF amplitude should ideally be much higher than the separation of signals, $\nu_1 \gg \Delta\nu_{IS}$, whereas in this case $\nu_1 = 2.6$ kHz and $\Delta\nu_{IS} = 1$ kHz. The use of Sinc pulses diminished the errors of the measurements (Fig 2.5.2.1) - the fitted relaxation rate constants were $R_{LLS} = 0.14$ s$^{-1}$ with both sequences, with errors of 1.5 % and 1.1 % for the WALTZ-16 and the Sinc sequences, respectively. Thus, the RF sequence that has the larger bandwidth in terms of the average offset $\Delta\nu$ also has the ability of better sustaining the LLS in molecules where the differences in chemical shifts $\Delta\nu_{IS}$ are large. In this way, the use of various decoupling sequences facilitates the efficient sustaining of LLS even for wide ranges of offsets and in the molecules where chemical shift differences are large.

## 2.6 Broadband Excitation of LLS in 1D Spectroscopy

In the last section, it has been discussed how the broadband excitation of LLS can be achieved in a 2D fashion. In cases where spectral overlap is significant, it is better to resort to 2D spectroscopy, but in cases where spectral overlap is not significant, two-dimensional techniques are unnecessarily time-consuming, and 1D broadband excitation methods of LLS are better adapted. In the following section, a pulse sequence for broadband excitation of LLS in 1D spectroscopy is described.

### 2.6.1 Methods

The efficiencies of sequence I (Fig. 2.2.1) and sequence II (Fig. 2.3.1) depend on the amplitude of antiphase single-quantum coherence $AP = 2I_xS_z + 2I_zS_x$ at time point 'b'.

Maximization of this coherence over a range of $J_{IS}$ can be achieved by insertion of the block in Fig. 2.6.1.1 in place of the spin–echo. If a rotation $\beta$ is brought about an axis with a plane $\theta$ = 0, a subsequent rotation $2\beta$ around another axis with $\theta = 2\pi/3$ compensates for the first order errors in $B_1$ inhomogeneities.[30] This idea of M. Levitt was adapted for heteronuclear INEPT by Wimperis and Bodenhausen.[31] If $\beta = \left(\dfrac{\pi}{2}\right)_0 - \tau_1 - \left(\pi\right) - \tau_1 - \left(\dfrac{\pi}{2}\right)_{180}$ then the pulse sequence in Fig. 2.6.1.1 can carry out broadband conversion of in-phase terms (- $I_y$ - $S_y$) into antiphase terms ($AP = 2I_xS_z + 2I_zS_x$) over a range of $J_{IS}$.
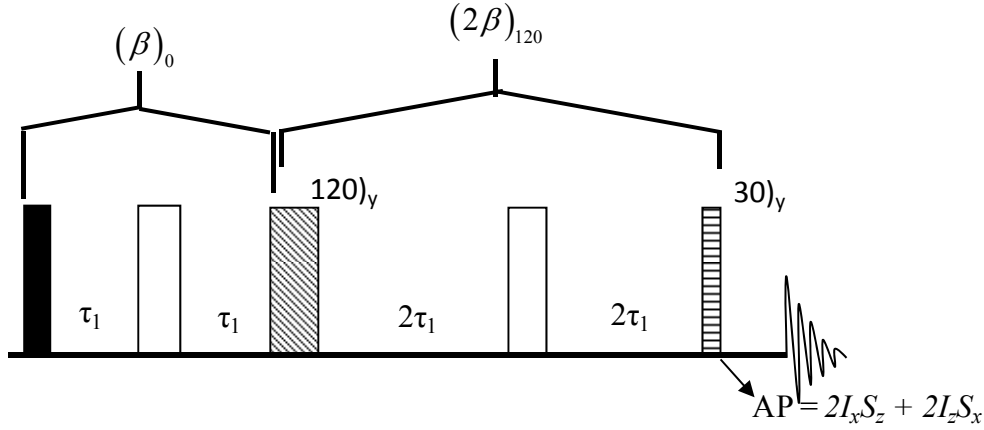


Fig. 2.6.1.1. Pulse sequence designed to perform broadband rotation over a range of $J_{IS}$.

The efficiency of the new sequence, $E^{bb}$, can be evaluated by calculating the expectation value of $AP = 2I_xS_z + 2I_zS_x$ at the end of the sequence:

$$E^{bb} = \left(1 + \frac{\cos^2 \beta}{2}\right)\sin \beta \qquad (2.6.1.1)$$

Fig. 2.6.1.2 shows its comparison to the $\sin\beta$ profile, obtained using a simple spin-echo:
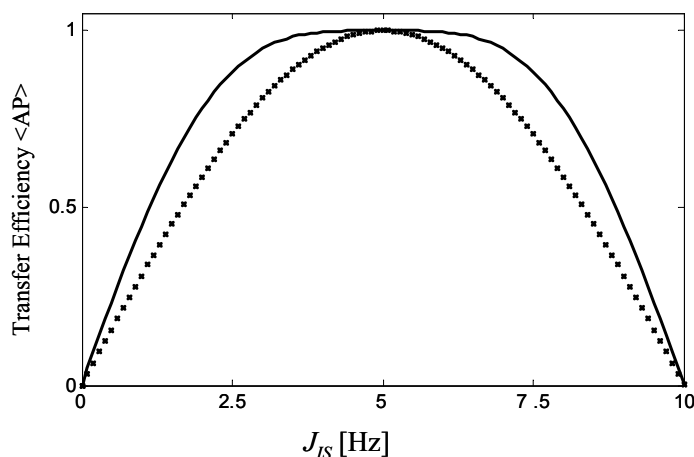
Figure 2.6.1.2. Theoretical plot of the efficiency of the conversion from in-phase to antiphase coherence using the broadband sequence (full line), compared to that of a spin-echo sequence (dotted line), using an interval $2\tau_I = 0.1$ s (yielding optimal transfer for $J_{IS} = 5$ Hz).

Following is a pulse sequence with the implementation of the broadband excitation idea, referred to as BB-LLS-DOSY,[32] which can be used for measuring diffusion in mixture of molecules:
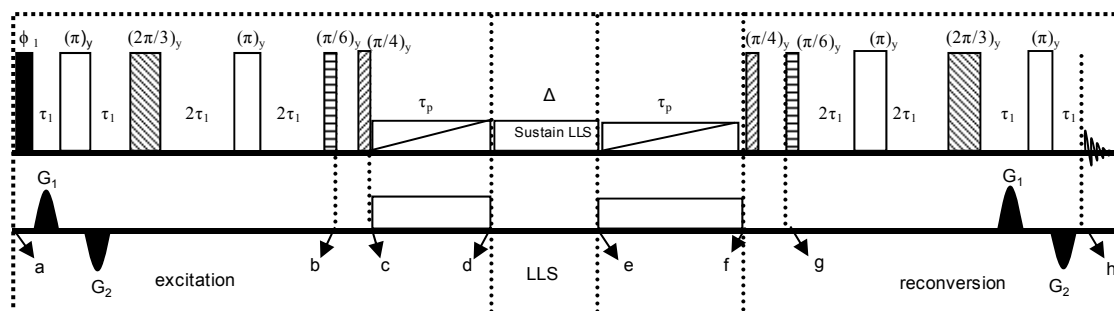


Figure 2.6.1.3. Method for broadband LLS diffusion ordered spectroscopy (BB-LLS-DOSY). The hatched rectangles stand for pulses with various flip angles, as indicated. During the intervals 'c-d' and 'e-f', T. K filters are inserted. Typical T. K. filters used in our experiments had durations $\tau_p = 12$ ms, sweep-widths of 80 kHz and peak radio-frequency amplitudes of 1.78 kHz; the amplitudes of the gradients were 14.6 and 17.8 G/cm for time intervals 'c-d' and 'e-f', respectively. During the interval $\Delta$ where the LLS are sustained, a sequence of sinc-shaped pulses of 400 µs duration each and a maximum radio-frequency amplitude of 5.7 kHz was applied.[25] The recommended phase cycle in the sequence is $\phi_1 = (x, -x)$ and $\phi_{rec} = (x, -x)$.

The broadband conversion is carried out with respect to the angle $\beta = 2\pi J_{IS}\tau_1$, consequently, if $\tau_1$ is fixed, with respect to the coupling constant $J_{IS}$. Thus, the spin-echo part 'a-b' of sequence

II (Fig. 2.3.1) can be replaced by the composite sequence 'a-b' (Fig. 2.6.1.1). A symmetric sequence (*g-h*) can be used to obtain in-phase signals before detection.

The efficiency of step 'a-b' in the BB-LLS-DOSY sequence was tested over a range of rotation angles $\beta = 2\pi J_{IS}\tau_1$ using simulations (Fig. 2.6.1.4 A) and by varying the interval $\tau_1$ in experiments on 2,3,6-trichlorobenzaldehyde (denoted by **I**) with $J_{IS} = J^{(1)} = 8.8$ Hz (Fig. 2.6.1.4 (B)). In Fig. 2.6.1.4 (B), the antiphase coherences were converted into in-phase magnetization prior to detection by appending a spin-echo with $\tau = 1/(4 J^{(1)})$, i.e., with $\beta = \pi/2$. Both simulations and experiments confirm that the transformation taking in-phase coherence $-(I_y + S_y)$ to antiphase coherence is sufficiently broadband over a range $0.25\pi < \beta < 0.75\pi$, in the sense that the signal amplitude $S(\beta)$ varies within a small range, $0.8 < S(\beta) < 1$.
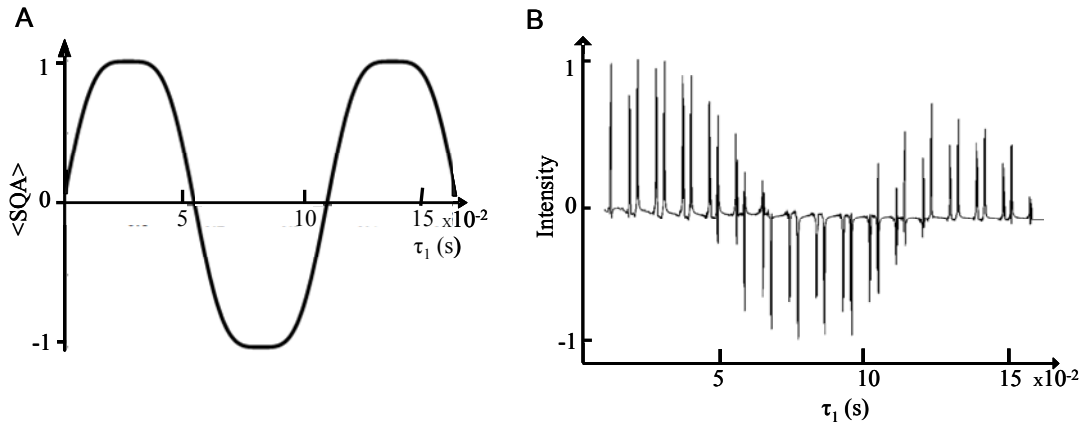


Figure 2.6.1.4 A. Simulations of the expectation values of antiphase single-quantum coherence $AP = 2I_xS_z + 2I_zS_x$ in a system with two coupled spins $I$ and $S$ with $J_{IS} = 8.8$ Hz, at time point 'b' in the BB-LLS-DOSY sequence of Fig. 2.6.1.3, as a function of the delay $\tau_1$. B. Experimental signal intensities of the four peaks of 2,3,6-trichlorobenzaldehyde (**I**), where $J_{IS} = 8.8$ Hz, using the pulse sequence explained in the text.

The excited antiphase terms are converted into a superposition of $2I_zS_z$ and $2I_xS_x$, under the effect of a $\pi/4$ pulse. Subsequently, a pulsed field gradient combined with a frequency-modulated pulse in the manner of a T. K. filter[22] allows the removal of the transverse terms, leading to a density operator at time-point 'd':

$$\sigma(d) = -2I_zS_z$$

which generates the required population difference between singlet and triplet states when the RF irradiation is switched on.

Step 'c-d' is also broadband with respect to the chemical shift difference $\Delta \nu_{IS}$, as the magnetization transferred from points 'c' to 'd' corresponds to longitudinal two-spin order $2I_zS_z$, that does not evolve under the shifts of the spins. Step 'd-e' can be rendered broadband by the use of various decoupling sequences (described in Section 2.5), thus making the pulse sequence suitable for broadband excitation and sustaining of LLS.

*2.6.2 Results*

To test the ability of the BB-LLS-DOSY sequence to determine simultaneously the diffusion coefficients of different molecules in solution using weak encoding/decoding gradients $G$ and long diffusion intervals $\Delta$, we have investigated a sample containing 2,3,6-trichlorobenzaldehyde (**I**) and 2-chloroacrylonitrile (**II**), each possessing a pair of *J*-coupled protons with coupling constants $J^{(\mathbf{I})} = 8.8$ Hz and $J^{(\mathbf{II})} = 3.3$ Hz, where long-lived states can be excited in separate series of experiments. The experiments were carried out at $B_0 = 14.1$ T (600 MHz) and T = 286 K, in a solvent consisting of 40 % $D_2O$ and 60 % DMSO-$d_6$. The concentration of each of the species in solution was ~ 20 mM. The LLS lifetimes were found to be $T_{LLS}$ (**I**) $= 12.5 \pm 0.3$ s and $T_{LLS}$ (**II**) $= 31.5 \pm 0.4$ s under our experimental conditions (without degassing), while the relaxation time constants of longitudinal magnetization were $T_1$ (**I**) $= 4.0 \pm 0.2$ s and $T_1$ (**II**) $= 3.8 \pm 0.2$ s.

The diffusion constants of these two molecules were first measured using the conventional stimulated-echo (STE) method[33] (Fig. 2.6.2.1 (A)). The signal intensities were fitted with two parameters, the diffusion coefficient $D$ and the initial signal intensity $S_0$, as a function of the parameter $\kappa$ which depends on the peak amplitude $G$ and duration $\delta$ of the pulsed field gradients:

$$\kappa = 2\gamma Gps\delta \qquad\qquad\qquad\qquad\qquad (2.6.2.1)$$

where $\gamma$ is the gyromagnetic ratio of protons. The factor 2 reflects the fact that bipolar pulse pairs (BPP) are used before and after the diffusion interval $\Delta$, $p$ is the coherence order (in the present case, $p = 1$ since single-quantum coherences are encoded), $s$ is a shape factor ($s = 2/\pi$ for a PFG with a sinusoidal envelope). The diffusion delay was chosen to be $\Delta = 0.6$ s in our basic STE experiments, and the peak amplitude $G$ of the sine-shaped encoding and decoding gradients was varied up to 90 % of the upper limit allowed for the probe. This results in spin-echo amplitudes which are in a convenient range $0.1 < S(\kappa)/S(\kappa = 0) < 1$ (Fig. 2.6.2.1A).

Using the simple LLS-SQ-DOSY sequence[9], the diffusion constants of compounds **I** and **II** in the mixture could only be measured in two separate series of experiments because the scalar coupling constants $J^{(I)}$ and $J^{(II)}$ are quite different. The intervals of the LLS-SQ-DOSY sequence for maximizing AP coherences were set to $\tau_1 = 1/(4J^{(I)}) = 28$ ms and $\tau_1 = 1/(4J^{(II)}) = 76$ ms, respectively. The diffusion delay could be set to $\Delta = 4$ s in both experiments, well below the lifetimes of the LLS populations in either of the two molecules, i.e., $\Delta \ll T_{LLS}(\mathbf{I}) < T_{LLS}(\mathbf{II})$. Consequently, the simple LLS-SQ-DOSY sequence allowed us to reduce the maximum gradients by a factor of $\sim 2$ compared to the basic STE sequence (Fig. 2.6.2.1 (B) – (C)). It is noteworthy that this feature of LLS-DOSY experiments allows one to determine diffusion coefficients of large, slowly-diffusing molecules, using regular NMR probes while reducing the strain on the required gradient amplitudes significantly.
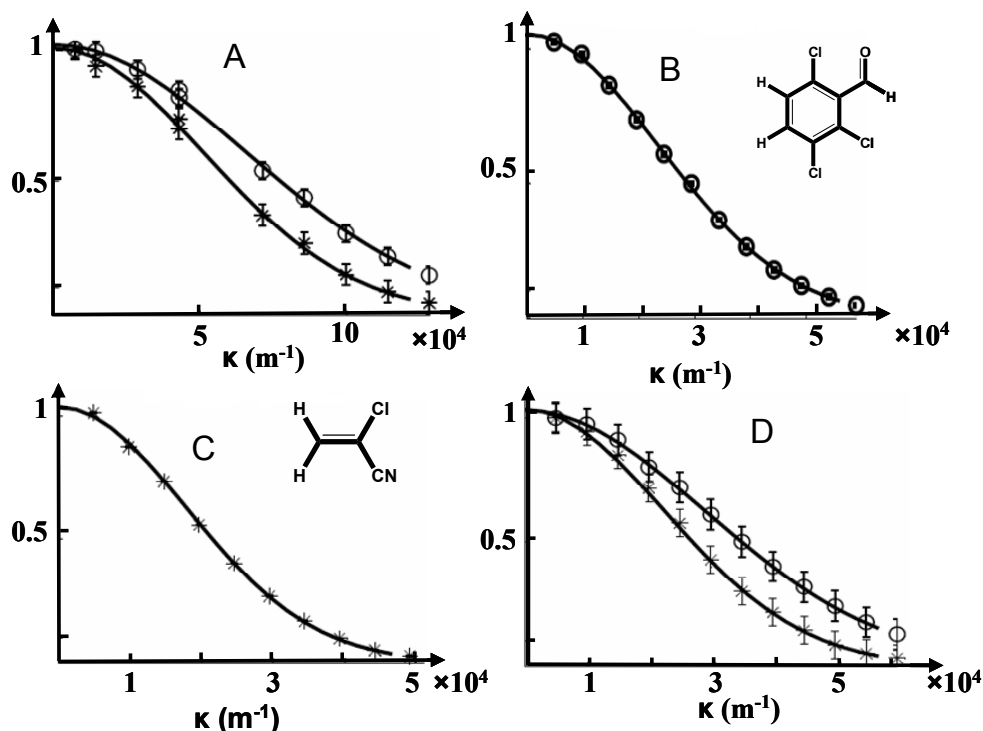
Figure 2.6.2.1. Experimental study of translational diffusion in a mixture of 2,3,6-trichlorobenzaldehyde (**I**) and 2-chloroacrylonitrile (**II**) at T = 286 K and $B_0$ = 14.1 T (600 MHz for protons). The experimental intensities of resonances of **I** and **II** are indicated by circles and stars, respectively. The diffusion coefficients determined from the curves are given in the Table 2.6.2.1. A. Conventional stimulated echo sequence (STE) with a diffusion delay $\Delta$ = 0.6 s; the peak amplitudes of the encoding and decoding gradients of duration $\delta$ = 0.8 ms were stepped through $2.6 < G < 43$ G/cm. B. LLS-SQ-DOSY with $\Delta$ = 4 s and a delay $\tau_1 = 1/(4J^{(I)}) = 28$ ms matched for compound **I**, with gradients of duration $\delta$ = 0.55 ms and amplitudes $3 < G < 31$ G/cm. C. Same sequence, with $\tau_1 = 1/(4 J^{(II)}) = 76$ ms matched for compound **II** and $3 < G < 26$ G/cm. D. The method for broadband LLS diffusion-ordered spectroscopy (BB-LLS-DOSY) with a diffusion delay $\Delta$ = 3 s and a compromise interval $\tau_1 = 41$ ms $\approx 1/[2(J^{(I)} + J^{(II)})]$, with gradients of duration $\delta$ = 0.55 ms and amplitudes $3 < G < 31$ G/cm.

The method for broadband LLS diffusion ordered spectroscopy (BB-LLS-DOSY) was used to determine the diffusion coefficients of the two molecules **I** and **II** simultaneously (Fig. 2.6.2.1 (D)). The interval 'a-b', as well as the corresponding refocusing interval in the sequence in Fig. 2.6.1.3, were chosen to maximize the function $f = \sin(2\pi J^{(I)}\tau_1) + \sin(2\pi J^{(II)}\tau_1)$ over the interval $0 < \tau_1 < 1/(4J^{(II)})$. Note that $\tau_1 \sim 1/[2(J^{(I)} + J^{(II)})]$ which corresponds to $\tau_1 = 41$ ms.

The diffusion coefficients obtained for both molecules with (using LLS-DOSY) and without irradiation (using STE) during the diffusion delay (Table 2.6.2.1) are similar, which shows that heating by the radio-frequency irradiation was minimal.

31

| Diffusion coefficients $D$ / $10^{-10}$ m$^2$s$^{-1}$ at $T = 286$ K | STE | LLS-SQ – DOSY $\tau_1 = 1/(4J^{(I)})$ = 28 ms | LLS-SQ-DOSY $\tau_1 = 1/(4J^{(II)})$ = 76 ms | BB-LLS-DOSY $\tau_1 = 1/[2(J^{(I)} + J^{(II)})] = 41$ ms |
|---|---|---|---|---|
| Trichlorobenzaldehyde (I) (circles in Fig. 2.6.2.1) | $2.0 \pm 0.1$ | $2.2 \pm 0.1$ | - | $2.0 \pm 0.1$ |
| Chloroacrylonitrile (II) (stars in Fig. 2.6.2.1) | $3.1 \pm 0.2$ | - | $3.7 \pm 0.2$ | $3.3 \pm 0.2$ |

Table 2.6.2.1. Diffusion coefficients $D$ of the two compounds **I** and **II** determined from the six curves in Fig. 2.6.2.1, corresponding to four different experiments: basic stimulated echoes (STE), LLS-SQ-DOSY, and the broadband LLS diffusion ordered spectroscopy (BB-LLS-DOSY).

In brief, broadband excitation of LLS in 1D and 2D spectroscopy alleviates the dependence on various parameters, thus making it widely applicable. In the next chapter, relaxation properties of LLS are discussed.

# Chapter - 3

# **Relaxation properties of long-lived states**

Long-lived states (LLS) have extraordinarily long lifetimes because the dipolar relaxation, which is the dominant relaxation mechanism in many situations, is inactive for these states. The dipole-dipole interaction between nuclei is not able to couple singlet states, which are antisymmetric with respect to the exchange of the two nuclei, to the symmetric triplet states. It is important to shed light upon relaxation of LLS in detail because of their interesting relaxation properties. The relaxation properties of LLS under various mechanisms have been described in this chapter.

## **3.1 Semi classical approach to relaxation**

Relaxation is the phenomenon by which the spin system returns back to an equilibrium state where all the coherences are zero and the populations of various energy levels follow a Boltzmann distribution. NMR relaxation is a consequence of the coupling of the spin system with the *surroundings*, termed as 'lattice'. The lattice has quasicontinuous energy levels, populated at Boltzmann distribution, and is assumed to be in thermal equilibrium all the time. The lattice modifies the local magnetic fields at the location of the nuclei by weak coupling to the spin system which causes relaxation. In the simplest form, relaxation can be described by Bloch's phenomenological equations, which provide a qualitative picture of relaxation, and phenomenological relaxation rate constants can be measured experimentally. Bloch's formulation does not provide any microscopic explanation of the origin or the magnitude of these rate constants.

To explain relaxation on a microscopic level, a semiclassical theory was formulated by Bloch, Wangsness and Redfield which is often used to describe NMR relaxation. In this theory, the

nuclear spins are treated quantum mechanically but the lattice classically. This treatment has the drawback that it does not predict how the spin system reaches the physical equilibrium state, i.e., Boltzmann distribution. This defect can be overcome by treating the relaxation fully quantum mechanically. In this chapter, the semi classical approach and its application to predict the relaxation rates of LLS under various relaxation mechanisms are described.

*3.1.1 Master equation of relaxation*

In the semiclassical approach, the Hamiltonian that acts on the spin system is the sum of the deterministic Hamiltonian, $H_0$, and the stochastic Hamiltonian, $H_1(t)$, which couples the spin system to the surroundings. The deterministic part $H_0$ can be constant or time-dependent, while $H_1(t)$ is randomly time-dependent, with the property that its time average is zero. The Liouville–von Neumann equation of motion of the density operator under the effect of the sum of the two Hamiltonians is given by:[34]

$$\frac{d\sigma(t)}{dt} = -i\left[H, \sigma(t)\right] = -i\left[H_0 + H_1(t), \sigma(t)\right] \tag{3.1.1.1}$$

The explicit dependence on $H_0$ can be removed by transforming the Liouville equation into the interaction frame, i.e., the reference frame of $H_0$. The density operator and stochastic Hamiltonian in the interaction frame ($\sigma^T(t)$ and $H_1^T(t)$) are given by:

$$\sigma^T(t) = \exp(iH_0 t)\sigma(t)\exp(-iH_0 t) \tag{3.1.1.2}$$

$$H_1^T(t) = \exp(iH_0 t)H_1(t)\exp(-iH_0 t) \tag{3.1.1.3}$$

From Eqns. (3.1.1.1), (3.1.1.2) and (3.1.1.3), the following equation of motion of the transformed density operator can be derived:

$$\frac{d\sigma^T(t)}{dt} = -i\left[H_1^T(t), \sigma^T(t)\right] \tag{3.1.1.4}$$

On integrating Eq. (3.1.1.4) over $t$:

$$\sigma^T(t) - \sigma^T(0) = \int_0^t -i\left[H_1^T(t'), \sigma^T(t')\right]dt' \tag{3.1.1.5}$$

Substituting the value of $\sigma^T(t)$ from Eq. (3.1.1.5) into Eq. (3.1.1.4):

$$\frac{d}{dt}\sigma^T(t) = -i\left[H_1^T(t), \sigma^T(0)\right] - \int_0^t \left[H_1^T(t), \left[H_1^T(t'), \sigma^T(t')\right]\right]dt' \tag{3.1.1.6}$$

An approximate solution can be obtained by setting $\sigma^T(t') = \sigma^T(t)$:

$$\frac{d}{dt}\sigma^T(t) = -i\left[H_1^T(t), \sigma^T(0)\right] - \int_0^t \left[H_1^T(t), \left[H_1^T(t'), \sigma^T(t)\right]\right]dt' \tag{3.1.1.7}$$

This can be rationalized because $\sigma^T(t')$ varies slowly, under the effect of randomly time-dependent $H_1^T(t)$. Now by replacing $t' = t - \tau$:

$$\frac{d}{dt}\sigma^T(t) = -i\left[H_1^T(t), \sigma^T(0)\right] - \int_0^t \left[H_1^T(t), \left[H_1^T(t-\tau), \sigma^T(t)\right]\right]d\tau \tag{3.1.1.8}$$

Taking the ensemble average on both sides:

$$\frac{d}{dt}\overline{\sigma^T(t)} = -i\overline{\left[H_1^T(t), \sigma^T(0)\right]} - \int_0^t \overline{\left[H_1^T(t), \left[H_1^T(t-\tau), \sigma^T(t)\right]\right]}d\tau \tag{3.1.1.9}$$

The first term vanishes if $H_1^T(t)$ and $\sigma^T(0)$ are uncorrelated since $\overline{H_1^T(t)} = 0$, by definition. The limit of the integral can be extended to infinity because of the short correlation times of $H_1^T(t)$ with respect to the change of the density operator. Including these assumptions in Eq. (3.1.1.9):

$$\frac{d}{dt}\overline{\sigma^T(t)} = -\int_0^\infty \overline{\left[H_1^T(t), \left[H_1^T(t-\tau), \sigma^T(t)\right]\right]}d\tau \tag{3.1.1.10}$$

The Hamiltonian $H_1(t)$ can be expanded in terms of irreducible tensor operators, which have very well established rotational properties:

$$H_1(t) = \sum_{q=-k}^{k} F_k^q(t) A_k^q \qquad (3.1.1.11)$$

where $F_k^q(t)$ is a random function of spatial variables and $A_k^q$ is a tensor spin operator. $A_k^q$ are chosen such that they have the following property:

$$\left[ I_z, A_k^q \right] = q\, A_k^q \text{ .We get } A_k^{qT} = \exp(i\omega_q t) A_k^q \text{ and } A_k^{q\dagger T} = \exp(-i\omega_q t) A_k^{q\dagger}$$

Substituting for $H_1(t)$ in Eq. (3.1.1.10):

$$\frac{d}{dt}\sigma^T(t) = -\sum_{q,q'} \int_0^\infty \overline{F_k^{q\dagger}(t) F_k^{q'}(t-\tau)} \exp(-i\omega_q \tau) d\tau \, \exp\left\{ i\left(\omega_{q'} - \omega_q\right) t \right\} \left[ A_k^{q\dagger}, \left[ A_k^{q'}, \sigma^T(t) - \sigma_0 \right] \right]$$

(3.1.1.12)

(Here, $\overline{\sigma^T(t)}$ has been replaced by $\sigma^T(t)$ and a correction term $\sigma_0$ has been introduced so that the final equilibrium form of the density operator leads to a Boltzmann distribution of populations.)

The terms in which $\left| \omega_{q'} - \omega_q \right| \gg 0$ are *nonsecular* and do not affect the long time behavior of $\sigma^T(t)$ because the rapidly oscillating factor $\exp\left\{ i\left(\omega_{q'} - \omega_q\right) t \right\}$ averages to zero much more rapidly than relaxation occurs. Therefore, only terms where $q = q'$ will contribute to relaxation:

$$\frac{d}{dt}\sigma^T(t) = -\sum_q \int_0^\infty \overline{F_k^{q\dagger}(t) F_k^q(t-\tau)} \exp(-i\omega_q \tau) d\tau \left[ A_k^{q\dagger}, \left[ A_k^q, \sigma^T(t) - \sigma_0 \right] \right] \qquad (3.1.1.13)$$

Considering only the real part:

$$\frac{d}{dt}\sigma^T(t) = -\sum_q J^q(\omega_q) \left[ A_k^q, \left[ A_k^{q\dagger}, \sigma^T(t) - \sigma_0 \right] \right] \qquad (3.1.1.14)$$

where $J^q(\omega_q)$ is the power spectral density function, given by:

$$J^q(\omega_q) = \text{Re}\left\{ \int_0^\infty \overline{F_k^{q\dagger}(t)F_k^q(t-\tau)} \exp(-i\omega_q\tau)d\tau \right\}$$ (3.1.1.15)

For relaxation in isotropic liquids in the high temperature limit:

$$J^q(\omega_q) = (-1)^q J^0(\omega_q) = (-1)^q J(\omega_q)$$ (3.1.1.16)

Therefore, only one spectral density function needs to be calculated. The relaxation mechanism here arises from tensor operators of rank $k = 2$. The random function $F_2^0(t)$, for a rigid spherical molecule undergoing Brownian motion, can be written as:

$$F_2^0(t) = c_0 Y_2^0[\Omega(t)]$$ (3.1.1.17)

where $c_0$ is a function of physical constants and $Y_2^0[\Omega(t)]$ is a spatial variable in the form of a second-order spherical harmonic function. Therefore,

$$J(\omega_q) = \text{Re}\left\{ c_0^2 \int_0^\infty \overline{Y_2^0[\Omega(t)]Y_2^0[\Omega(t+\tau)]}\exp(-i\omega\tau)d\tau \right\}$$ (3.1.1.18)

For isotropic rotational diffusion of a rigid rotor:

$$J(\omega_q) = c_0^2 \frac{2}{5}\frac{\tau_c}{(1+\omega_q^2\tau_c^2)} = c_0^2 j(\omega_q)$$ (3.1.1.19)

Where $j(\omega_q) = \dfrac{2}{5}\dfrac{\tau_c}{(1+\omega_q^2\tau_c^2)}$ is the orientational spectral density function.

Eq. (3.1.1.14) can be used to calculate the evolution of any physical observable $Q$ in the interaction frame:

$$\frac{d}{dt}\overline{Q} = Tr\left\{ Q\frac{d}{dt}\sigma^T(t) \right\} = -\sum_q(-1)^q J(\omega_q)Tr\left\{ Q\left[A_k^q,\left[A_k^{q\dagger},\sigma^T(t)-\sigma_0\right]\right] \right\}$$ (3.1.1.20)

$$= -\sum_q(-1)^q J(\omega_q)Tr\left\{ \left[\left[Q,A_k^q\right],A_k^{q\dagger}\right]\left(\sigma^T(t)-\sigma_0\right) \right\}$$ (3.1.1.21)

Several operators describing the spin lattice couplings can have the same time dependence in the interaction frame. Therefore a general equation can be written in this case:[35]

$$\frac{d}{dt}\overline{Q}=Tr\left\{Q\frac{d}{dt}\sigma^T(t)\right\}=-\sum_{i,j}\sum_{q}(-1)^q J(\omega_q)Tr\left\{\left[\left[Q,A_{ki}^q\right],A_{kj}^{q\dagger}\right]\left(\sigma^T(t)-\sigma_0\right)\right\}$$

(3.1.1.22)

The non zero terms where $i \neq j$ are referred to as cross-correlation between two relaxation mechanisms. In the next sections, Eqs. (3.1.1.21) and (3.1.1.22) have been used to predict the relaxation behavior of LLS under various mechanisms.

**3.2 Dipolar Relaxation**

For spin-½ nuclei, dipolar relaxation is the major relaxation mechanism. LLS have very long relaxation time constants because the intramolecular dipolar interaction is ineffective. In this section, the effect of dipolar interactions on LLS is discussed.

For a homonuclear two-spin ½ system, the dipolar Hamiltonian has the following form in the molecular frame:[35]

$$H_{DD} = b_{ij}\left\{\vec{I}\cdot\vec{S}-3I_Z S_Z\right\} \tag{3.2.1}$$

where $b_{ij} = -\left(\frac{\mu_0}{4\pi}\right)\frac{\gamma^2\hbar}{r_{ij}^3}$ is the strength of the dipolar interaction. The Z-axis can be defined to lie along the main magnetic field, i.e., in the laboratory frame of reference. After carrying out the frame transformation, one obtains:

$$H_{DD}' = \sum_{q=-2}^{2}F_2^q(\theta,\phi)A_2^q = \sum_{q=-2}^{2}c_0 Y_2^q(\theta,\phi)A_2^q \quad \text{where } c_0 = b_{ij} = -\left(\frac{\mu_0}{4\pi}\right)\frac{\gamma^2\hbar}{r_{ij}^3} \tag{3.2.2}$$

and $\theta$ and $\phi$ are the polar angles which connect the two frames discussed above. Table 3.2.1 shows the components of the tensors.

Table 3.2.1

| $q$ | $Y_2^q(\theta,\phi)$ | $A_2^q$ | $\omega_q$ |
|---|---|---|---|
| 0 | $\sqrt{\dfrac{3}{2}}\left(3\cos^2\theta-1\right)$ | $\dfrac{1}{\sqrt{6}}\left(3I_zS_z-I.S\right)$ | 0 |
| $\pm 1$ | $\pm 3\sin\theta\cos\theta\exp\left(\pm i\phi\right)$ | $\mp\dfrac{1}{2}\left(I_\pm S_z+I_z S_\pm\right)$ | $\omega$ |
| $\pm 2$ | $\dfrac{3}{2}\left(\sin^2\theta\right)\exp\left(\pm 2i\phi\right)$ | $\dfrac{1}{2}\left(I_\pm S_\pm\right)$ | $2\omega$ |

Considering isotropic rotational diffusion of a rigid rotor,

$$J^q(\omega_q)=(-1)^q c_0^{\,2}\,\frac{2}{5}\,\frac{\tau_c}{(1+\omega_q^{\,2}\tau_c^{\,2})} \tag{3.2.3}$$

The relaxation matrix can be expressed in the orthonormal basis of Liouville operators that can be chosen depending on the ranks of the spherical tensors, i.e., coherence orders. Due to the secular approximation, there are no terms which connect different orders of coherences as the relaxation matrix is block-diagonal in this particular basis. The Liouville basis described according to coherence orders can be written as shown in table 3.2.2.

Table 3.2.2

| Coherence order | Operators |
|---|---|
| 0 | $E, I_z, S_z, 2I_zS_z, \sqrt{2}ZQ_x, \sqrt{2}ZQ_y$ |
| $\pm 1$ | $\dfrac{1}{\sqrt{2}}I_+, \dfrac{1}{\sqrt{2}}I_-, \dfrac{1}{\sqrt{2}}S_+, \dfrac{1}{\sqrt{2}}S_-, \sqrt{2}I_+S_z, \sqrt{2}I_-S_z, \sqrt{2}I_zS_+, \sqrt{2}I_zS_-$ |
| $\pm 2$ | $\sqrt{2}DQ_x, \sqrt{2}DQ_y$ |

where
$$ZQ_x = \left(I_x S_x + I_y S_y\right)$$
$$ZQ_y = \left(I_y S_x - I_x S_y\right)$$
and
$$DQ_x = \left(I_x S_x - I_y S_y\right)$$
$$DQ_y = \left(I_y S_x + I_x S_y\right)$$

The relaxation matrix corresponding to the dipolar interaction in the basis defined above is:[21]



$$\Gamma_{DD} = \begin{pmatrix} \begin{array}{|c|} \hline 6\times6 \\ \Gamma_{DD}^{0} \\ \hline \end{array} & & 0 \\ & \begin{array}{|c|} \hline 8\times8 \\ \Gamma_{DD}^{\pm1} \\ \hline \end{array} & \\ 0 & & \begin{array}{|c|} \hline 2\times2 \\ \Gamma_{DD}^{\pm2} \\ \hline \end{array} \end{pmatrix}$$

where

$$\Gamma_{DD}^0 = \begin{bmatrix} 0 & 0 & 0 & 0 & 0 & 0 \\ 0 & -R_{I_z}^{auto} & R_{I_z \leftrightarrow S_z}^{cross} & 0 & 0 & 0 \\ 0 & R_{I_z \leftrightarrow S_z}^{cross} & -R_{S_z}^{auto} & 0 & 0 & 0 \\ 0 & 0 & 0 & -R_{2I_z S_z}^{auto} & R_{2I_z S_z \leftrightarrow ZQ_x}^{cross} & 0 \\ 0 & 0 & 0 & R_{2I_z S_z \leftrightarrow ZQ_x}^{cross} & -R_{ZQ_x}^{auto} & 0 \\ 0 & 0 & 0 & 0 & 0 & -R_{ZQ_y}^{auto} \end{bmatrix} \qquad (3.2.4)$$

$$\Gamma_{DD}^{\pm 1} = \begin{bmatrix} -R_{I_+}^{auto} & 0 & -R_{I_+ \leftrightarrow S_+}^{cross} & 0 & 0 & 0 & 0 & 0 \\ 0 & -R_{I_-}^{auto} & 0 & -R_{I_- \leftrightarrow S_-}^{cross} & 0 & 0 & 0 & 0 \\ -R_{I_+ \leftrightarrow S_+}^{cross} & 0 & -R_{S_+}^{auto} & 0 & 0 & 0 & 0 & 0 \\ 0 & -R_{I_- \leftrightarrow S_-}^{cross} & 0 & -R_{S_-}^{auto} & 0 & 0 & 0 & 0 \\ 0 & 0 & 0 & 0 & -R_{I_+ S_z}^{auto} & 0 & -R_{I_+ S_z \leftrightarrow I_z S_+}^{cross} & 0 \\ 0 & 0 & 0 & 0 & 0 & -R_{I_- S_z}^{auto} & 0 & -R_{I_- S_z \leftrightarrow I_z S_-}^{cross} \\ 0 & 0 & 0 & 0 & -R_{I_+ S_z \leftrightarrow I_z S_+}^{cross} & 0 & -R_{I_z S_+}^{auto} & 0 \\ 0 & 0 & 0 & 0 & 0 & -R_{I_- S_z \leftrightarrow I_z S_-}^{cross} & 0 & -R_{I_z S_-}^{auto} \end{bmatrix}$$

(3.2.5)

and

$$\Gamma_{DD}^{\pm 2} = \begin{bmatrix} -R_{DQ_x}^{auto} & 0 \\ 0 & -R_{DQ_y}^{auto} \end{bmatrix}$$

(3.2.6)

## 3.2.2 Effect of dipolar relaxation on LLS

It is necessary to define a proper orthonormal basis to describe the evolution of the singlet and triplet states under coherent and fluctuating Hamiltonians. It has been shown earlier that the relaxation matrix is block-diagonal with respect to the coherence orders, due to the secular approximation. The LLS is comprised of operators with zero coherence order. Therefore, it is sufficient to consider only the zero quantum block of the relaxation matrix to examine the relaxation properties of LLS. Here, we use the basis of Liouville operators in the zero quantum block, as in Pileio et al:[20]

$$\{ST\}_0 = \left\{ \begin{array}{l} \dfrac{1}{2}\left(|S_0\rangle\langle S_0| + |T_+\rangle\langle T_+| + |T_0\rangle\langle T_0| + |T_-\rangle\langle T_-|\right), \\[2mm] Q_{LLS}, \\[2mm] \dfrac{1}{\sqrt{2}}\left(|T_+\rangle\langle T_+| - |T_-\rangle\langle T_-|\right), \\[2mm] \dfrac{1}{\sqrt{6}}\left(-|T_+\rangle\langle T_+| + 2|T_0\rangle\langle T_0| - |T_-\rangle\langle T_-|\right), \\[2mm] L_+, \\[2mm] L_- \end{array} \right\} \qquad (3.2.2.1)$$

where 
$$\begin{array}{l} L_+ = |S_0\rangle\langle T_0| \\ L_- = |T_0\rangle\langle S_0| \end{array} \quad \text{and}$$

$$Q_{LLS} = N_{LLS}\left[|S_0\rangle\langle S_0| - \frac{1}{3}\left(|T_0\rangle\langle T_0| + |T_+\rangle\langle T_+| + |T_-\rangle\langle T_-|\right)\right] \qquad (3.2.2.2)$$

It is now possible to calculate the elements of the relaxation matrix in the basis defined in Eq. (3.2.2.1). The matrix representation of the relaxation superoperator assuming extreme narrowing limit (i.e., $J\left(\omega_q\right) = J\left(0\right)$):

$$\Gamma_{DD}^{ST} = \begin{pmatrix} 0 & 0 & 0 & 0 & 0 & 0 \\ 0 & 0 & 0 & 0 & 0 & 0 \\ 0 & 0 & \dfrac{-3b_{ij}^2\tau_c}{2} & 0 & 0 & 0 \\ 0 & 0 & 0 & \dfrac{-9b_{ij}^2\tau_c}{10} & 0 & 0 \\ 0 & 0 & 0 & 0 & \dfrac{-b_{ij}^2\tau_c}{2} & 0 \\ 0 & 0 & 0 & 0 & 0 & \dfrac{-b_{ij}^2\tau_c}{2} \end{pmatrix} \qquad (3.2.2.3)$$

It can be seen that $Q_{LLS}$, the population difference between the singlet and the mean of the three triplet states, is immune to the dipolar interaction, thus has a long lifetime. Therefore, it is necessary to point out how one can see these long lifetimes by experiments, or in other words, when the similarity transformation becomes relevant to describe a physical phenomenon. In fact, in the experiments described in this thesis, the basis transformation

becomes relevant when the system evolves under RF irradiation. In low field experiments,[14] this occurs when the sample is taken out of the magnetic field. In both cases, the eigenoperators of the spin system become the eigensystem of the isotropic scalar coupling Hamiltonian (which has been described in Section 2.1). In high field experiments, coherent processes can induce a leakage from the LLS to other fast-relaxing states as has been described in details elsewhere.[19-20] In the following section, relaxation caused by other mechanisms, such as the Chemical Shift Anisotropy (CSA), is discussed.

## 3.3 Relaxation of LLS caused by CSA

The chemical shift (CS) Hamiltonian of a nuclear spin, in the principal axes of the CS tensor, is given by:

$$H_{CS}^I = \gamma_I \vec{I} \cdot \vec{\sigma} \cdot \vec{B} \tag{3.3.1}$$

Where $\vec{\sigma}$ is chemical shielding tensor and $\vec{B}$ is the magnetic field.

In the frame of the principal axes of CS tensor, the Hamiltonian is given by:[35]

$$H_{CS}^I = \gamma_I \sum_{a=x,y,z} I_a \sigma_{aa} B_{0a} \tag{3.3.2}$$

It is possible to split Eq. (3.3.2) into an isotropic term, which is invariant under rotation, and an anisotropic term which causes relaxation. The anisotropic part has the following form:

$$H_{CSA}^I = \gamma_I \frac{\sigma_{\parallel} - \sigma_{\perp}}{3} \left( \vec{B}_0 \cdot \vec{I} - 3B_Z I_Z \right) \tag{3.3.3}$$

Here the CS tensor has been assumed to have a cylindrical symmetry with $\sigma_{\parallel} = \sigma_{xx}$, $\sigma_{\perp} = \sigma_{yy} = \sigma_{zz}$.

For convenience, the same frame transformation for obtaining Eq. (3.2.2) from Eq. (3.2.1) can be carried out for Eq. (3.3.3) to obtain:

$$H_{CSA}^I = \sum_{q=-2}^{2} F_2^q (\theta, \phi) A_2^q \qquad (3.3.4)$$

The main component of the magnetic field is along the z-direction. All other components of $B_0$ vanish. We shall address the effects of CSA interactions on the relaxation of an LLS in a system with only two spins $I$ and $S$. The principal axes and orientations of the CSA tensors characteristic for a planar molecule are defined in Fig. 3.3.1.
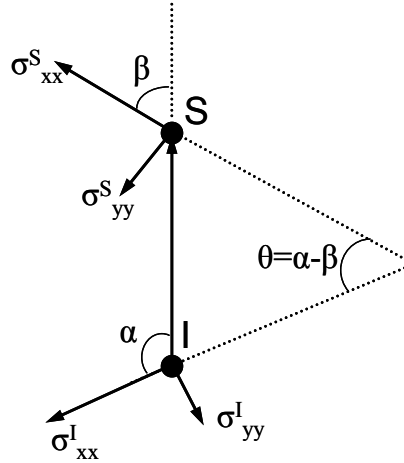


Figure 3.3.1. Principal values and relative orientations of CSA tensors in a system of two spins $I$ and $S$ such as two aromatic protons. The zz components (not shown) of the two CSA tensors are assumed to be both perpendicular to the plane of the paper and hence to the internuclear vector $r_{IS}$. The $\sigma_{xx}^I$ and $\sigma_{xx}^S$ components subtend an angle $\theta$.

The tensor operators for the CSA interactions of spins $I$ and $S$, along with the relevant frequencies, are given in Table 3.3.1.

| q | $F_2^q$ | $A_2^q$ |
|---|---------|---------|
| 0 | $4a \dfrac{\Delta\sigma_{jj}^K \omega_0}{3} \sqrt{\dfrac{3}{2}} \left(3\cos^2\theta - 1\right)$ | $K_z$ |
| ±1 | $b \dfrac{\Delta\sigma_{jj}^K \omega_0}{3} \mp 3\sin\theta\cos\theta \exp(\pm i\phi)$ | $\mp K^{\pm}$ |
| ±2 | - | - |

Table 3.3.1. Tensor operators with $a = \dfrac{1}{2}$, $b = \sqrt{\dfrac{3}{2}}$. The other symbols have their usual meaning. The tensor operators $A_2^q$ for the CSA interaction of spins $I$ or $S$ are defined using $\Delta\sigma_{jj} = \sigma_{jj} - \sigma_{zz}$, $j = x, y$.

It is now possible to use the master equation (Eq. (3.1.1.21)) to evaluate the rates of various observables under CSA relaxation. As the procedure is the same as described for the dipolar interaction, we shall focus on the relaxation behavior of LLS under CSA.

The LLS eigenoperator $Q_{LLS}$, which decays with a relaxation rate $R_{LLS}$, corresponds to the difference between the population of the singlet state and the mean of the populations of the three triplet states as defined in Eq. (3.2.2.2). Since $Q_{LLS}$ commutes with all tensor operators that represent the $I$-$S$ dipole-dipole (DD) interaction, it is not affected by dipolar relaxation between the two active spins, i.e., $\Gamma_{Q_{LLS}}^{DD} = 0$ if there are no further spins. On the other hand, the contribution of the CSA interactions of spins $I$ and $S$ to the relaxation of $Q_{LLS}$ is:[18]

$$R_{LLS}^{CSA} = \Gamma_{Q_{LLS}}^{CSA} = -\sum_{q} \sum_{L,M=I,S} \sum_{i,j=x,y} J^q\left(\omega_q\right) Tr\left\{\left[\left[Q, A_k^{(L_i)q}\right], A_k^{(M_j)q\dagger}\right]\left(\sigma^T\left(t\right)-\sigma_{eq}\right)\right\} \cdot P_2(\cos\phi(\sigma_{ii}^I,\sigma_{jj}^S))$$

(3.3.5)

where $P_2$ is the Legendre polynomial and $\phi(\sigma_{ii}^I,\sigma_{jj}^S)$ is the angle between the principal axes $\sigma_{ii}^I$ and $\sigma_{ii}^S$ of the CSA tensors of the two spins. The tensor operators with A = $I$ or $S$ are given in Table 3.3.1. If both CSA tensors have cylindrical symmetry (e.g., if $\sigma_{xx}^I \neq \sigma_{yy}^I = \sigma_{zz}^I$, $\sigma_{xx}^S \neq \sigma_{yy}^S = \sigma_{zz}^S$), using the notations $\Delta\sigma^{I,S} = \Delta\sigma_{xx}^{I,S}$, the CSA contributions to the auto-relaxation rate of an LLS involving the spins $I$ and $S$ are given by:[18]

$$R_{LLS}^{CSA} = \frac{2}{3}\left[\left(\frac{\Delta\sigma^I\omega_0}{3}\right)^2 + \left(\frac{\Delta\sigma^S\omega_0}{3}\right)^2\right]\left[2J\left(0\right)+3J\left(\omega_0\right)\right]$$
$$-\frac{4}{3}\left(\frac{\Delta\sigma^I\omega_0}{3}\right)\left(\frac{\Delta\sigma^S\omega_0}{3}\right)\left[2J\left(0\right)+3J\left(\omega_0\right)\right]\cdot\frac{3\cos^2\theta-1}{2}$$

(3.3.6)

where $\theta = (\sigma_{xx}^I,\sigma_{xx}^S)$ is the angle between the principal axes $\sigma_{xx}^I$ and $\sigma_{xx}^S$.

*3.3.1 Similar CSA tensors with non-parallel principal axes*

In some cases, it can be inferred from molecular symmetry that the principal values of the CSA

tensors of spins *I* and *S* must be similar. In this case, it may be possible to determine the

relative orientations of the two tensors from the relaxation rates of LLS. If the two CSA tensors

are similar and axially symmetric, we can further simplify the notation by using

$\Delta\sigma = \Delta\sigma^I = \Delta\sigma^S$, and Eq. (3.3.6) becomes:

$$R_{LLS}^{CSA} = 2\left(\frac{\Delta\sigma\omega_0}{3}\right)^2 \left(1-\cos^2\theta\right)\cdot\left[2J\left(0\right)+3J\left(\omega_0\right)\right] \tag{3.3.1.1}$$

where $\theta = (\sigma^I, \sigma^S)$ is again the angle between the principal axes of the tensors $\sigma^I$ and $\sigma^S$. The

auto-relaxation rate of Eq. (3.3.1.1) depends only on the chemical shift anisotropy $\Delta\sigma$ and on

the relative orientation $\theta$ of the two tensors (Fig. 3.3.1.1(A)).
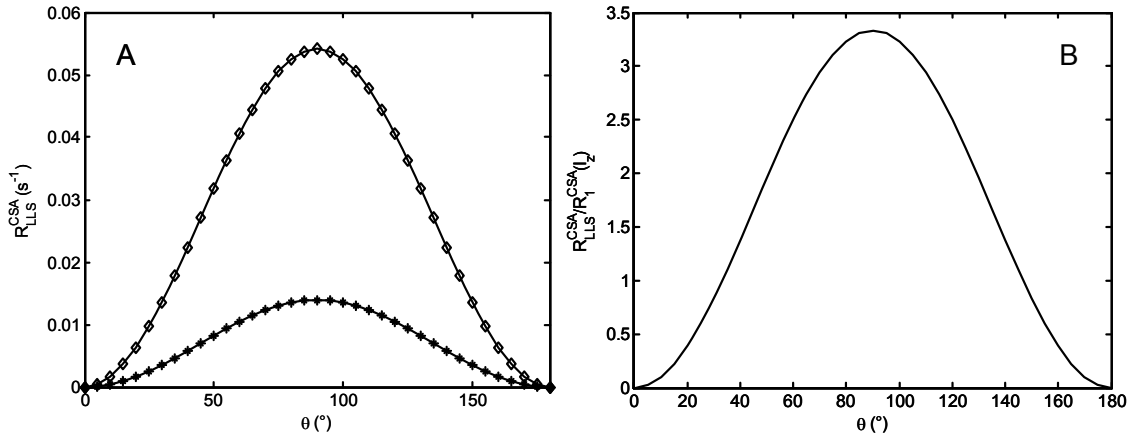


Figure 3.3.1.1. (A) Theoretical CSA contributions $R_{LLS}^{CSA}$ to the relaxation rates of LLS in the system of Fig. 3.3.1 at 400 MHz (stars) and 800 MHz (diamonds), considering two CSA tensors with cylindrical symmetry ($\sigma_{xx} \neq \sigma_{yy} = \sigma_{zz}$) and with the same anisotropy ($\sigma_{xx} - \sigma_{zz}$) = 10 ppm for both spins *I* and *S*, as a function of the angle θ = α − β between the orientations of the $\sigma_{xx}^I$ and $\sigma_{xx}^S$ components. The rates were calculated for a correlation time $\tau_c$ = 0.05 ns. (B) Theoretical ratio of $R_{LLS}^{CSA}$ to the CSA contribution to the longitudinal relaxation rates $R_1^{CSA}$ ($I_z$) = $R_1^{CSA}$ ($S_z$) of the individual spins as a function of the angle $\theta$. This ratio does not depend on the static field $B_0$.

In the extreme narrowing limit we have:

$$R_{LLS}^{CSA} = 10\left(\frac{\Delta\sigma\omega_0}{3}\right)^2 J(0)(1-\cos^2\theta) \tag{3.3.1.2}$$

This rate can be compared with the CSA contributions to the longitudinal relaxation rates $R_1 = 1/T_1$ of the individual spins:

$$R_1^{CSA}(I_z) = \Gamma_{I_z,I_z}^{CSA} = R_1^{CSA}(S_z) = \Gamma_{S_z,S_z}^{CSA} = 3\left(\frac{\Delta\sigma\omega_0}{3}\right)^2 J(0) \tag{3.3.1.3}$$

Therefore, the ratio between the CSA contributions $R_{CSA}^{LLS}$ to the auto-relaxation rate of an LLS and the CSA contributions $R_1^{CSA}$ to the longitudinal relaxation rates of the individual spins yields:

$$R_{LLS}^{CSA} / R_1^{CSA} = 10(1-\cos^2\theta)/3 \tag{3.3.1.4}$$

thus providing direct information about the relative orientation of the two CSA tensors, i.e., about the angle subtended between their principal axes (Fig. 3.3.1.1(B)). Note that one must exclude the dipolar contributions $R_{LLS}^{DD}$, $R_1^{DD}(I_z)$ and $R_1^{DD}(S_z)$, which are field-independent in the extreme narrowing limit, to the relaxation rates.

### 3.3.2 Different CSA tensors with parallel principal components

If the principal components of the CSA tensors are parallel ($\theta = 0$) and the CSA tensors have cylindrical symmetry (e.g., if $\sigma_{xx}^I \neq \sigma_{yy}^I = \sigma_{zz}^I$, $\sigma_{xx}^S \neq \sigma_{yy}^S = \sigma_{zz}^S$), the rate only depends on the difference $\Delta\sigma^I - \Delta\sigma^S = \left[\left(\sigma_{xx}^I - \sigma_{zz}^I\right) - \left(\sigma_{xx}^S - \sigma_{zz}^S\right)\right]$

$$R_{LLS}^{CSA} = \frac{2}{3}\left(\frac{\Delta\sigma^I\omega_0}{3} - \frac{\Delta\sigma^S\omega_0}{3}\right)^2 \left[2J(0) + 3J(\omega_0)\right] \tag{3.3.2.1}$$

Thus, for two protons with $\Delta\sigma^I - \Delta\sigma^S = 5$ ppm in the extreme narrowing limit ($\tau_c = 0.05$ ns), the relaxation rates calculated are $R_{LLS}^{CSA} = 0.0012$ s$^{-1}$ at 400 MHz and 0.0045 s$^{-1}$ at 800 MHz.

These rates increase to $R_{LLS}^{CSA}$ = 0.0472 and 0.1876 s$^{-1}$ for $\tau_c$ = 5 ns. These rates vanish regardless of the static field if the two CSA tensors are parallel in orientation and equal in magnitudes. These calculations, done using Eq. (3.3.2.1), were confirmed numerically by using the GAMMA program[36], as described in the Simulations section.

In a two-spin system where the CSA tensors are known to have cylindrical symmetry ($\sigma_{xx} \neq \sigma_{yy} = \sigma_{zz}$) and have a known relative orientation $\theta$, the variation of the relaxation rate $R_{LLS}^{CSA}$ of LLS as a function of the B$_0$ field can provide a measure of the difference between the anisotropies of the two spins, $\Delta\sigma^I - \Delta\sigma^S$ (Fig. 3.3.2.1). The profiles of $R_{LLS}^{CSA}$ in the slow motion limit are very similar to those for extreme narrowing in Fig. 3.3.2.1, since J($\omega_0$) << J(0).
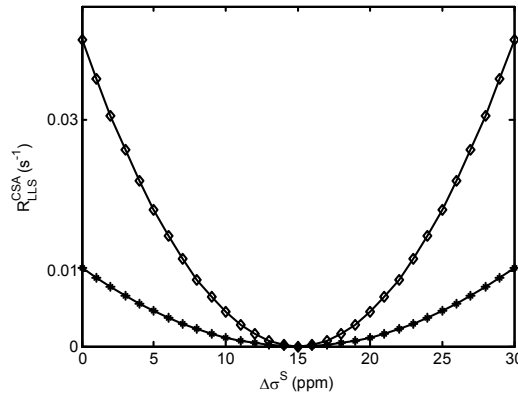


Figure 3.3.2.1. Theoretical CSA contributions $R_{LLS}^{CSA}$ to the relaxation rates of LLS in the spin system of Fig. 3.3.1 at 400 MHz (stars) and 800 MHz (diamonds), considering two CSA tensors with cylindrical symmetry ($\sigma_{xx} \neq \sigma_{yy} = \sigma_{zz}$) with parallel principal components ($\theta = 0$) as a function of the anisotropy ($\sigma_{xx}^S - \sigma_{zz}^S$) that is varied in the range $0 < (\sigma_{xx}^S - \sigma_{zz}^S) < 2(\sigma_{xx}^I - \sigma_{zz}^I)$ with ($\sigma_{xx}^I - \sigma_{zz}^I$) = 15 ppm. The rates were calculated for a correlation time $\tau_c$ of 0.05 ns.

## 3.4 Experimental evidence

In order to obtain information about molecular symmetry and structure using Eqs. (3.3.1.2) and (3.3.1.3), the CSA contributions $R_1^{CSA}(I_z)$ and $R_1^{CSA}(S_z)$ to the longitudinal relaxation rates of the two active spins need to be known. In practice, this may be difficult for protons, since dipolar interactions tend to mask CSA effects, often by more than an order of magnitude, even in high magnetic fields. In order to obtain the desired information, the longitudinal relaxation rates $R_1^{CSA}(I_z)$ and $R_1^{CSA}(S_z)$ need to be measured in a similar molecule where the spin under investigation (say, spin $I$) has a similar environment, while the dipolar interaction with the other spin ($S$) is removed by substitution, for instance by a chlorine atom.

The longitudinal and LLS relaxation rates have been measured in two related molecules (Fig. 3.4.1): pentachlorobenzene (which contains an isolated $I = ½$ proton that is predominantly relaxed through CSA) and trichlorophenol (with two coupled protons that experience both dipolar and CSA interactions). We shall assume for simplicity that the CSA tensors of the protons are the same in the two molecules. The measurements were carried out at static fields of 9.4 T and 14 T (400 and 600 MHz for protons). In order to eliminate possible contributions from interactions other than the CSA's, we considered ratios of differences between rates measured at different fields, rather than the ratios between the rates directly:

$$F = \frac{R_{LLS}^{CSA}(600MHz) - R_{LLS}^{CSA}(400MHz)}{R_1^{CSA}(I_z)(600MHz) - R_1^{CSA}(I_z)(400MHz)} \qquad (3.4.1)$$



pentachlorobenzene          trichlorophenol
(OH →OD)

A                  B
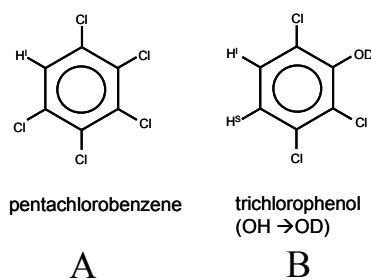
Figure 3.4.1.  (A) Pentachlorobenzene, containing an isolated proton I predominantly relaxed by chemical shift anisotropy, with a CSA tensor assumed to be axially symmetric. (B) Trichlorophenol with a deuterated hydroxyl group, containing two protons I and S with CSA tensors that have similar anisotropies $(\sigma_{xx}^S - \sigma_{zz}^S) \approx (\sigma_{xx}^I - \sigma_{zz}^I)$.

The experimental ratio was found to be F > 2.6. With reference to Fig. 3.3.1.1(B), this ratio implies that the relative orientation θ of the most shielded components of the two CSA tensors $\sigma^I$ and $\sigma^S$ must fulfill the inequality θ > 60°. The errors of 30 % in the calculated ratio F, and therefore in θ, are relatively large.

In short, LLS have special relaxation properties for isolated spin pairs because the dipolar relaxation mechanism is inoperative. In the next chapter, the analysis of LLS for larger spin systems is described.

## 3.5 Simulations

To calculate contributions of various relaxation mechanisms to the Liouvillian, we considered two protons separated by a distance $|\vec{r}_{IS}| = 2\,\text{Å}$ with two axially symmetric CSA tensors $(\sigma^I_{xx} \neq \sigma^I_{yy} = \sigma^I_{zz}$ and $\sigma^S_{xx} \neq \sigma^S_{yy} = \sigma^S_{zz})$ with different anisotropies $\sigma^I_{xx} - \sigma^I_{zz} = 15$ ppm and $\sigma^S_{xx} - \sigma^S_{zz} = 10$ ppm, and with correlation times $\tau_c = 0.05$ or 5 ns. The theoretical relaxation rates were compared with GAMMA simulations[36] incorporating coherent evolution under the full spin Hamiltonian (expressed in units of ħ as usual), in addition to dipolar and CSA relaxation mechanisms:

$$H = \omega_I I_z + \omega_S S_z + 2\pi J_{IS} I \cdot S + \omega_1 (I_x + S_x)$$   (3.5.1)

The simulations were performed considering a difference between the chemical shifts $(\omega_I - \omega_S)/(2\pi) = 74$ Hz, a scalar coupling $J_{IS} = -12$ Hz, and a radio-frequency amplitude $\omega_1/(2\pi) = 500$ kHz. The decay of the populations of LLS was monitored for 1000 different relaxation intervals. The decays were then fitted to exponential functions using three fitting parameters.

# Chapter - 4

# Long-lived states in multiple-spin systems

 The coherent and relaxation properties of long-lived states (LLS) in systems containing a pair of coupled protons (or other homonuclear spins) have been described in the previous chapters. However, it is not usual to find isolated spin pairs, and therefore the applications of LLS to the study of slow dynamic phenomena are rather limited. The applications of LLS should become increasingly widespread provided they can be excited in systems with more than two coupled spins.

There has been significant progress towards extending the applications of LLS to systems featuring diverse spin patterns. For instance, spin states with long lifetimes can be excited in symmetric molecules like 4-hydroxybenzoic acid, citric acid, etc. (AA´XX´-type systems) with lifetimes $T_{LLS}$ up to $8T_1$.[37] E. Vinogradov and A. Grant[38-39] have given a theoretical analysis of the molecular geometries of systems that can sustain LLS. The magnetization transferred from *para*-hydrogen can also be used to enhance LLS.[40-41]

For an *n*-spin system where $n > 2$, relaxation-favored spin permutation properties for eigenstates of the *J*-coupling Hamiltonian are harder to find, which makes the existence of LLS less obvious in multiple-spin systems. G. Pileio and M. Levitt have shown by theoretical analysis of LLS in the AMX type of systems that an effective way of identifying LLS in arbitrary spin systems is the diagonalization of their Liouvillians,[42] which was also proposed by K. *Gopalakrishnan* and G. Bodenhausen.[19]

Here, LLS are analyzed in some common amino-acids such as serine, aspartic acid etc., where the aliphatic protons form a coupled three-spin system.[43] LLS, once identified in these molecules, can be excited and sustained by designing a suitable pulse sequence. We also

demonstrated that LLS can be found in systems with larger number of spins, such as taurine and glycerol.

**4.1 Theory**

The equation of motion of the density operator, in the presence of coherent and stochastic interactions, is given by:

$$\frac{d}{dt}\sigma(t) = \hat{L}\sigma(t)$$ (4.1.1)

Where the Liouvillian superoperator $\hat{L}$ can be expressed as:

$$\hat{L} = -i\hat{H} + \hat{T}$$ (4.1.2)

Here, $\hat{H}$ is the coherent evolution superoperator, associated with the Hamiltonian, $H$, of the system and $\Omega_{rs}$ is the characteristic frequency of the associated basis operator:

$$\Omega_{rs} = <B_r|[H, B_s]>$$ (4.1.3)

while $\hat{T}$ is the relaxation superoperator, generated by fluctuations of random fields:

$$\hat{T} = -\sum_q J^q(\omega_q)\left\langle B_r\left|\left[A_k^q,\left[A_k^{q\dagger}, B_s\right]\right]\right]\right\rangle$$ (4.1.4)

The Liouvillian superoperator $\hat{L}$ can be expressed as an $N^2 \times N^2$ matrix in Liouville space, where $N$ is the number of spin states, given by $2^n$ for the case of $n$ coupled spins - ½. The superoperator $\hat{L}$ can be diagonalized to obtain $N^2$ eigenvalue-eigenoperator pairs:

$$\hat{L}B_q = b_q B_q$$ (4.1.5)

where $q \in (1,2,3\dots,N^2)$.

The eigenvalues $b_q$ are complex with negative real parts, and can be expressed as:

$$b_q = -\lambda_q + i\omega_q$$ (4.1.6)

where $\lambda_q$ and $\omega_q$ are real.

The eigenoperators with real eigenvalues correspond to spin-state populations and remain conserved under coherent evolution, but decay with their respective relaxation rates $\lambda_q$. Sorting the values $\lambda_q$ in ascending order yields the slowest-relaxing states $B_1, B_2, B_3, \ldots B_N{}^2$, where $B_1$ measures the sum of all populations and has the eigenvalue zero. In this way, Liouvillian diagonalization can provide the Liouville state (operator) with the slowest decay rate, i.e., the LLS.[42] As the Liouvillian consists of both coherent and relaxation terms, the structure of the LLS depends on the chemical shifts and $J$-couplings, as well as on molecular properties like internuclear distances and CSA tensors.[18,44]

## 4.2 Simulations

The Liouvillian for a three spin-½ scalar coupled system was constructed and diagonalized using GAMMA libraries.[36] The Liouvillian diagonalization yields 64 eigenstates for a three-spin system. For instance, acrylic acid is a suitable system and has been shown to possess long lifetimes if its magnetization is enhanced by chemical reduction of its precursor propiolic acid (CH≡C-COOH) with *para*-hydrogen.[40] The structure of acrylic acid, along with its 1D proton spectrum is shown in Fig. 4.2.1.
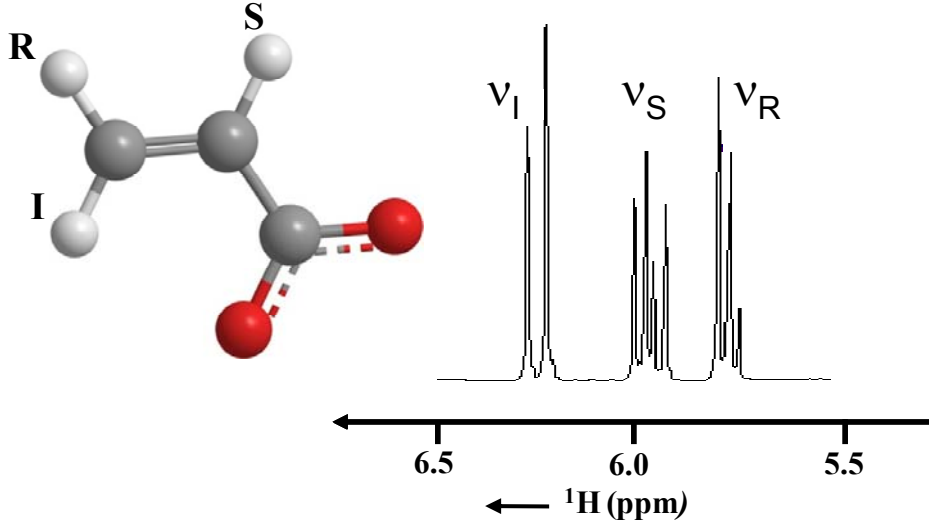
Figure 4.2.1. The molecular structure of acrylic acid and its 1D proton NMR spectrum at 500 MHz ($B_0 = 11.75$ T) and 298 K. The three protons *I*, *S*, and *R* are coupled by $J_{IS} = 17.3$ Hz, $J_{IR} = 1.4$ Hz, and $J_{SR} = 10.4$ Hz.

One type of states with small real eigenvalues, and therefore long lifetimes, can be expressed as follows:

$$Q^{ISR} = \frac{1}{\sqrt{3}} \left( \lambda_{IS}\vec{I}\cdot\vec{S} + \lambda_{IR}\vec{I}\cdot\vec{R} + \lambda_{SR}\vec{S}\cdot\vec{R} \right)$$

$$(4.2.1)$$

We call them *quadratic states* because they can be expressed as combinations of bilinear or quadratic operators.

Another type of LLS, which we call *cubic states*, contain trilinear products of operators:

$$C^{ISR} = \mu_x T_x + \frac{\mu_{IS}}{\sqrt{3}}\left[\left(\vec{I}\cdot\vec{S} - E/4\right)R_x - T_x\right] + \frac{\mu_{IR}}{\sqrt{3}}\left[\left(\vec{I}\cdot\vec{R} - E/4\right)S_x - T_x\right] + \frac{\mu_{SR}}{\sqrt{3}}\left[\left(\vec{S}\cdot\vec{R} - E/4\right)I_x - T_x\right]$$

$$(4.2.2)$$

where $E$ is the identity operator, and $T_x = I_x S_x R_x$ is the cubic (trilinear) product of Cartesian spin operators.

The coefficients $\lambda$ and $\mu$ reflect the coherent part of Hamiltonian, as well as the geometry of the system which determines the randomly fluctuating dipole-dipole interactions of the Liouvillian that leads to relaxation.[44]

For the simulations, the rotational correlation times for various molecules were obtained from the initial spin-lattice recovery time constants of protons $I$, $R$ and $S$ (Fig. 4.2.1) and the atomic coordinates were obtained from the crystal structures. A continuous-wave RF field with an amplitude $\gamma B_{1x}/(2\pi) = 5$ kHz, with the carrier set at the mean frequency of spins $I$ and $R$, $\nu_0 = (\nu_I + \nu_R)/2$, was used to suppress the chemical shifts.

In the case of acrylic acid, the coefficients obtained from the molecular geometry were:

for state $Q^{ISR}$ of Eq. (4.2.1): $\lambda_{IS} = -0.23$, $\lambda_{IR} = 0.93$, and $\lambda_{SR} = 0.28$, and

for state $C^{ISR}$ of Eq. (4.2.2): $\mu_x = 0.51$, $\mu_{IS} = -0.19$, $\mu_{IR} = 0.80$, and $\mu_{SR} = 0.24$.

The squares of these coefficients sum up to 1, since the states are normalized. Considering only the dipolar relaxation mechanism, the relaxation time constants for the *quadratic* and *cubic* states are predicted to be $T_{LLS}(Q^{ISR}) = 37$ s and $T_{LLS}(C^{ISR}) = 50$ s for a rotational correlation time $\tau_c = 22$ ps. When one takes into consideration the contributions to relaxation stemming from anisotropies of the chemical shift tensors, the lifetime of $C^{ISR}$ is shorter than that of $Q^{ISR}$, so the latter is likely to be the longest-lived state under realistic conditions.

Some amino acids such as aspartic acid, serine, asparagine, cysteine and histidine feature coupled three-spin systems ( -CH$^\alpha$-CH$_2{}^\beta$-) and can be even more interesting to analyze because of their biological importance. Fig. 4.2.2 shows an assigned 1D spectrum of aspartic acid. For aspartic acid, the coefficients of the *quadratic state* are as follows:

$\lambda_{IS} = 0.11$, $\lambda_{SR} = -0.07$, and $\lambda_{IR} = -0.97$.
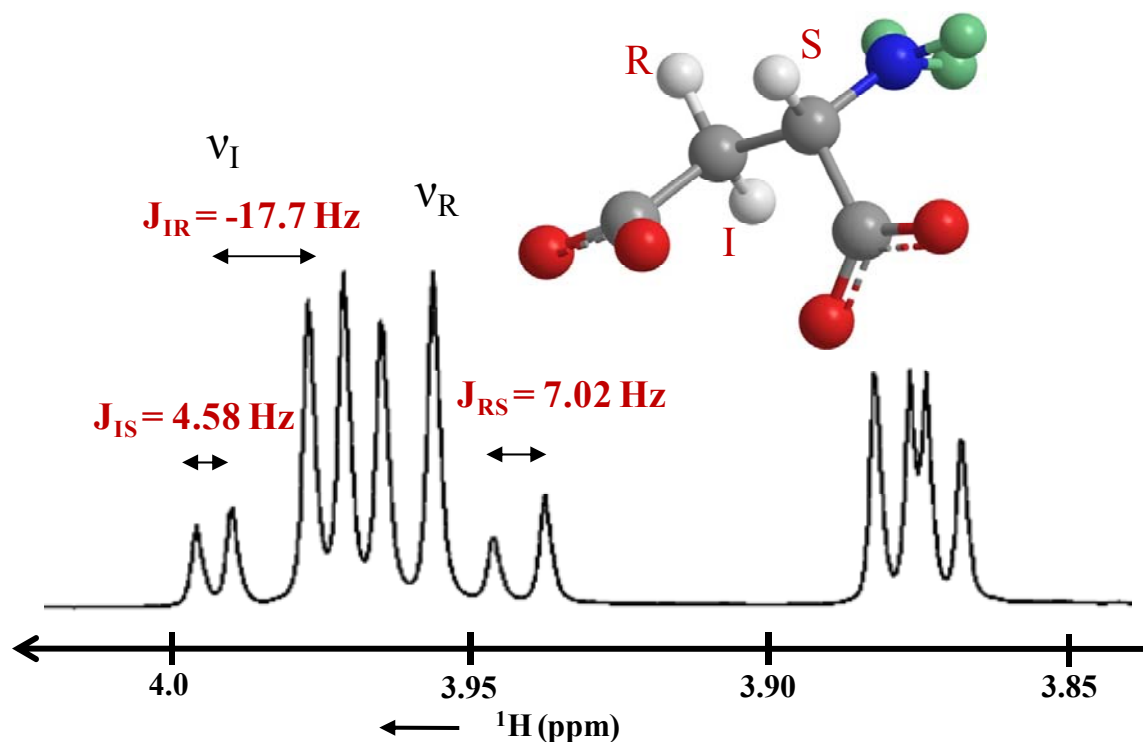
Figure 4.2.2. The molecular structure of aspartic acid and its 1D proton NMR spectrum at 500 MHz ($B_0$ = 11.75 T) and 298 K, in a $D_2O$ solution without buffer. The three protons $I$, $S$, and $R$ are coupled by $J_{IS}$ = 4.58 Hz, $J_{IR}$ = -17.7 Hz, and $J_{SR}$ = 7.02 Hz.

After identifying the LLS, a pulse sequence was optimized *in silico* in order to populate this state. Since the state $Q^{ISR}$ is a linear combinations of states $Q^{JK}$ (where $J,K \in \{I,S,R\}$) involving pairs of spins, the starting point is a sequence designed to excite LLS of the former type (Pulse sequence I of section 2.2). The delays in the pulse sequence shown in Fig. 4.2.3 were optimized to excite $Q^{ISR}$ operators for various molecules in table 4.3.1, sustain these states by continuous-wave irradiation and re-convert them to detectable coherences.

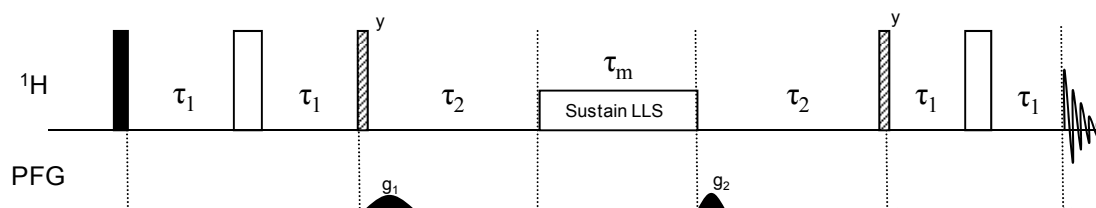Figure 4.2.3. A pulse sequence designed to populate LLS where the delays were optimized to excite $Q^{ISR}$. The pulses with $\pi$, $\pi/2$ and $\pi/4$ are indicated by open, filled and hatched rectangles, respectively. The phases of the pulses are along the x axis unless otherwise specified.

For instance, in the case of aspartic acid, the delays $\tau_1$ and $\tau_2$, optimized by simulations to obtain a maximum coefficient of the state $Q^{ISR}$, were found to be $\tau_1 = 14$ ms and $\tau_2 = 15.5$ ms. Using these values, the yield of the desired state at the beginning of the sustaining period $\tau_m$ was 0.9. Unwanted coherences were destroyed by gradients.

## 4.3 Experimental results and discussion

Table 4.3.1 shows the experimentally-measured relaxation time constants for various molecules.[43] For systems featuring two close spins $I$ and $R$, such as the $H^\beta$ protons in the amino acids mentioned above, and a spin $S$ further away from the first two, e.g., the $H^\alpha$ proton in these amino acids, the spin-lattice relaxation of spin $S$ has a time constant that is larger than those of spins $I$ and $R$ (i.e., $(T_1^S = T_1^{max})$) while spins $I$ and $R$ have similar $T_1$ $(T_1^I \approx T_1^R)$. In table 4.3.1, the spin-lattice relaxation time constants $(T_1)$, fitted from initial recovery for the spins $I$, $R$ and $S$ of different molecules, are compared to the $T_{LLS}$ achieved. The gain in lifetimes afforded by the use of LLS, as quantified by the $T_{LLS}/T_1^{I,R}$ ratio, is approximately a factor between five to nine while the ratio $T_{LLS}/T_1^{max}$ is approximately two for all systems except for histidine, where dipolar interactions with nearby aromatic protons significantly reduce $T_{LLS}$.

| Molecule | $T_1^{I,R}$ (s) | $T_1^S$ (s) | $T_{LLS}$ ($Q^{ISR}$) (s) | $T_{LLS}/T_1^{I,R}$ | $T_{LLS}/T_1^S$ |
|---|---|---|---|---|---|
| Acrylic Acid | $5.7 \pm 0.3$ | $22 \pm 1$ | $53 \pm 3$ | 9.2 | 2.3 |
| Aspartic Acid | $1.22 \pm 0.05$ | $5.8 \pm 0.3$ | $10.9 \pm 0.5$ | 9.1 | 1.9 |
| Asparagine | $1.20 \pm 0.05$ | $5.4 \pm 0.3$ | $11.2 \pm 0.6$ | 9.3 | 2.1 |
| Serine | $1.7 \pm 0.1$ | $7.6 \pm 0.4$ | $13.6 \pm 0.7$ | 7.9 | 1.8 |
| Cysteine | $1.7 \pm 0.1$ | $7.7 \pm 0.4$ | $12.4 \pm 0.6$ | 7.3 | 1.6 |
| Histidine | $1.0 \pm 0.05$ | $4.9 \pm 0.3$ | $5.3 \pm 0.3$ | 5.1 | 1.1 |

Table 4.3.1. Experimental time constants $T_1$ and $T_{LLS}(Q^{ISR})$ of protons in various molecules dissolved in $D_2O$ at 500 MHz ($B_0$ = 11.75 T) and 298 K. The paramagnetic oxygen content in the sample was reduced by bubbling gaseous nitrogen.

The slow decay of the LLS in aspartic acid is compared in Fig. 4.3.1 with the decay of the deviation from equilibrium of the longitudinal magnetization of spin $H^S$.
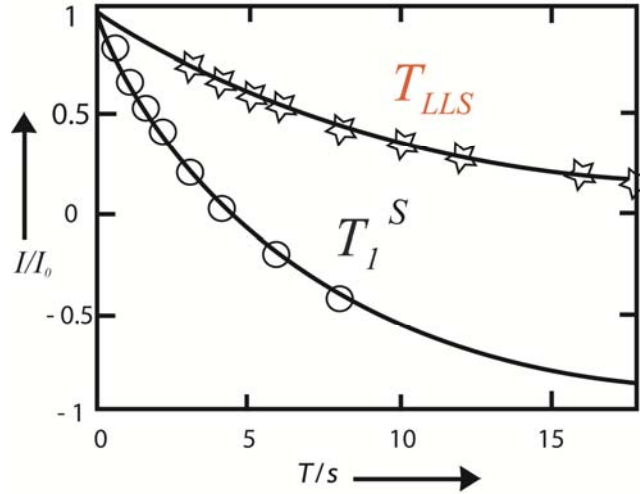


Figure 4.3.1. Exponential decay of the longest-lived Zeeman magnetization in aspartic acid (insert), with $T_1(H^\alpha) = T_1^{max} = 5.8 \pm 0.3$ s, compared with the decay of the long-lived state $Q^{ISR}$, with $T_{LLS} = 10.9 \pm 0.5$ s.

We have explored the existence of LLS in molecules containing a larger number of spins, namely taurine and glycerol dissolved in $D_2O$. In taurine (Fig. 4.3.2), the four methylene protons constitute an $A_2X_2$ system. Long-lived states of the type $Q^{IS}$, with $I$ = A and $S$ = X,

have been found to have lifetimes longer than the $T_1^{max}$ in this system, with $T_{LLS} = 2.7 \pm 0.1$ s, while $T_1^{max} = 1.02 \pm 0.03$ s at 800 MHz and 298 K. In glycerol, the five protons constitute an AA′BB′X system featuring long-lived states of the type $Q^{ISR}$, with $I = A$, $S = B$, and $R = X$. Nearly exponential decays with $T_{LLS} = 7.34 \pm 0.3$ s were obtained, while the maximum spin-lattice relaxation time constant was $T_1^{max} = 3.6 \pm 0.2$ s at 500 MHz and 298 K.
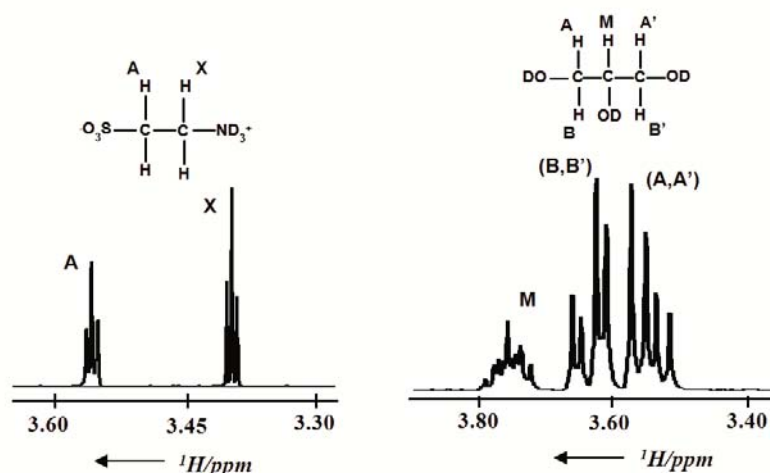


Figure 4.3.2 Molecular formulae and 1D spectra measured at 400 MHz and 298 K for taurine (left) and glycerol (right) dissolved in $D_2O$.

In brief, the applications of LLS can be extended to larger spin systems, including some common amino acids such as aspartic acid, serine, etc., as well as to taurine and glycerol. In the next chapter, the applications of LLS to small peptides and proteins are demonstrated.

## 4.4 Experimental details

The experiments were carried out at 500 MHz ($B_0 = 11.75$ T) and 298 K using ~ 20 mM solutions in deuterated water. Gaseous nitrogen was bubbled through the samples for five minutes prior to the experiments in order to decrease dissolved oxygen. Eight transients were acquired for each LLS experiment using a relaxation delay of 30 s. Experimental relaxation time constants $T_1$ and $T_{LLS}$ were obtained by fitting normalized spectral intensities to mono-

exponentially decaying functions. Continuous-wave irradiation with an amplitude $\nu_1 = 2.5$ kHz was used to sustain the LLS.

Chapter - 5

# Applications of long-lived states: from peptides to proteins

The lifetimes of long-lived states (LLS), $T_{LLS}$ are immune to dipolar interactions between the spins involved, but are attenuated by external spins and paramagnetic species. There have been discussions about how the lifetimes of LLS are affected by the presence of other spins, connected by either scalar or dipolar couplings.[39,42] For example, in the case of a partially deuterated saccharide, where a scalar coupled two-spin system is well isolated, $T_{LLS} = 26 \pm 3$ s has been observed while in the presence of external protons, i.e., when the molecule is not partially deuterated, the $T_{LLS}$ decreases to $1.5 \pm 0.2$ s.[16] LLS can also be excited and preserved in symmetric molecules like citric acid (with spin patterns of the AA´XX´ type)[37] for lifetimes $T_{LLS}$ up to $8T_1$.

In the case of small peptides and mobile parts of proteins, LLS can be excited and preserved over timescales longer than $T_1$ without any sort of deuteration, which is the concern of present chapter. LLS have been found in small peptides like Ala-Gly and in mobile parts of Ubiquitin, and used to measure diffusion coefficients with moderate pulsed field gradients (PFG's).[45]

**5.1 LLS in a dipeptide, Ala-Gly**

The aliphatic $CH^{\alpha}_2$ protons in monomeric glycine $NH_2CH^{\alpha}_2COOH$ are magnetically equivalent, but they become diastereotopic in peptides and proteins. We have excited and preserved LLS in the dipeptide DL-Ala-Gly, where the spins $I$ and $S$ ($I = H_{\alpha}^{1}$ and $S = H_{\alpha}^{2}$) have a geminal $J$-coupling $J_{IS} = -17.4$ Hz and a chemical shift difference $\Delta v_{IS} = 0.12$ ppm (61.4 Hz at 11.75 T, Fig. 5.1.1). Methods for creating such states in diastereotopic pairs of scalar-coupled protons in high magnetic fields $B_0$ have been demonstrated by the group of M. Levitt and by ourselves[15-16] and have been discussed in chapter 2.
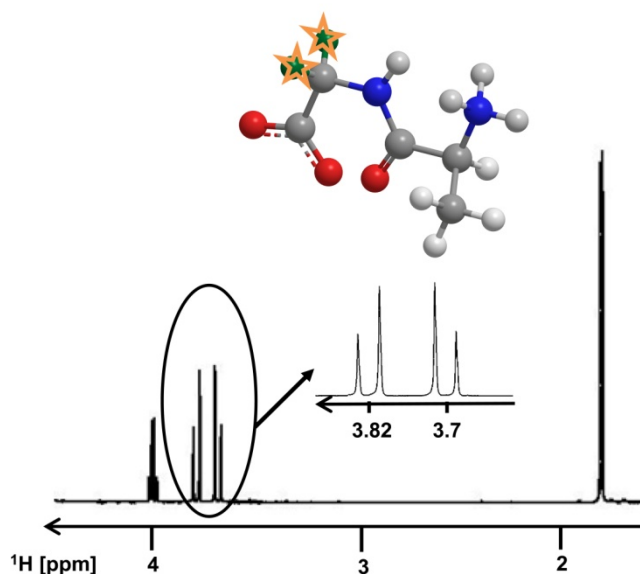
Figure 5.1.1. 1D proton NMR spectrum of DL-Ala-Gly in aqueous solution at 11.75 T (500 MHz for protons) and 25 °C. The resonances of the diastereotopic $CH_2$ protons of Gly are shown in the expanded region.

Table 5.1.1 compares the values of $T_{LLS}$ and $T_1$ for DL-Ala-Gly dissolved in $D_2O$. Lifetimes $T_{LLS} \approx 22$ s are observed, which increase to 42 s when the $O_2$ concentration is reduced to a significant extent by bubbling $N_2$ through the solution (Fig. 5.1.2), while $T_1$ does not change with $N_2$ bubbling, so that the ratio $T_{LLS}/T_1$ increases from 13 to 25.

| T | $T_1$ (s) (Without $N_2$ bubbling) | $T_{LLS}$ (s) (Without $N_2$ bubbling) | $T_{LLS}/T_1$ | $T_1$ (s) (After $N_2$ bubbling) | $T_{LLS}$ (s) (After $N_2$ bubbling) | $T_{LLS}/T_1$ | $D *$ $10^{-10}$ $(m^2s^{-1})$ |
|---|---|---|---|---|---|---|---|
| 294 K | $1.7 \pm 0.1$ | $22 \pm 1$ | **13** | $1.7 \pm 0.1$ | $42 \pm 2$ | **25** | $4.9 \pm 0.5$ |

Table 5.1.1. Lifetimes $T_1$ and $T_{LLS}$ of the long-lived state associated with the diastereotopic $CH^{\alpha}_2$ protons of Gly in DL-Ala-Gly dissolved in $D_2O$.
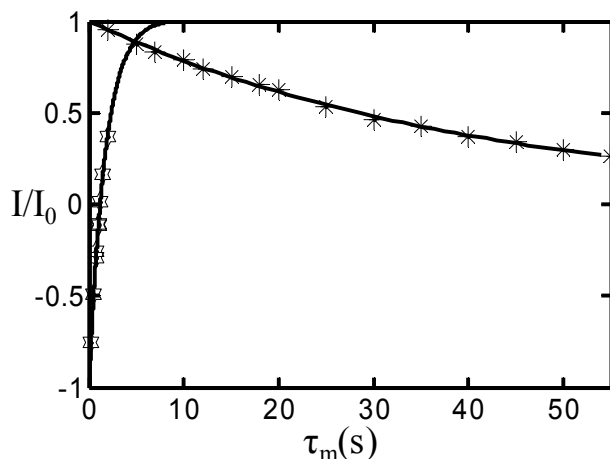
Figure 5.1.2. Exponential fits of the relaxation time constants $T_{LLS}$ and $T_1$ of the diastereotopic $CH^{\alpha}_2$ protons of DL-Ala-Gly dissolved in $D_2O$. $N_2$ was bubbled so as to reduce the concentration of $O_2$. The experiments were performed at 14.1 T (600 MHz for protons).

*The $T_{LLS}$* of the $CH^{\alpha}_2$ pair are mainly affected by intra-molecular dipolar interactions with the protons of the neighbouring alanine residue. These interactions are modulated by the rotational correlation time of the dipeptide in solution. It can be seen from numerical simulations (Table 5.1.2) that the dipolar interactions with methyl protons of alanine mainly affect $T_{LLS}$, to a larger extent than for $H^{\alpha}$ of alanine.

| Protons considered | Simulated $T_{LLS}$(s) | Simulated $T_1$(s) | Experimental $T_1$(s) |
|---|---|---|---|
| Gly-$H^{\alpha}$, $H^{\beta}$ and Ala- $H^{\alpha}$ | 98 | 1.68 | $1.7 \pm 0.1$ |
| Gly-$H^{\alpha}$,$H^{\beta}$ | 103 | 1.71 | -- |

Table 5.1.2. GAMMA simulations incorporating the evolution under the full spin Hamiltonian, consisting of the coherent part and relaxation, including DD and CSA interactions. The rotational correlation time $\tau_c$ was obtained by matching the $T_1$ obtained from experiments. Atomic coordinates were obtained from the crystal structure of (Ala-Gly)$_2$-Ser-Gly peptide.[46] An RF amplitude $\nu_{rf} = 2.5$ kHz was used for sustaining LLS.

The $T_{LLS}$ are also shortened by inter-molecular dipolar interactions, especially with dissolved paramagnetic oxygen. $T_{LLS}$ increases from 22 s to 42 s (Table 5.1.1), when $N_2$ is bubbled for several minutes in order to reduce the content of dissolved $O_2$ in the solution.

Another sample of DL-Ala-Gly was prepared in a mixture of deuterated water and deuterated DMSO, which remains liquid at temperatures well below 273 K, thus allowing one to explore a wide range of rotational correlation times. Table 5.1.3 compares $T_{LLS}$ with $T_1$ at various temperatures yielding the ratio $T_{LLS}/T_1 = 7$ even in the presence of oxygen, when molecular tumbling is considerably slowed down at 270 K.

| T | $T_1$ (s) (without $N_2$ bubbling) | $T_{LLS}$ (s) (without $N_2$ bubbling) | $T_{LLS}/T_1$ | $T_1$ (s) (After $N_2$ bubbling) | $T_{LLS}$ (s) (After $N_2$ bubbling) | $T_{LLS}/T_1$ | $D$ x $10^{-10}$ ($m^2s^{-1}$) |
|---|---|---|---|---|---|---|---|
| 294 K | 0.84 ± 0.04 | 11.6 ± 0.5 | 14 | 0.99 ± 0.05 | 16.3 ± 0.8 | 17 | 2.17 ± 0.09 |
| 270 K | 0.65 ± 0.03 | 4.8 ± 0.2 | 7 | 0.65 ± 0.03 | 8.2 ± 0.4 | 13 | 0.91 ± 0.05 |

Table 5.1.3. $T_1$ and $T_{LLS}$ of diastereotopic $CH^{\alpha}_2$ protons of Gly in DL-Ala-Gly dissolved in a mixture of 70% $D_2O$ and 30% deuterated DMSO at two temperatures.

## 5.2 Diffusion measurements on Ubiquitin using LLS

At 270 K, the diffusion coefficient $D = (0.91 \pm 0.09)$ x $10^{-10}$ $m^2s^{-1}$ of DL-Ala-Gly is smaller than the typical diffusion constant of a small protein in water at room temperature, e.g., $D = 1.77\pm0.02$ x $10^{-10}$ $m^2s^{-1}$ for Ubiquitin (76 amino acids, mass ca. 9 kDa) at 298 K.[47] We measured the LLS lifetimes of the $CH^{\alpha}_2$ pairs of the glycine residues in Ubiquitin dissolved in $D_2O$ at 310 K, having bubbled $N_2$ to reduce $O_2$ concentration before the experiments. Under these conditions, the $T_{LLS}$ of the terminal Gly-75 and Gly-76 (Fig. 5.2.1) were found to be $T_{LLS}$

= 6.3 ± 0.3 and 6.4 ± 0.4 s, respectively. These values represent a gain in the lifetime of spin memory by a factor $T_{LLS}/T_1 > 6$ for the $CH_2^\alpha$ protons in the same amino-acids, since their $T_1$ values are of the order of 1 s.
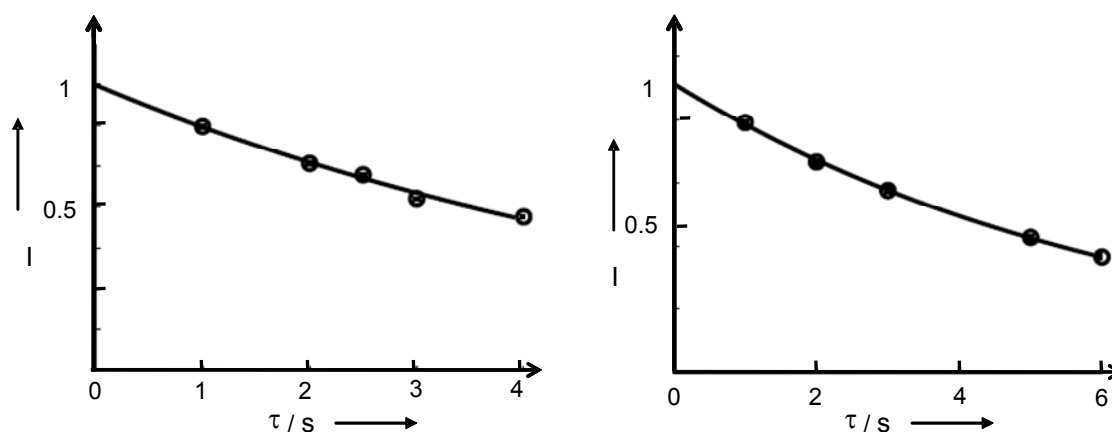


Figure 5.2.1. Exponential fits of $T_{LLS}$ of long-lived spin states of the diastereotopic $CH_2^\alpha$ protons in Gly-75 (left) and Gly-76 (right) in Ubiquitin. The experiments were performed at 14.1 T (600 MHz for protons).

One can assign Gly-75 and Gly-76 in the TOCSY spectrum of ubiquitin at 600 MHz (Fig. 5.2.2) though the cross peaks are not well separated from the diagonal peaks, as the shift difference between the α-protons of Gly-75 and Gly-76 is very small (~ 50 Hz at 11.4 T or 600 MHz).
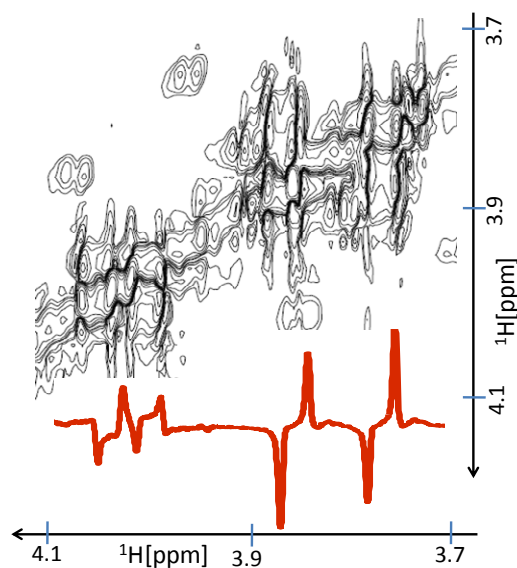
Figure 5.2.2. Zoom from a TOCSY spectrum of Ubiquitin at 11.4 T (600 MHz), acquired using a mixing time 50 ms. The signals obtained from an LLS experiment are plotted along the abscissa.

The long lifetimes $T_{LLS}$ of the $CH^{\alpha}_2$ pairs in glycine residues of the highly mobile $C$-terminus are due to the fact that, on average, these protons are relatively remote from the bulk of the protein, so that dipolar interactions with spins belonging to the compact folded part of the protein are partly averaged out. From the simulations in Table 5.2.1, it can be seen that dipolar interactions with the protons of the adjacent residue give a significant contribution to shortening the lifetimes of LLS.

| Residue | Spins included in simulations | $T_{LLS}$(s) |
|---------|------------------------------|--------------|
| Gly-76 | Gly 76 -$H^{\alpha 1}$ and $H^{\alpha 2}$ | $> 400$ |
| Gly-76 | Gly 76- $H^{\alpha 1}$ and $H^{\alpha 2}$, Gly 75- $H^{\alpha 1}$ and$H^{\alpha 2}$ | 28 |
| Gly-75 | Gly 75 - $H^{\alpha 1}$ and $H^{\alpha 2}$ | $> 400$ |
| Gly-75 | Gly 76- $H^{\alpha 1}$ and $H^{\alpha 2}$, Gly 75- $H^{\alpha 1}$ and $H^{\alpha 2}$ | 24 |

Table 5.2.1. GAMMA simulations incorporating the evolution under the full spin Hamiltonian, consisting of the coherent part and relaxation, including DD interactions. A rotational correlation time, $\tau_c$ = 4 ns was used and atomic coordinates were obtained from the crystal structure.[48] An RF amplitude $\nu_{rf}$ = 2.5 kHz was used for sustaining LLS.

The $T_{LLS}$ of the $CH^{\alpha}_2$ pairs of the other Gly residues (G10, G35, and G47) that are buried inside the core of the protein were also determined, but these lifetimes were found to be similar to their $T_1$ ($T_{LLS} \approx T_1 < 1$ s). It is noteworthy that the methods presented here are by no means limited to glycine residues, as methods to excite LLS in other amino-acids have been developed [43] and discussed in chapter 4. For instance, it is possible to excite LLS in scalar-coupled three-spin systems like serine, cysteine, aspartate, etc. but again their $T_{LLS}$ were found to be similar to their $T_1 \approx 1$s (Table 5.2.2).

| Residue | $T_{LLS}$ (s) |
|---------|---------------|
| Gly-47 | $0.3 \pm 0.1$ |
| Gly-35 | $0.6 \pm 0.1$ |
| Asp-52 | $0.6 \pm 0.04$ |
| Asp-32,39 | $0.5 \pm 0.05$ |
| Ser-20 | $0.12 \pm 0.02$ |
| Gly-10 | $0.3 \pm 0.03$ |

Table 5.2.2. $T_{LLS}$ in various residues of Ubiquitin. Experiments were done by adapting the chemical shift differences and *J*-couplings for each residue, respectively.

Diffusion studies were carried out on Ubiquitin at 294 K in order to compare the necessary gradient strengths required for classical methods and for LLS method. The signal intensities (*S*) were fitted with the function:

$$\frac{S}{S_0} = \exp(-D\kappa^2\Delta) \tag{5.2.1}$$

and two adjustable parameters, the diffusion coefficient D and the initial intensity $S_0$, as a function of the parameter $\kappa$, which depends on the *amplitude G* and the *duration* δ *of* the *PFG's:*

$$2\kappa = 2\delta\gamma psG \tag{5.2.2}$$

where $\gamma$ is the gyromagnetic ratio, $p = 1$ is the coherence order, $\delta$ is the gradient duration, and the factor $s = 2/\pi$ describes the surface of the sine-shape of the gradients.[49] A long diffusion interval ($\Delta_{LLS} = 2$ s) can be used because of the lifetime $T_{LLS} = 6.5$ s (Fig. 5.2.3), as compared to the shorter interval ($\Delta_{STE} = 0.55$ s for $T_1 \approx 1$ s) used in the conventional STE sequence, thus allowing one to limit the product of the duration $\delta$ (or the strength $G_{max}$) of the PFG with diffusion delay $\Delta$, by a factor of $(\Delta_{LLS}/\Delta_{STE})^{1/2} \sim 2$. The $CH^{\alpha}_2$ proton pair of Gly-76 has a chemical shift difference $\Delta\nu_{IS} = 55.7$ Hz at 500 MHz and a scalar coupling $J_{IS} = -17.3$ Hz. Very similar values for the diffusion coefficient $D = (1.264\pm0.002) \times 10^{-10}$ m$^2$s$^{-1}$ were obtained by both methods (less than 1% deviation between the two measurements).
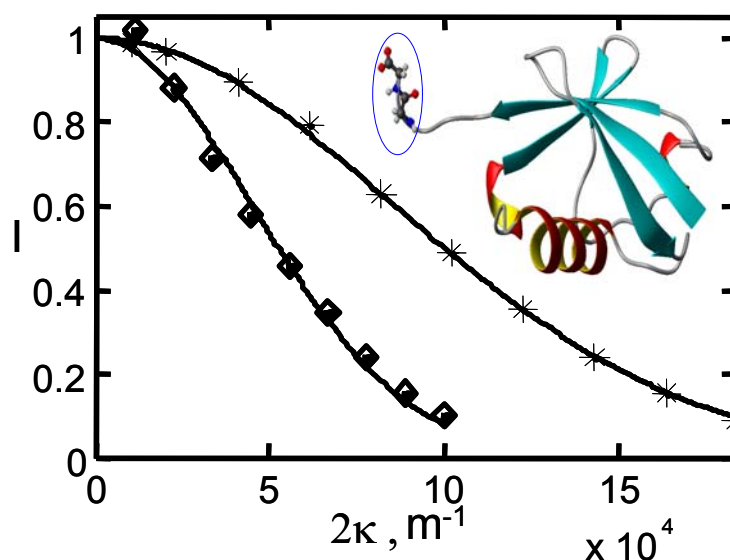


Figure 5.2.3. Experimental study of translational diffusion in ~ 2 mM Ubiquitin dissolved in D$_2$O at T = 298 K and B$_0$ = 11.7 T (500 MHz) using long-lived states (LLS) (diamonds) and conventional STE (stars). The gradient amplitudes ranged between $3 < G < 45$ Gcm$^{-1}$ in the two experiments, while the gradient pulse durations were $\delta$ = 650 and 1200 $\mu$s, respectively. The diffusion intervals were $\Delta$ = 2 and 0.55 s, respectively. Very similar values for the diffusion coefficient $D = (1.264\pm0.002) \times 10^{-10}$ m$^2$s$^{-1}$ were obtained by both methods (less than 1% deviation between the two measurements).

In brief, LLS can have significantly longer lifetimes than $T_1$ in the mobile parts of proteins but the dipolar interactions with external spins, e.g., in case of the residues inside the core of

Ubiquitin, the lifetimes $T_{LLS}$ decrease very fast, which makes LLS very sensitive probe to detect any structural changes. We followed the unfolding of Ubiquitin by addition of urea and varying pH which is described in next chapter.

**5.3 Experimental Section**

The experiments to measure $T_{LLS}$ for DL-ala-gly were carried out at 500 MHz ($B_0 = 11.75$ T) and ~ 20 mM solutions in deuterated water and in a mixture of 70% $D_2O$ and 30% deuterated DMSO at two temperatures, 294K and 270K. Gaseous nitrogen was bubbled through the samples for ten minutes prior to the experiments in order to reduce the concentration of dissolved oxygen. Eight transients were acquired for each LLS experiment using a relaxation delay of 30 s and an acquisition time of 2.73 s. Experimental $T_1$ and $T_{LLS}$ values were obtained by fitting normalized spectral intensities to mono-exponentially decaying functions. Continuous-wave irradiation with an amplitude $\nu_1 = 2.5$ kHz was used for sustaining LLS.

The experiments to measure $T_{LLS}$ and 2D-TOCSY on Ubiquitin were carried out at 600MHz and ~ 2 mM solution in $D_2O$. Gaseous nitrogen was bubbled through the sample for ten minutes prior to the experiments in order to reduce the concentration of dissolved oxygen. During the sustaining period, Sinc pulses[23] were used to sustain the long-lived state, the carrier was placed at the water frequency and a presaturation pulse of 1 s was applied before the beginning of the sequence. 128 transients were acquired for each LLS experiment using a relaxation delay of 10 s and an acquisition time of 2.73 s.

**5.4 Simulations**

To calculate contributions of various relaxation mechanisms to the Liouvillian, we carried out numerical simulations using GAMMA libraries,[36] incorporating DD and CSA relaxation mechanisms in addition to coherent evolution under the full spin Hamiltonian. The atomic

coordinates of spins were taken from crystal structure while chemical shifts and *J*-couplings were measured from the 1D NMR spectrum. The decay of the populations of LLS was monitored for 100 different relaxation intervals. The decays were then fitted to exponential functions using three fitting parameters (initial amplitude, decay rate and an additive constant). RF amplitude, $v_{rf} = 2.5$ kHz was used for sustaining LLS.

# Chapter - 6

# **Long-lived states to study unfolding of Ubiquitin**

Protein folding and unfolding is a very fundamental but complex phenomenon which remains very difficult to characterize, even after numerous methodological advancements in bio-analytical techniques. Proteins undergo various conformational changes after their biosynthesis by the ribosome and molecular chaperons play a significant role in their folding. The phenomenon of folding is described by the energy landscape theory as a sequence of partially folded states leading to a three-dimensional native state.[50]

Protein misfolding or unfolding lead to various diseases because folding of a protein into a correct three-dimensional structure is important for it to function properly.[51] Therefore, understanding the phenomenon of protein folding is necessary to have insights into various cellular activities. Various methods like MD simulations, one- and two-dimensional NMR, fluorescence spectroscopy, etc., have been employed to shed light upon various pathways of protein folding but still the area has numerous ambiguities and remains a challenging objective.

Ubiquitin is a small, highly-structured and stable protein with 76 amino acids that remains folded even up to $100^0C$.[52] It is involved in targeting proteins for proteosomal degradation and cellular signalling pathways. It exists within eukaryotic cells both as monomer and polymeric forms called polyubiquitin chains.[53] The crystal structure of Ubiquitin has been solved[48] and was confirmed by multidimensional NMR.[54] A large number of the amino acids ($\approx$ 85 %) are involved in the H-bonded secondary structure, thus making it unusually stable.

Unfolding of Ubiquitin has been extensively studied by various methods including two dimensional NMR, 2D–IR spectroscopy and MD simulations. Schanda et al[55] have studied H/D exchange kinetics in Ubiquitin combining fast acquisition techniques with 2D NMR,

using rapid sample mixing in the NMR magnet. They have observed that H/D exchange of amide protons is the slowest for residues in β1-β2 strands and α-helix whereas the exchange is much faster in β-sheets at the C-terminal part of Ubiquitin. Brutscher et al[56] have studied the backbone dynamics of the partially folded A state of Ubiquitin by NMR. They have observed that this state, which appears at low pH in a 60 % / 40 % methanol / water mixture, retains a native-like structure at N–terminal (β1-β2 strands and α-helix) where as the C-terminal part undergoes a transition from a β-sheets to a structure with predominantly helical character. Cordier and Grzesiek[57] have shown by following scalar J couplings across H bonds in Ubiquitin with increasing temperature that H-bonds between the β1-β5 antiparallel sheets are the least stable and that E64 → Q2 is the weakest H-bond. The kinetics of thermal unfolding of Ubiquitin has also been studied by molecular dynamics simulations.[58-59] The conclusion is that β-sheets in Ubiquitin are less stable than the α-helix, the weakest being the β structure at the C-terminus. Even after numerous studies of Ubiquitin unfolding, there still remain open questions, especially regarding the early steps of the process.

The lifetimes of LLS are immune to the mutual dipolar interaction of the spins involved but are more sensitive than $T_1$ or $T_2$ to relaxation by external spins.[60] We have measured the lifetimes of LLS in various amino acids of wild-type Ubiquitin while denaturing it by addition of urea and pH changes in order to extract information about the structural changes and its mobility during unfolding. In addition, we compared the values of relaxation time constants $T_{LLS}$ in various residues of Ubiquitin mutants,[53] L69S and L67S with those in wild-type Ubiquitin.

## 6.1 Ubiquitin denaturation using urea

As it has been discussed in sections 4.3 and 5.1, LLS can be excited in amino acids like serine, aspartic acid, etc., as well as in Gly residues of dipeptide, Ala-Gly. Though LLS with

significant lifetimes have been observed in the mobile *C*-terminus in native state of Ubiquitin, $T_{LLS}$ in amino acids buried inside the core of Ubiquitin are similar to $T_1$ because of the dipolar interactions with protons in the vicinity (as discussed in section 5.2), and therefore can provide information about structural changes during unfolding of Ubiquitin. We measured the $T_{LLS}$ in various amino acid residues of wild-type Ubiquitin after addition of 8 M urea at various pH (Table 6.1.1). LLS with significant lifetimes ($T_{LLS} > T_1$) were obtained in Gly-76, Gly-75 and Ser-65 but for other residues LLS lifetimes ($T_{LLS}$) were similar to $T_1$.

| Urea (M) | pH | $T_{LLS}$(s) in Gly-76 | $T_{LLS}$(s) in Gly-75 | $T_{LLS}$(s) in Ser-65 |
|----------|-----|------------------------|------------------------|------------------------|
| 0 | 7 | 6.5 ± 0.4 | 6.3 ± 0.3 | <1 |
| 8 | 7 | 6.4 ± 0.3 | 3.85 ± 0.6 | 12 ± 1 |
| 8 | 4.5 | 6.4 ± 0.3 | 2.9 ± 0.2 | 11± 1 |
| 8 | 3 | 8.7 ± 0.4 | --- | 11± 1 |

Table 6.1.1. The lifetimes $T_{LLS}$ for aliphatic protons in Gly-76, Gly-75 and Ser-65 of wild-type Ubiquitin while varying urea concentration and pH.

The $T_{LLS}$ time constant of Gly-76 aliphatic protons remains unchanged upon addition of 8 M urea and even upon changing the pH from 7 to 4.5. However, $T_{LLS}$ increases from 6.4 s to 8.7 s when the pH is further increased to 3, thus indicating increased mobility at the *C*-terminus. Under these conditions (8 M urea and pH = 3), the proton chemical shifts obtained by TOCSY experiments are similar to the chemical shifts of unfolded Ubiquitin,[61] thus indicating unfolding of the protein.

In Gly-75, the $T_{LLS}$ time constant of the aliphatic protons decreases from 6.3 s to 4 s upon addition of urea and further decreases to 2.9 s when the pH is decreased to 4.5. It was not possible to measure $T_{LLS}$ in Gly-75 when the protein is completely denatured (at pH = 3)

because of spectral overlap. $T_{LLS}$ might decrease because of dipolar interactions with external protons arising from structural changes at the $C$-terminus. For instance, Arg-74 has a long side chain which might come closer to protons of Gly-75 due to structural changes.

In Ser-65, the $T_{LLS}$ time constant is shorter than 1 s in the absence of denaturant (pH = 7), when the protein is in its most stable conformation and folded in its native state. While $T_{LLS}$ = 12 s is observed after addition of 8 M urea, the $T_1$ remains unchanged ($\approx$ 1 s), thus the ratio $T_{LLS}/T_1 \approx 12$. The increase in lifetimes $T_{LLS}$ indicates structural changes in β5 which allow Ser-65 to move out of the proton-rich core of Ubiquitin.

**6.2 Correlation experiments to study changes in chemical shifts with denaturation**

We performed TOCSY experiments in order to observe proton chemical shifts at various urea concentrations and various pH values, seeking information about possible structural changes occuring under these conditions. Fig. 6.2.1 shows the overlay of $^1$H - $^1$H correlation spectra obtained by TOCSY experiments at pH = 7, with urea (in red) and without urea (in green). The spectra do not differ significantly and information about possible structural changes induced by the addition of urea is difficult to obtain from this type of experiments. The spectra remain the same till pH = 4 but the chemical shifts collapse suddenly when the pH is changed from 4 to 3, thus indicating complete denaturation, as confirmed by the chemical shift assignment of denatured Ubiquitin in the literature.[61]
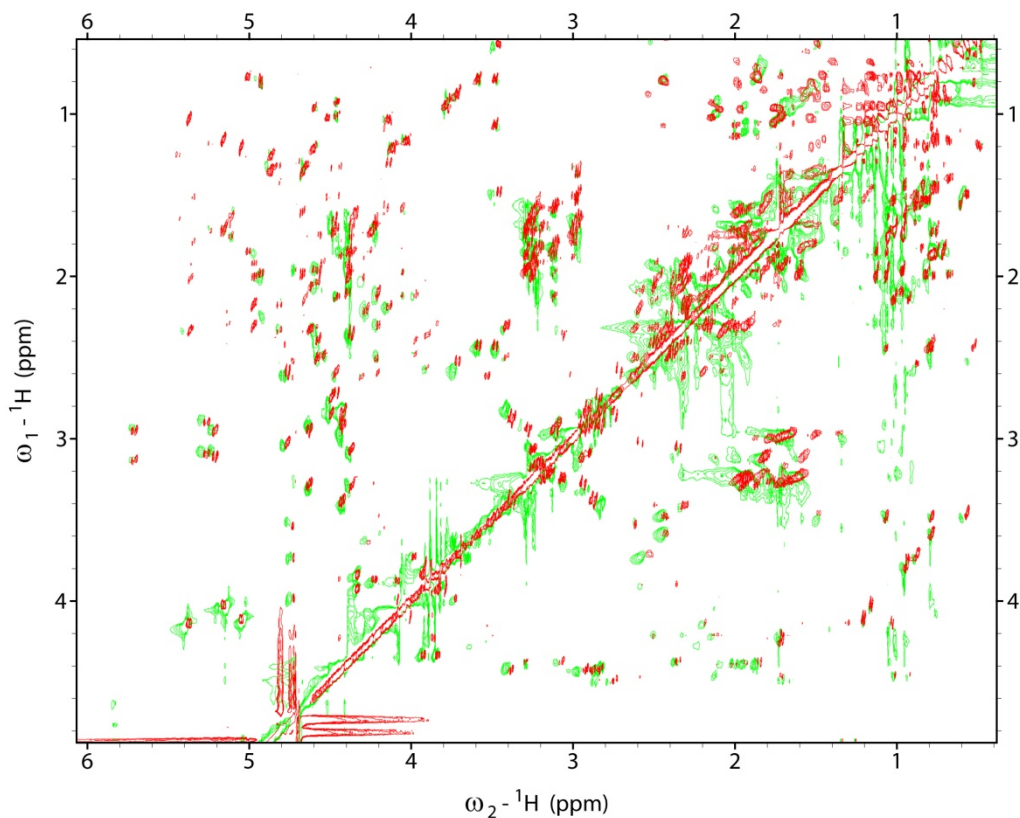
Figure 6.2.1. $^1H$ - $^1H$ correlation obtained from TOCSY experiments [62] at pH = 7 and T = 300 K, for native Ubiquitin (green), and after addition of 8 M urea (red).The experiments were carried out at 14.1 T (600 MHz for protons) with a mixing time $\tau_m$ = 80 ms.

Fig. 6.2.2 (A) shows $^{15}N$ - $^1H$ correlations obtained by HSQC experiments on wild-type Ubiquitin (with natural abundance of the $^{15}N$ isotope), dissolved in 90% $H_2O$ and 10% $D_2O$ at pH = 7 and after addition of 8 M urea. Many residues are found to be shifted significantly, thus indicating structural changes upon addition of urea. Most of these residues belong to either β1 or β5 (Fig. 6.2.2 (B)).
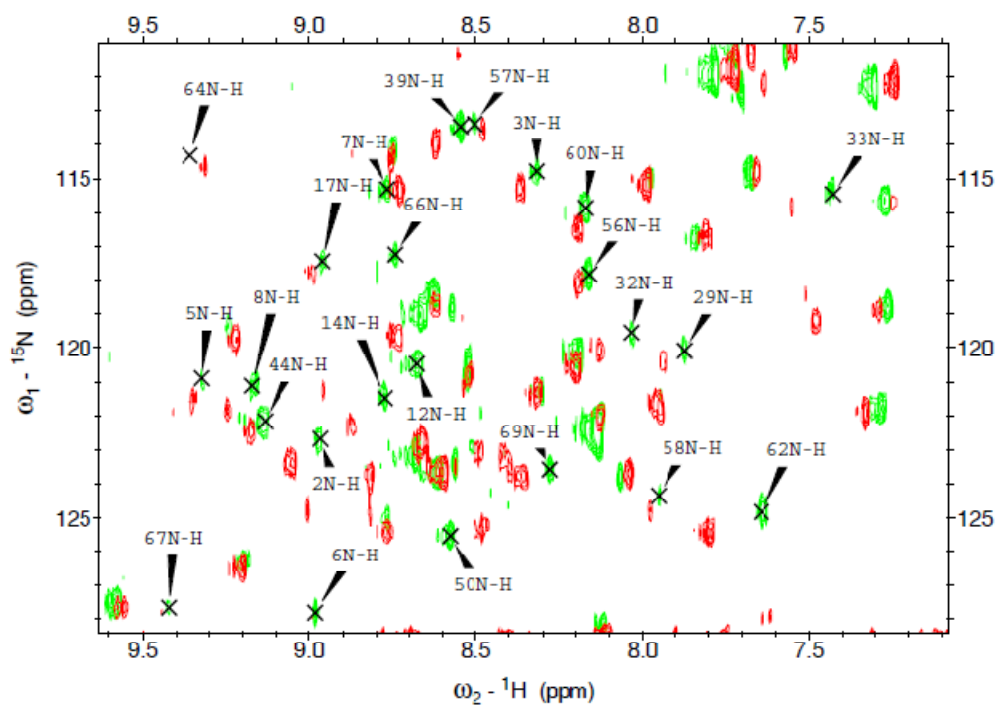
Figure 6.2.2. (A). $^{15}$N - $^{1}$H correlation obtained from HSQC experiments (with natural abundance of the $^{15}$N isotope) at pH = 7, native Ubiquitin (green), after addition of 8 M urea (red). The experiments were carried out at 18.8 T (800 MHz for protons).
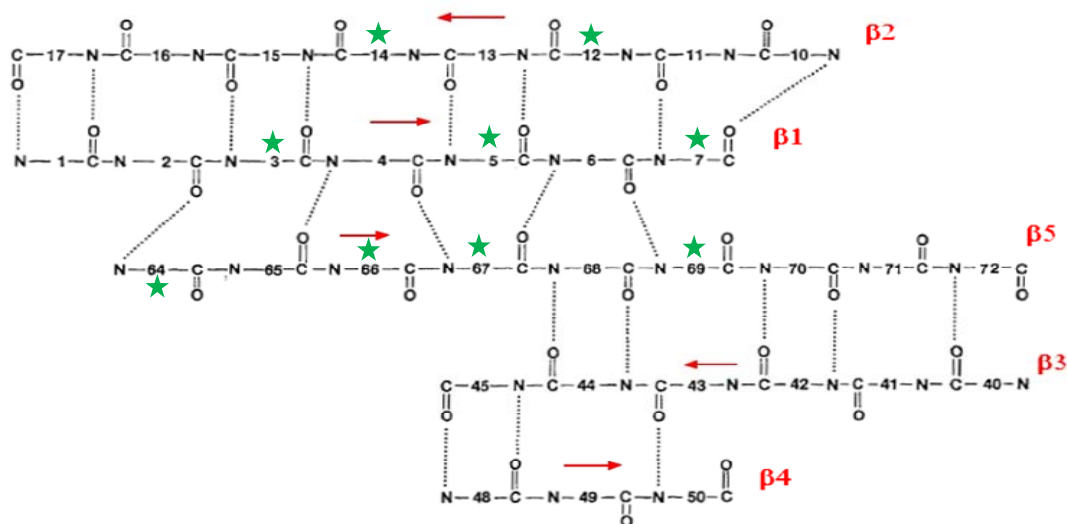


Figure 6.2.2. (B). β-sheet structure in Ubiquitin. Stars indicate the residues which show a difference between chemical shifts in $^{15}$N - $^{1}$H HSQC spectra in Fig. 6.2.2 (A).

Fig. 6.2.3 shows the signal intensity in LLS experiments with a sustaining period $\tau_{LLS}$ = 1 s at pH = 7 as a function of urea concentration (varying from 0 to 8 M). $T_{LLS}$ of various residues

change with initial addition of urea but maintains a constant value (same as Table 6.1.1) when urea concentration is increased from 2 M to 8 M. The intensity of signals of Gly-76 and 75 decreases but the intensity of signal of Ser-65 increases, which means that by addition of urea a conformer with long lifetimes $T_{LLS}$ of Ser-65 starts to appear.
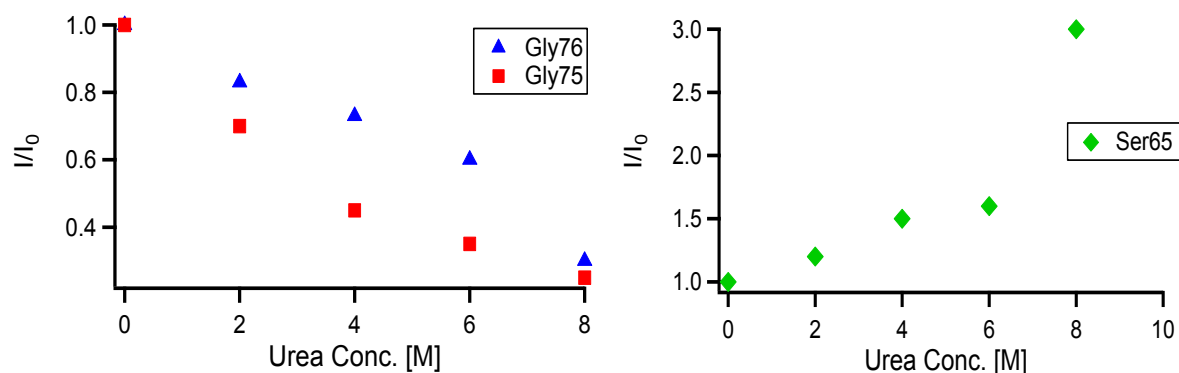


Figure 6.2.3. Normalized intensity of signals of Gly-75, Gly-76 (left) and Ser-65(right) using a sustaining period, $\tau_{LLS}$ = 1 s with increasing concentration of urea from 0 to 8 M. The Ser-65 signal intensity increases, while the Gly-75, -76 signal intensities decrease.

## 6.3 Similarities with the mutants L69S and L67S

We also measured $T_{LLS}$ in two mutants of Ubiquitin, L69S and L67S. Replacement of the hydrophobic leucine by a polar serine induces a loss of hydrophobic interactions, resulting in increase of the distances between α-β₃ and α-β₅ that makes the *C*-terminus of the protein more mobile.[53] Fig. 6.3.1 shows the chemical shift assignment of Ser-65 and Ser-69 on TOCSY spectrum of L69S Ubiquitin compared with the spectrum from an LLS experiment (inset) where the spectral parameters of serine were used. It can be seen that LLS with significant lifetimes exist on Ser-65.
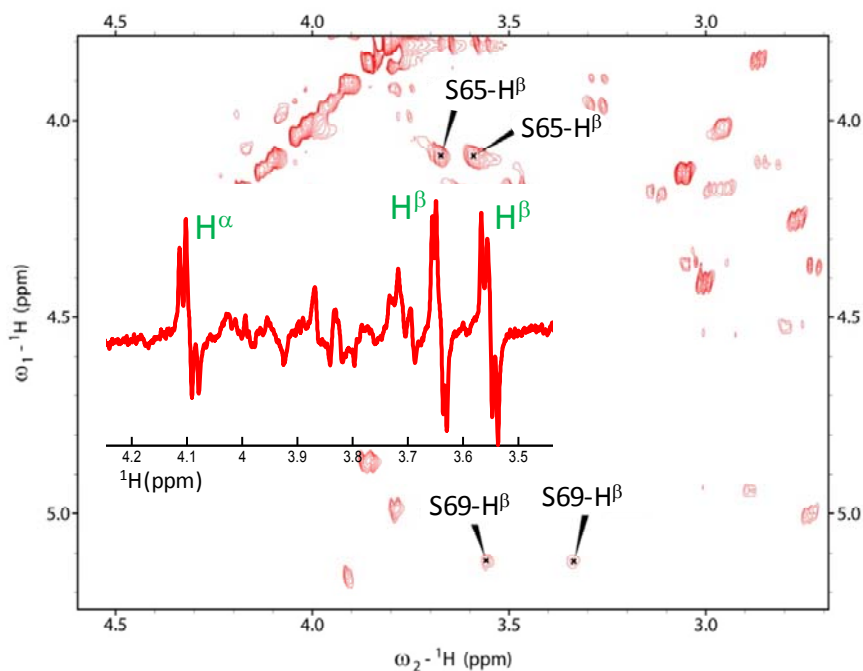
Figure 6.3.1. Selected region of $^1H$ - $^1H$ correlation spectra obtained from TOCSY experiments of Ubiquitin L69S. Chemical shifts of S69 and S65 have been assigned. The experiments were carried out at 14.1 T (600 MHz for protons) with a mixing time, $\tau_m$ = 80ms. Inset - LLS spectrum of Ubiquitin-L69S showing the signals from the three side chain protons of Ser-65. $\tau_m$ = 1 s was used for sustaining LLS.

Table 6.3.1 shows comparison of the lifetimes $T_{LLS}$ between mutated and wild-type Ubiquitin at pH = 7. In mutants, $T_{LLS} \approx 15$ s is observed in Ser-65 which is similar to the case of Ubiquitin with addition of 8 M urea. Also, the lifetimes of Gly-75 residue are shorter than those of Gly-76 which is also observed with addition of urea to wild-type Ubiquitin, leading to the conclusion that $C$-terminus of mutants has structural similarities with Ubiquitin at pH = 7 and in presence of 8 M urea.

78

| Urea (M) | Protein type | $T_{LLS}$ (s) in Gly-76 | $T_{LLS}$ (s) in Gly-76 | $T_{LLS}$ (s) in Ser-65 |
|---|---|---|---|---|
| 0 | Wild -Type | 6.5 ± 0.4 | 6.3 ± 0.2 | <1 |
| 8 | Wild - Type | 6.41 ± 0. 3 | 3.85 ± 0. 6 | 12 ± 1 |
| 0 | L69S | 4.2 ± 0. 3 | 1.4 ± 0. 1 | 15.0 ± 0.2 |
| 0 | L67S | 2.9 ± 0. 3 | --- | 16.4 ± 0.2 |

Table 6.3.1 The lifetimes $T_{LLS}$ of Gly-76, Gly-75 and Ser-65 in wild-type Ubiquitin at pH=7 and various urea concentration, compared with the lifetimes of same residues in mutants of Ubiquitin (L69S and L67S).

## 6.4 T$_{1\rho}$ measurements

We measured values $T_{1\rho}$[63] in the corresponding amino acid residues of Ubiquitin at increasing urea concentrations, as well as for the L69S mutant Ubiquitin. Table 6.4.1 compares the values of $T_{1\rho}$ and $T_{LLS}$ in Gly-76 and Gly-75 of wild-type Ubiquitin at pH = 7, before and after the addition of 8M urea. Not much change in $T_{1\rho}$'s is observed upon the addition of urea while $T_{LLS}$ in Gly-75 changes significantly upon addition of 8M urea. Before the $T_{1\rho}$ pulse sequence a *J*-filter was inserted, consisting of a combination of π-pulses and gradients for dephasing the undesired coherences obtained from other residues.

| Residue | $T_{1\rho}$ (ms) Urea conc. = 0 M | $T_{1\rho}$ (ms) Urea conc. = 8 M | $T_{LLS}$ (s) Urea conc. = 0 M | $T_{LLS}$ (s) Urea conc. = 8 M |
|---|---|---|---|---|
| Gly-75 | 110 ± 5 | 115 ± 5 | 6.3 ± 0.3 | 3.85 ± 0.6 |
| Gly-76 | 195 ± 10 | 190 ± 10 | 6.5 ± 0.4 | 6.41 ± 0.3 |

Table 6.4.1. The comparison of lifetimes, $T_{1\rho}$ and $T_{LLS}$ in Gly-76, Gly-75 of wild-type Ubiquitin at pH = 7, with and without addition of urea.

Table 6.4.2 shows $T_{1\rho}$ values for L69S. The $T_{1\rho}$ of Ser-65 is similar to Gly-76 which indicates that the Ser-65 is quite mobile, which is the reason why $T_{LLS}$ = 15.0 ± 0.2 s is obtained for this amino acid.

| Residue | $T_{1\rho}$ (ms) |
|---------|---------|
| Gly-76 | $120 \pm 5$ |
| Ser-65 | $200 \pm 10$ |

Table 6.4.2. $T_{1\rho}$ in various amino acids of Ubiquitin, L69S at pH = 7 and T = 298 K.

## 6.5 Discussion

In light of the above observations, the stability of Ubiquitin decreases in the presence of urea. Under these conditions, H- bonds in β1-β2 hairpin and β1-β5 antiparallel sheets are affected, which can be seen by the comparison of HSQC experiments at pH = 7 in the presence and absence of urea (Figs 6.2.2 (A) and 6.2.2 (B)). The increase in $T_{LLS}$ of Ser-65 after the addition of urea indicates increased mobility of β5 because of the breaking of weaker H-bond interactions in the antiparallel β1-β5 sheet, which is in accordance with evidences reported in the literature about unfolding pathways of Ubiquitin where the β structure of Ubiquitin at the C-terminus has been found to be the least stable.

## 6.6 Experimental Section

The experiments to measure $T_{LLS}$ and 2D-TOCSY on Ubiquitin were carried out at 600MHz and ~ 2 mM solution in $D_2O$. Gaseous nitrogen was bubbled through the sample for ten minutes prior to the experiments in order to reduce the concentration of dissolved oxygen. Before addition, urea was lyophilized twice in $D_2O$ for exchanging acidic protons with deuterium. pH of the solution was adjusted by concentrated HCl. For each residue, LLS experiments were run using the method described by Sarkar et al.[16] During the sustaining period, the carrier was placed at the water frequency, Sinc pulses[23] were used, and a presaturation pulse of 1 s was applied before the beginning of the sequence. 128 transients

were acquired for each LLS experiment using a relaxation delay of 10 s and an acquisition time of 2.73 s. Experimental $T_{LLS}$ values were obtained by fitting normalized spectral intensities to mono-exponentially decaying functions. 2D-HSQC for obtaining $^{15}$N - $^{1}$H correlations were carried out at 800 MHz on 2 mM Ubiquitin dissolved in a mixture of 90% $H_2O$ and 10% $D_2O$.

# Chapter - 7

# Long-lived coherences in high-field NMR

In conventional NMR spectroscopy, narrowing homogeneous line widths is regarded as a considerable challenge. For large molecules, lines are very broad because of fast transverse relaxation, thus making NMR of large molecules and supramolecular assemblies difficult. This holds equally true for zero-, single-, and multiple-quantum spectroscopy. Though inhomogeneous line broadening can be reduced by using spin echoes,[64] achieving further narrowing is a difficult task. Homogeneous broadening results from transverse relaxation due to stochastic interactions, and therefore its elimination by the experimentalist is hard.

In some fortunate cases, stochastic interactions may cancel out mutually, thus leading to line narrowing. For instance, the fluctuations of dipole-dipole interactions and anisotropic chemical shifts can partially cancel each other if they have favorable relative orientations, a phenomenon which is used in Transverse Relaxation Optimized SpectroscopY (TROSY).[65-71] Similar types of interferences between several dipolar interactions can also be observed in methyl groups.[72] These effects have brought major advances by increasing the size of proteins and protein complexes that are amenable to structural and dynamic studies by NMR from about 20 to 50 kDa.

In this chapter, another approach to narrow line-widths, inspired by the work of M. Levitt and co-workers, has been demonstrated. In analogy to LLS, which have remarkably long lifetimes, excitation of long-lived coherences (LLC's) can lead to significant sensitivity and resolution enhancement. A transition between singlet and triplet states is normally symmetry-forbidden and therefore has a vanishing transition probability. However, under certain circumstances, the *coherent superpositions across these forbidden transitions* can be excited, and we refer to such superpositions as long-lived coherences (LLC's).[73-74] In contrast to the populations of long-

lived states (LLS), which decay monoexponentially, the time-dependence of LLC's is oscillatory and can be mapped in the manner of two-dimensional (2D) spectroscopy. For an LLC experiment, a control of the symmetry of quantum states is required that can be simply achieved, in conventional NMR, by switching a radio-frequency (RF) field on or off: if the RF field is switched on, the states are symmetric or antisymmetric under a permutation of the spins, i.e., singlet and triplet states; if it is switched off, the states have no permutation symmetry as the spins become nonequivalent because of their different Larmor frequencies. Recently, M. Levitt and co-workers have discussed similar transitions between symmetric and antisymmetric states in zero field, where a Rabi nutation of the two-level system, comprising the singlet and central triplet states, is brought about by irradiation with an electromagnetic field at extremely low frequency (ELF), typically on the order of a few tens of Hz.[75]

LLC lifetimes can be significantly longer than the transverse relaxation times $T_2$ of single quantum coherences ($3 < T_{LLC}/T_2 < 9$), depending on the correlation times. Therefore, monitoring the slow oscillatory decays of LLC's by two-dimensional spectroscopy allows one to obtain very narrow lines with half widths at half height $\Delta v_{LLC} = (\pi T_{LLC})^{-1} << \Delta v = (\pi T_2)^{-1}$. This chapter comprises the experimental demonstration of excitation methods of LLC's in small molecules, as well as in proteins.


## 7.1 Theory

If a continuous-wave (CW) radio frequency (RF) with an amplitude $|v_1|$ is applied and the RF carrier, $v_{RF}$, is placed half-way between the two chemical shifts:

$$v_{RF} = v_{av} = (v_I + v_S)/2 \tag{7.1.1}$$

The truncated Hamiltonian for a two spin-½ system, in a frame rotating at $v_{av}$, can be written as (described in detail in section 2.1):

$$H = v_1(I_x + S_x) + J\vec{I} \cdot \vec{S} \tag{7.1.2}$$

This Hamiltonian is symmetric under the permutation of the spins $I$ and $S$. Therefore, the spin system can be well described in singlet-triplet basis $\Phi_{STB}$.

The part of the total Liovillian, considering the deterministic Hamiltonian in Eq. (7.1.2) and the stochastic Hamiltonian for the dipolar interaction between spins $I$ and $S$ (described in section 3.2), can be written as follows:

$$\Gamma^{ST}_{total} = \begin{pmatrix} 0 & 0 & 0 & 0 & 0 & 0 \\ 0 & 0 & 0 & 0 & 0 & 0 \\ 0 & 0 & -R_1 & 0 & 0 & 0 \\ 0 & 0 & 0 & -\left(\dfrac{5}{3}\right)R_1 & 0 & 0 \\ 0 & 0 & 0 & 0 & 2\pi iJ - \dfrac{R_1}{3} & 0 \\ 0 & 0 & 0 & 0 & 0 & -2\pi iJ - \dfrac{R_1}{3} \end{pmatrix} \qquad (7.1.3)$$

in the following basis:

$$\{ST\}_0 = \left\{ \begin{array}{l} \dfrac{1}{2}\left(|S_0\rangle\langle S_0| + |T_+\rangle\langle T_+| + |T_0\rangle\langle T_0| + |T_-\rangle\langle T_-|\right), \\ Q_{LLS}, \\ \dfrac{1}{\sqrt{2}}\left(|T_+\rangle\langle T_+| - |T_-\rangle\langle T_-|\right), \\ \dfrac{1}{\sqrt{6}}\left(-|T_+\rangle\langle T_+| + 2|T_0\rangle\langle T_0| - |T_-\rangle\langle T_-|\right), \\ L_+, \\ L_- \end{array} \right\} \qquad (7.1.4)$$

where $\begin{array}{l} L_+ = |S_0\rangle\langle T_0| \\ L_- = |T_0\rangle\langle S_0| \end{array}$ and

$$Q_{LLS} = N_{LLS}\left[|S_0\rangle\langle S_0| - \frac{1}{3}\left(|T_0\rangle\langle T_0| + |T_+\rangle\langle T_+| + |T_-\rangle\langle T_-|\right)\right]$$

$R_1 = -\left(\langle I_z + S_z | \Gamma_{DD} | I_z + S_z \rangle\right) = \left(\dfrac{3}{2}\right) b_{IS}^2 \tau_c$ is defined as the longitudinal relaxation rate. The Liouvillian was calculated under the extreme narrowing limit where $R_1 = R_2$.

From Eqs. (7.1.3) and (7.1.4), it can be seen that either of $|S_0\rangle\langle T_0|$ or $|T_0\rangle\langle S_0|$ (the 5th and 6th diagonal elements in the matrix), decay with the relaxation rate $R_{LLC}$, which is three times smaller than $R_1$ or $R_2$.

Their linear combination, $Q_{LLC}$, can be written as follows:

$$Q_{LLC} = |S_0\rangle\langle T_0| + |T_0\rangle\langle S_0| \tag{7.1.5}$$

We call these *coherent superpositions between the singlet and central triplet states* long-lived coherences (LLC's).

Their expression can be converted into Cartesian angular momentum operators:

$$Q_{LLC} = |S_0\rangle\langle T_0| + |T_0\rangle\langle S_0| = I_z{}' - S_z{}' \tag{7.1.6}$$

In the absence of an RF field, the operators of spins $K = \{I, S\}$ need to be transformed back from the tilted interaction frame by:

$$\begin{pmatrix} K_x{}' \\ K_y{}' \\ K_z{}' \end{pmatrix} = \begin{pmatrix} \cos\theta_K & 0 & -\sin\theta_K \\ 0 & 1 & 0 \\ \sin\theta_K & 0 & \cos\theta_K \end{pmatrix} \begin{pmatrix} K_x \\ K_y \\ K_z \end{pmatrix} \tag{7.1.7}$$

When $\theta_{I,S} \sim \pi/2$, this simply amounts to relabeling $K_z{}' \rightarrow K_x$, as suggested by Eq. (7.1.7).

Therefore, $Q_{LLC}$ in the rotating frame of reference is expressed as:

$$Q_{LLC} = I_x - S_x \tag{7.1.8}$$

Thus, when the continuous RF field is suddenly switched on, the difference $(I_x - S_x)$ in the product base $\Phi_{PB}$ is converted into off-diagonal elements between the states $|S_0\rangle$ and $|T_0\rangle$ in the singlet-triplet base $\Phi_{STB}$. These off-diagonal elements correspond to long-lived coherences (LLC's).

The density operator of the form $Q_{LLC}$ in Eq. (7.1.8) does not commute with the isotropic scalar coupling Hamiltonian, which causes it to undergo an evolution:

$$\left[ I_x - S_x, \vec{I} \cdot \vec{S} \right] = i \left( 2I_y S_z - 2I_z S_y \right) \tag{7.1.9}$$

Therefore the evolution of LLC's under the coherent part of Hamiltonian, provided that the applied RF field amplitude is strong enough to mask the chemical shift difference between the two spins, can be written as follow:

$$Q_{LLC}(t) = (I_x - S_x)\cos(2\pi Jt) + (2I_y S_z - 2I_z S_y)\sin(2\pi Jt) \tag{7.1.10}$$

The LLC decay including both coherent effects and relaxation is given by:

$$\frac{d}{dt} Q_{LLC} = -\left( R_{LLC} + i2\pi J \right) Q_{LLC} \tag{7.1.11}$$

The LLC's oscillate with a frequency determined by the scalar coupling constant $J$ (the imaginary part), while the relaxation rate $R_{LLC}$ (the real part) governs the slow decay and is compared to $R_2$ to estimate the gain in line-width obtained by these methods.

In a system of two spin-½ nuclei, $I$ and $S$, the rate $R_2$, predominantly determined by the dipolar interaction between these spins,[34] is:

$$R_2 = \left( \frac{b_{IS}^2}{20} \right) \left[ 9J(0) + 15J(\omega) + 6J(2\omega) \right] + R_2^{ext} \tag{7.1.12}$$

where $b_{IS} = -\dfrac{\mu_0}{4\pi} \dfrac{\gamma^2 \hbar}{r_{IS}^3}$ is the strength of the homonuclear dipolar coupling, $r_{IS}$ the distance between the spins $I$ and $S$, and $J(\omega) = \dfrac{\tau_c}{1 + \omega^2 \tau_c^2}$ the spectral density function. The term $R_2^{ext}$ comprises contributions from external random fields, anisotropic chemical shifts (CSA), and dipole-dipole (DD) interactions to remote spins.

In contrast to 'longitudinal' LLS, which are not affected by the dipolar interaction between the two spins $I$ and $S$, the general formulation of the relaxation rate constant $R_{LLC}$ under the homonuclear dipolar interaction is given by:

$$R_{LLC} = \left(\frac{b_{IS}^2}{20}\right)\left[J(0) + 3J(\omega) + 6J(2\omega)\right] + R_{LLC}^{ext} \tag{7.1.13}$$

If the $R_{LLC}^{ext}$ term is small, the LLC has a slower relaxation rate than single-quantum coherences in all motional regimes, i.e., for arbitrary molecular tumbling rates. The ratio, $T_{LLC}/T_2 = \varepsilon = 3$ for fast-tumbling limit ($\tau_c \ll 1/\omega_0$), increases to $T_{LLC}/T_2 = \varepsilon = 9$ for slow tumbling ($\tau_c \gg 1/\omega_0$).[76] Thus, if the $R_{LLC}^{ext}$ terms may be neglected, the ratio of the relaxation times should increase from $T_{LLC}/T_2 = \varepsilon = 3$ in small molecules to $T_{LLC}/T_2 = \varepsilon = 9$ in macromolecules, thus making the gain more significant for large molecules.

## 7.2 Methods

### 7.2.1 Method I - Excitation of LLC's in a single pair of spins

A suitable pulse sequence for exciting and detecting LLC's[73] is shown in Fig. 7.2.1.1.
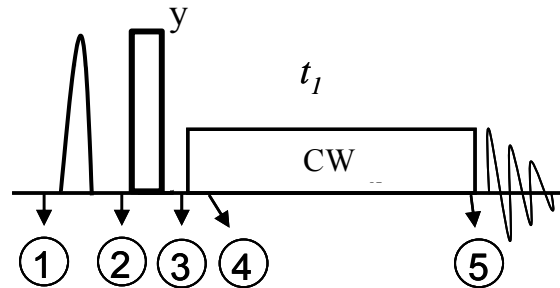


Figure 7.2.1.1. Basic experiment used for excitation, sustaining and detection of long-lived coherences (LLC's) for one pair of protons at a time. The time-points of the experiment, given in circles, are mentioned in the equations. The vertical open rectangle represents a non-selective $\pi/2$ pulse. All pulses are applied along the x

axis, unless specified. The $\pi$ pulse for semi-selective inversion has a sinc shape, a length of 70 ms, and a peak RF amplitude of 40 Hz.

In the beginning of the experiment, at point $\tau_1$ in the sequence, the density operator $\sigma_1$ comprises only populations in thermal equilibrium:

$$\sigma_1 = (I_z + S_z) \tag{7.2.1.1}$$

A semi-selective $(\pi)_x$ pulse is applied only to spin $S$ between $\tau_1$ and $\tau_2$:

$$R_{(1->2)} = \exp(-i\pi S_x) \tag{7.2.1.2}$$

so that the system at point $\tau_2$ is described by:

$$\sigma_2 = R_{(1->2)}\sigma_1 R_{(1->2)}^{-1} = I_z - S_z \tag{7.2.1.3}$$

After applying a non-selective $(\pi/2)_y$ pulse to both spins:

$$R_{(2->3)} = \exp\left[-i\frac{\pi}{2}(I_y + S_y)\right] \tag{7.2.1.4}$$

one obtains:

$$\sigma_3 = R_{(2->3)}\sigma_2 R_{(2->3)}^{-1} = I_x - S_x \tag{7.2.1.5}$$

Between points $\tau_3$ and $\tau_4$, a continuous RF irradiation is switched on, so that the eigenstates of the system are switched instantaneously to the symmetry-adapted states $\Phi_{STB}$. As explained in Eq. (7.1.7), we can now rewrite the density operator at time point $\tau_4$, since $\theta_{I,S} \sim \pi/2$:

$$\sigma_3 = I_x - S_x = I_z{}' - S_z{}' \tag{7.2.1.6}$$

The matrix representation of the density operator $\sigma_4$ in the product base $\Phi_{PB}$ can be transformed into the singlet-triplet base $\Phi_{STB}$:

$$\sigma_4 = I_z{}' - S_z{}' = |S_0><T_0| + |T_0><S_0| \tag{7.2.1.7}$$

which is $Q_{LLC}$, oscillating with the frequency same as $J$-coupling and decaying with the rate constant $R_{LLC}$.

For the detection, it is sufficient to switch off the RF field so that the two spins become non equivalent. The density operator $\sigma_5$ is given by:

$$\sigma_5 = I_x - S_x \qquad (7.2.1.8)$$

which is detectable through the RF coil.

### 7.2.2 Method II - Broadband excitation of several LLC's

LLC experiments are not limited to studying one pair of spins after another. The semi-selective inversion of several spins in rapid succession (i.e., within an interval shorter than $T_1$) allows several LLC's to be excited simultaneously in different subsystems. For instance, LLC's can be excited simultaneously in Gly-75 and Gly-76 of Ubiquitin.[74]

Fig. 7.2.2.1(a) shows the pulse sequence for simultaneous excitation of LLC's in G75 and G76. There are three important differences between the broadband and selective methods for detecting LLC's: *i)* a double-quantum (*DQ*) filter is inserted, prior to the LLC excitation. *ii)* Two semi-selective $\pi$ pulses are needed to invert the two doublets. *iii)* The RF carrier was placed at the mean position between the two averages $\{v_{av}(I,S)$ and $v_{av}(I^{'},S^{'})\}$ of the four chemical shifts during the sustaining period and a train of sinc shaped pulses was used to sustain the LLC's on both residues simultaneously because the use of a simple CW irradiation is not sufficient in this case. We also used presaturation by a continuous-wave RF field ('CW' in Fig. 7.2.2.1(a)) to attenuate the residual water signal.

The *DQ* filter has been used to suppress perturbing multiplets with smaller splittings that arise from other spin systems in the protein. This filter consists of a sequence of pulses, phase cycling to select double quantum coherences, pulsed field gradients, and matched delays $\tau = 1/(4J) = 14.7$ ms, since $|J| = 17$ Hz for all glycine residues (irrespective of their environment). This filter creates pure in-phase coherences of the form $(I_x + S_x)$ for Gly 75 and 76. Note that this filter also suppresses singlets quite efficiently. If no filters are used, the baseline for the

LLC experiment can be contaminated by unwanted signals from residues other than glycines, which degrade the signal purity and render the fitting process inaccurate. Fig. 7.2.2.1(b) shows the signal from both glycines at the end of the filter.
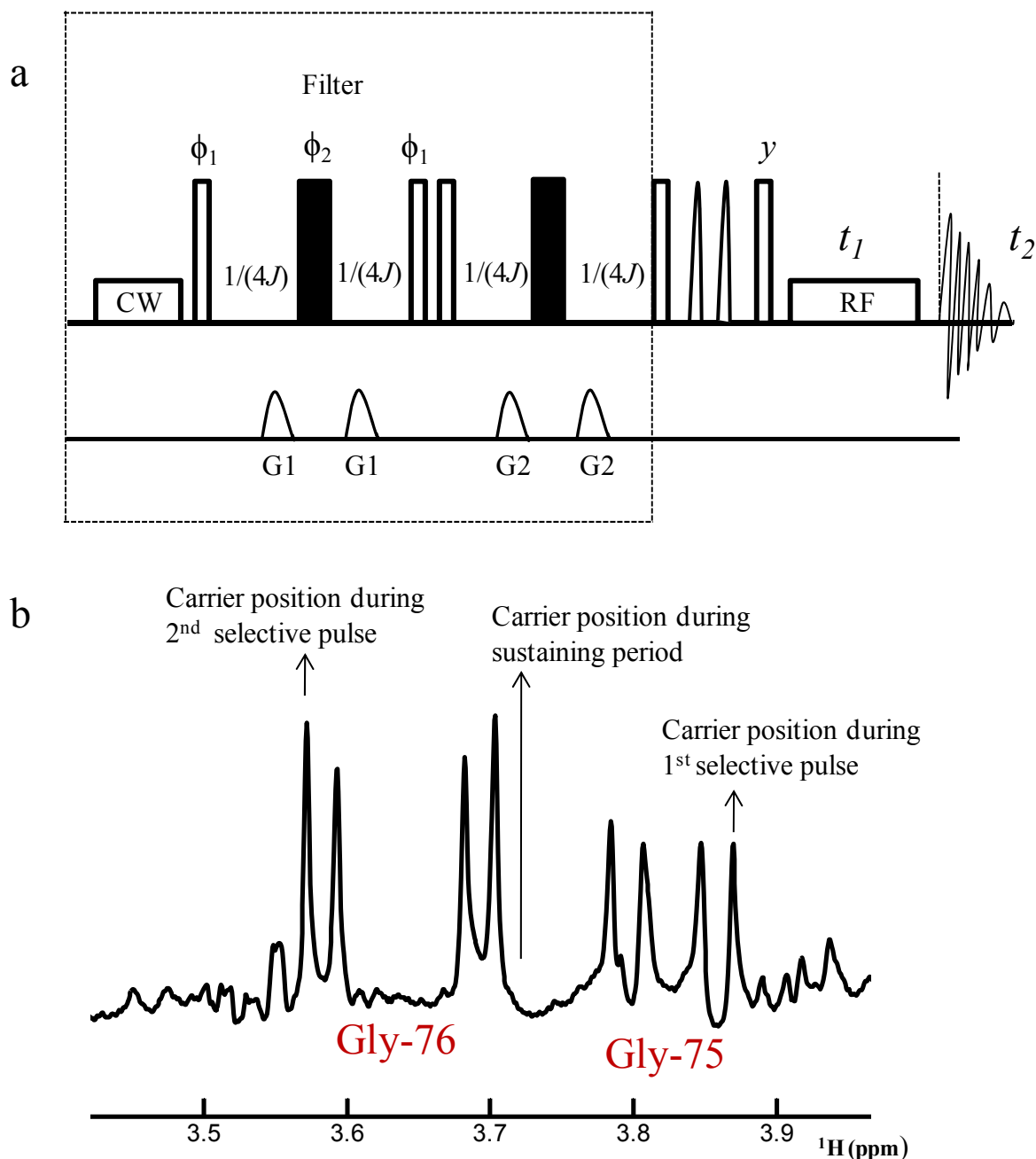


Figure 7.2.2.1 Simultaneous excitation and observation of long-lived coherences (LLC's) in high magnetic fields, illustrated for a system with two pairs of diastereotopic protons, i.e., Gly-75 and Gly-76 in ubiquitin (a) The sequence is preceded by a *DQ* filter described in the text. Open and filled rectangles represent non-selective $\pi/2$ and $\pi$ pulses, respectively. All pulses are applied along the x-axis, unless otherwise specified. The pulse phases are: $\phi_1 = x, y, -x, -y$; $\phi_2 = y, -x, -y, x$ and $\phi_{rec} = x, -x$. (b) Proton signals of Gly-75 and Gly-76 in ubiquitin obtained at

800 MHz with the pulse sequence (a) acquired after the *DQ* filter.  The positions of the RF carrier for exciting LLC's at different points are shown.

## 7.3 Results and discussion

### 7.3.1 LLC's in a small molecule

2,3,6-trichlorophenol, which contains two scalar-coupled aromatic protons, was used to determine the lifetimes of LLC's. The typical 1D spectrum of 2,3,6-trichlorophenol is shown in Fig. 7.3.1.1(a). The experiments were performed by *Method I* described in section 7.2.1, which is good enough to excite LLC's in one pair of spins. Fig. 7.3.1.1(b) shows the time-domain decay of LLC's in 2,3,6-trichlorophenol in a field $B_0$ = 9.4 T (400 MHz for protons) at room temperature, which yields a very precise value of $J$ = 8.760 ± 0.001 Hz and a slow relaxation rate $R_{LLC}$ = 0.10 ± 0.01 s$^{-1}$. A ratio $\varepsilon$ = $T_{LLC}/T_2$ ~2.4 has been observed, i.e., a resolution enhancement by a factor 2.4.[74]

In the 2D spectrum in Fig. 7.3.1.2(a), the chemical shifts can be seen in the direct $\omega_2$ dimension, whereas only a single peak at 9.0 ± 0.2 Hz is observed in the $\omega_1$ dimension. This corresponds to the magnitude of the coupling constant $J$. Here, the $\omega_1$ dimension was not sampled long enough to avoid truncation effects ($t_1^{max}$ = 14.3 s with 1024 points and $\Delta t_1$ = 14 ms).
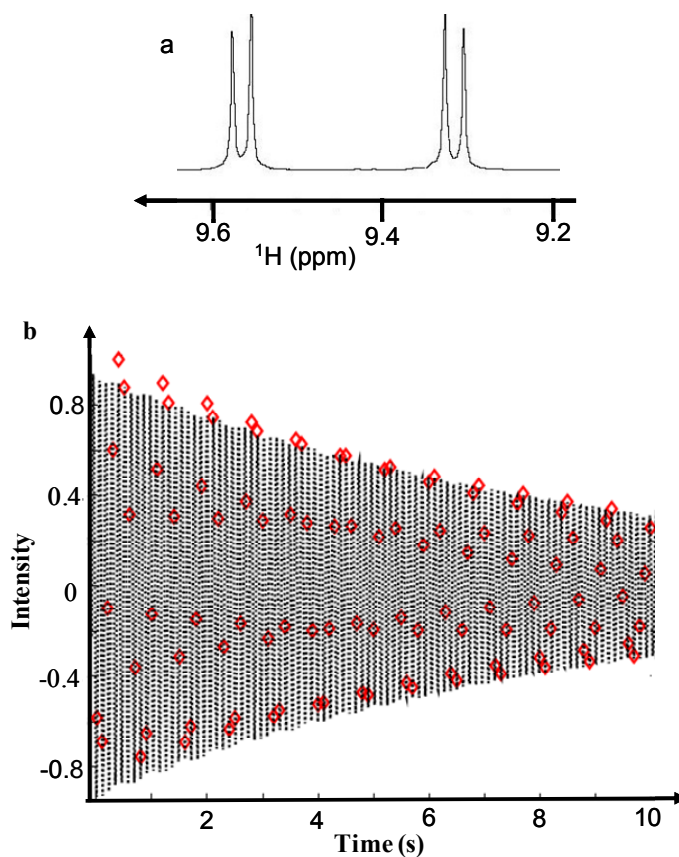
Figure 7.3.1.1 (a) Proton spectrum of the two weakly-coupled protons in 2,3,6 trichlorophenol at 400 MHz. (b) The experimental intensities (red lozenges) were plotted as a function of time $t_1$ and fitted with a function $I(t_1) = I_0 \cos(2\pi J t_1) \exp(-R_{LLC} t_1)$. The best-fit parameters were $J = 8.760 \pm 0.001$ Hz and $R_{LLC} = 0.10 \pm 0.01\,\mathrm{s}^{-1}$. The amplitude of the continuous RF irradiation was 2.5 kHz. Each experiment was performed with 4 transients with a relaxation delay of 30 s. $J = 8.8$ Hz was obtained from a conventional 1D spectrum.

To obtain the optimal linewidth permitted by this method, one has to sample the indirect dimension as far as $t_1^{max} = 5 T_{LLC}$. The 2D spectrum in Fig. 7.3.1.2 (b), was recorded by undersampling the indirect dimension ($t_1^{max} = 50$ s with $N_1 = 200$ points and $\Delta t_1 = 250$ ms). The linewidth is only 60 mHz, unaffected by truncation. The spectral width was reduced to 2 Hz in the indirect dimension, so that the signal appeared at the (aliased) frequency $\nu_1 = 0.24$ Hz.
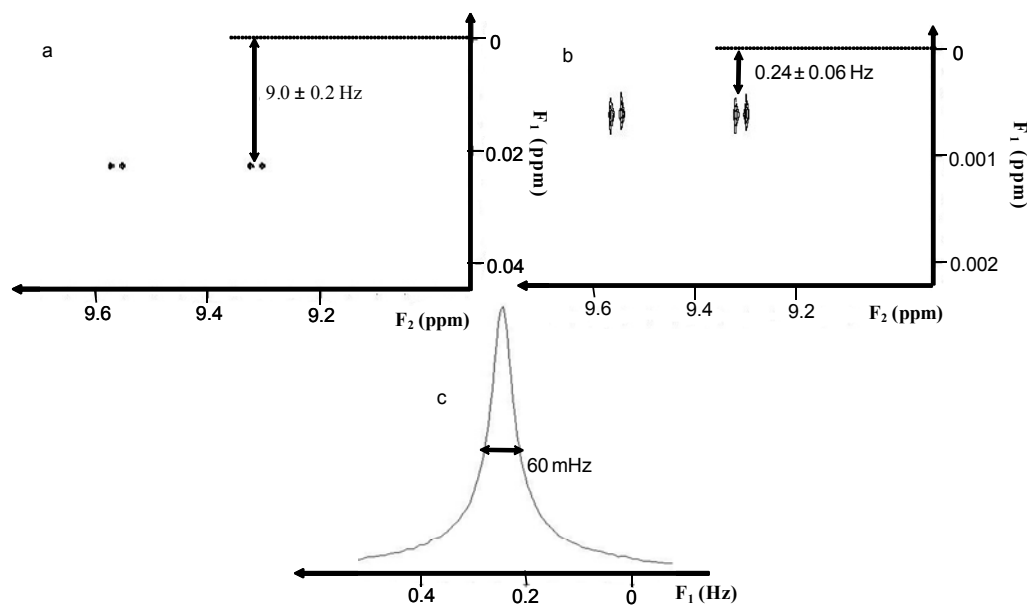
Figure 7.3.1.2 (a) 2D spectra of 2,3,6-trichlorophenol at 400 MHz, where the chemical shifts and doublets appear in the $\omega_2$ dimension and the $J$ coupling in the $\omega_1$ dimension. (b) Spectrum obtained with a spectral width reduced to 2 Hz in the $\omega_1$ dimension by under-sampling the $t_1$. The folded signals appear at a frequency of 0.24 Hz. Both 2D spectra were acquired in pure absorption mode using time-proportional phase increments (TPPI). (c) A column is extracted at $\omega_2 = 9.31$ ppm from spectrum. The linewidth is merely 60 mHz in the $\omega_1$ dimension.

## 7.3.2 LLC's in a protein

To determine LLC lifetimes in a protein, we used a sample of Ubiquitin dissolved in $D_2O$, where LLS were shown to exist in Gly-75 and Gly-76 (as described in section 5.2). Figs. 7.3.2.1(a) and (b) show the monoexponential decays from $R_{1\rho}$ experiment, and the oscillatory decay of an LLC experiment in Gly-76 of Ubiquitin. In the terminal residue Gly-76 of Ubiquitin, it was found that $\varepsilon = T_{LLC}/T_2 = 2.2$.[73]

The 2D experiment in Gly-76, performed with *Method I,* is shown in Fig. 7.3.2.1(c), where the full line-width at half-height of the signal was $\Delta \nu_{1/2} = 600$ mHz in the $\omega_1$ dimension.

Undersampling leads to spectral aliasing, but it is easy to correct for this effect and find that the aliased signal corresponds to $J = -17.17$ Hz.
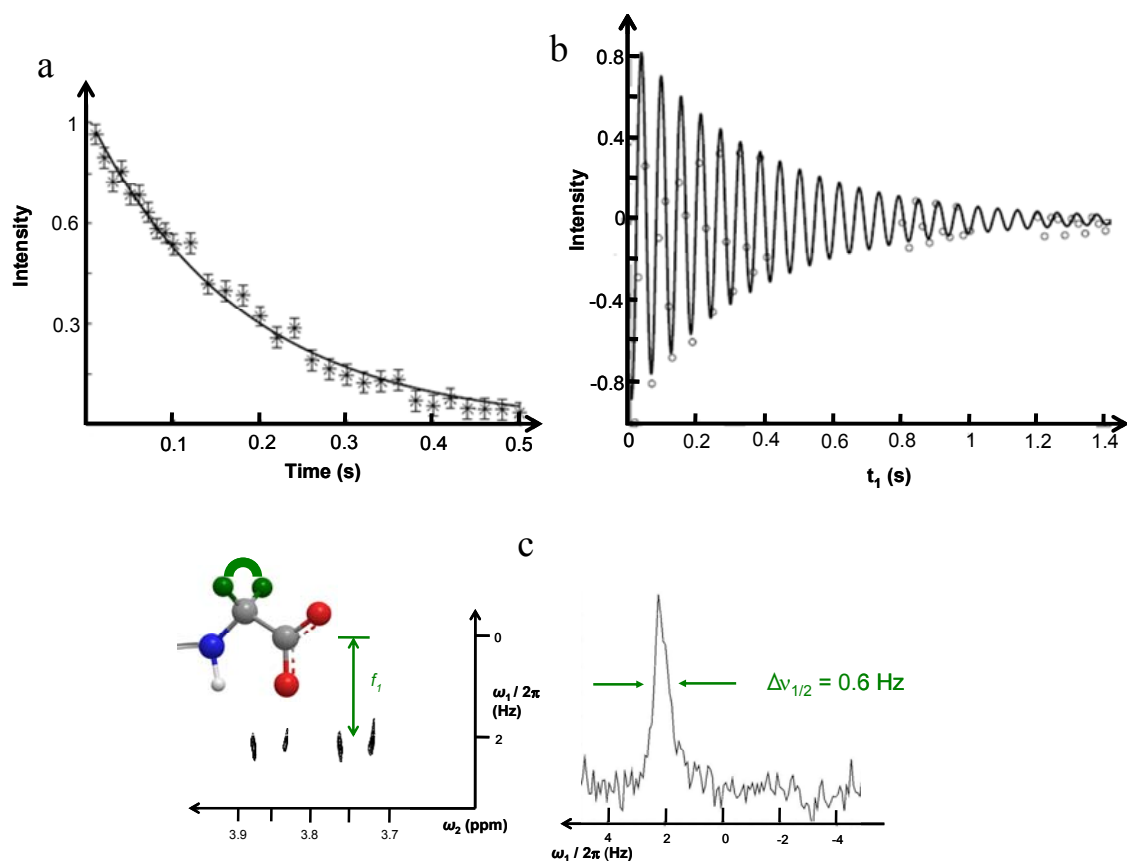
Figure 7.3.2.1 Excitation and observation of long-lived coherences (LLC's) in Gly-76 of Ubiquitin in high magnetic fields. (a) Experimental $T_{1\rho}$ decay of ordinary in-phase single-quantum coherences that are spin-locked by continuous-wave (CW) RF irradiation, yielding the homogeneous relaxation rate constant $R_{1\rho} = 1/ T_{1\rho} \approx R_2 = 1/ T_2 = 5.6$ s$^{-1}$, i.e., $T_2 = 180$ ms. (b) Oscillating signals (dots) due to the long-lived coherences (LLC's) obtained using *method I*. A fit to the function $I(t_1) = I_0 \cos(2\pi J_{IS} t_1) \exp(-R_{LLC} t_1)$ (solid line) yields $|J_{IS}| = 17.17 \pm 0.08$ Hz and $R_{LLC} = 2.5 \pm 0.7$ s$^{-1}$, i.e., $T_{LLC} = 400$ ms, yielding $T_{LLC}/T_2 = 2.2$. (c) (Left) 2D spectrum of the LLC comprising the two inequivalent protons $H_1^\alpha$ and $H_2^\alpha$ (green spheres) of the terminal amino acid Gly-76 in the protein Ubiquitin (molecular mass 7600 Da, correlation time $\tau_c = 4.5$ ns). The spectral window was reduced to 10 Hz in the $\omega_1$ dimension (shown only up to 3 Hz), so that the folded peaks appear at 2.17 Hz. (Right) Cross-section extracted from the 2D spectrum at $\omega_2 = 3.84$ ppm; the line-width in the $\omega_1$ dimension is 0.6 Hz.

### 7.3.3 Simultaneous excitation of several long-lived coherences (LLC's) in a protein

Fig. 7.3.3.1 shows 2D LLC spectrum of Gly-75 and 76 in Ubiquitin, obtained at 800MHz, using the double excitation method shown in Fig. 7.2.2.1 (*Method II*). The LLC's in G75 and G76 were also excited simultaneously in 1D fashion, but the filter was used *without* the selection of double quantum coherences, i.e., using the pulse sequence of *Method II* with only

Gradients and π-pulses. Fitting yielded modulation frequencies $v_1 = J = 17.00 \pm 0.02$ Hz for Gly-75 and $J = 17.20 \pm 0.01$ Hz for Gly-76. The relaxation rates were found to be $R_{LLC} = 2.6 \pm 0.1$ s$^{-1}$ for Gly-75 and $2.10 \pm 0.08$ s$^{-1}$ for Gly-76. These results were compared against standard, narrow-band LLC experiments in the manner of Fig. 7.2.1.1, performed separately for Gly-75 and 76. The agreement between the two methods was found to be satisfactory.
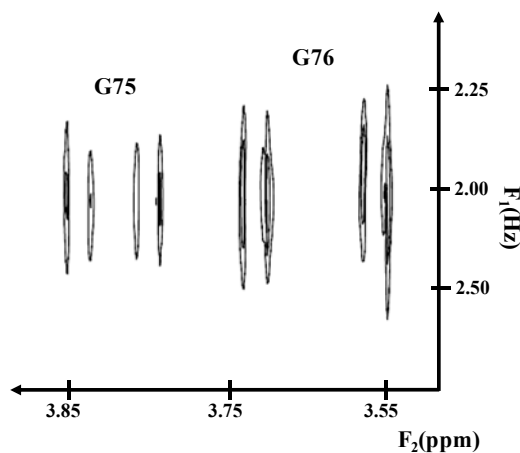


Figure 7.3.3.1 Simultaneous excitation and observation of two LLC's of the C-terminal Gly 75 and 76 residues in Ubiquitin: 2D LLC spectrum showing the signals arising from G75 and G76 at 800 MHz. The LLC's were sustained by a sequence of contiguous sinc pulses, each of 1.2 ms length with a peak amplitude of 2.5 kHz. The RF carrier was placed at the mean position between the four chemical shifts of the two residues. The π pulses for semi-selective inversion had a sinc shape, a length of 70 ms, and a peak RF amplitude of 40 Hz.

In brief, excitation of LLC's can lead to significant resolution enhancements in NMR spectroscopy, depending on the correlation times and could find their applications in assignments of proteins.

95

Chapter - 8

# Long-lived states of magnetization enhanced by *dissolution* Dynamic Nuclear Polarization

NMR spectroscopy is a major analytical technique because of the detailed information it can provide about structures, dynamics and interactions of biomolecules. Despite its many advantages, NMR suffers from poor sensitivity in comparison to other spectroscopic techniques. The reason behind the low sensitivity of NMR is the low magnetic energy of nuclear spins compared to the thermal energy at room temperature. Even the most sensitive nuclei, i.e., $^1$H, with 100 % natural abundance and a large gyromagnetic ratio, have a room-temperature polarization of 5 ppm in a magnetic field of 1.5 T, thus an improvement by a factor 200,000 is theoretically possible. For nuclei with low gyromagnetic ratios like $^{13}$C or $^{15}$N (1/4 for $^{13}$C and 1/10 for $^{15}$N compared to $^1$H), the theoretical enhancement factor is proportionately higher and can be even more beneficial because of the low natural abundance of the NMR-active isotope (1.1% for $^{13}$C and 0.36% for $^{15}$N). There have been significant technological advancements like introducing higher static magnetic fields and cooling the probe electronics in order to overcome this problem, which has made it possible to employ NMR successfully for structural determination and to study the dynamics of large biomolecules.

Sensitivity can be improved by coupling the nuclear Zeeman energy levels to other energy levels having larger separations. Many methods have been proposed to enhance the polarization of nuclear spins, e.g., optical pumping, para-hydrogen-induced polarization (PHIP) and dynamic nuclear polarization (DNP). Optical pumping is a technique which uses circularly-polarized light to polarize electronic spins of gaseous metal vapors. This enhances the nuclear spin polarization of noble gases through collision and spin exchange with gaseous

metal vapors. For $^{129}$Xe, an enhancement factor of $\approx 11{,}000$ compared to thermal equilibrium magnetization (at 9.4 T and $T = 298$ K ) has been observed by optical pumping, which corresponds to $\approx 10\%$ polarization.[77] In PHIP, *para*-hydrogen is inserted into a substrate molecule via catalytic hydrogenation. This method relies on the reduction of a double or triple bond in the molecule.[78]

DNP can enhance the nuclear polarization up to four orders of magnitude and was theoretically predicted by A. Overhauser in 1953.[79] Experimentally, it was demonstrated by T. R. Carver and C. Slichter when they detected a 100-fold increase in nuclear polarization, Li$^7$ in the solid state.[80] In our case, the technique requires the presence of unpaired electrons that are added to the sample in the form of an organic free radical like TEMPO and irradiating near electronic Larmor frequency so as to saturate the EPR transitions. The enhanced nuclear polarization can be utilized to carry out solid state NMR. This is done, in practice, by irradiating ESR transitions using gyrotrons in the same magnet where the NMR experiment is performed. This technique is known as *gyrotron* DNP and allows one to improve the signal-to-noise ratio by signal averaging or by recording multidimensional spectra, because the experiments can be repeated after a short time interval.[81]  DNP acquired rapid momentum for applications to routine liquid-state NMR experiments after J. H. Ardenkjaer-Larsen et. al. showed that a significant amount of polarization can be retained while the dynamically polarized solid sample is rapidly dissolved and transferred to an NMR magnet close to the polarizing magnet.[82] This technique has come to be known as *dissolution* DNP. For instance, in the case of urea, a maximum $^{13}$C polarization of 37% can be obtained after dissolution, yielding an enhancement of 44'000 compared to thermal equilibrium at 9.4 T and room temperature (RT). Dissolution DNP experiments are very useful, but they are expensive in terms of time and cryogenics, as the polarization requires several hours to build up. Enhanced magnetization obtained from these kinds of experiments should be utilized within $t < 5T_1$,

which makes it sensitive to *intrinsically short* spin-lattice relaxation lifetimes ($T_1$). The short lifetimes of the polarization is one of the most serious constraints in the application of the technique to various areas and has kept it limited to applications to low-$\gamma$ nuclei. The fact that spin order stored as LLS can last for time periods that are an order of magnitude longer than $T_1$, implies that it can be useful to store enhanced magnetization as LLS by reducing the constraint on the interval between polarization and NMR detection. LLS can be excited in diastereotopic $CH^{\alpha}_2$ protons of glycines in small peptides like Ala-Gly [45](as discussed in detail in section 5.1) and also in some amino acids like serine, aspartate, cysteine etc.[43] (as discussed in detail in section 4.3). In this chapter, the methods to store enhanced magnetization as LLS in various spin systems are discussed.

## 8.1 Long-lived states in a dipeptide via hyperpolarized carbon-13

It is favorable to store enhanced polarization on $^{13}C$ or $^{15}N$ nuclei while transferring the rapidly dissolved liquid sample to the NMR magnet, because they have longer $T_1$'s compared to protons. For instance, $T_1(^{15}N) \approx 189$ s in $(CD_3)_3{}^{15}N^+CH_2CH_2OH \cdot Cl^-$ in $D_2O$ can be used to preserve the enhanced polarization during the voyage, prior to transferring the magnetization from $^{15}N$ to $^1H$, via INEPT type experiments for detection, so as to benefit from better sensitivity of protons.[83] It is noteworthy that the obtained nuclear spin polarization may be partly converted into detectable magnetization so as to have an efficient utilization of the enhanced magnetization. Also, one can benefit in a similar way from single-scan 2D-NMR spectroscopy, in which the sample is virtually sliced by using pulsed filed gradients (PFG's).[84] In our case, natural-abundance $^{13}C$ in the dipeptide Ala-Gly was hyperpolarized and the magnetization of $^{13}CO$ of glycine was used to create LLS in $CH^{\alpha}_2$ protons of glycine.

*8.1.1 Methods*

The new experiment mainly consists of three steps (Fig. 8.1.1.1): (1) Hyperpolarization, consisting of polarizing the frozen beads of the sample in a home-built polarizer ($B_0 = 3.35$ T and $T = 1.2$ K) followed by dissolution with a burst of hot water and rapid transfer within 6s of the polarized sample to a high-resolution magnet (in our case, $B_0 = 7.05$ T and $T = 300$K); (2) INEPT-type transfer of the hyperpolarized magnetization from C-13 to protons; (3) Creation, sustaining and detection of LLS on protons.
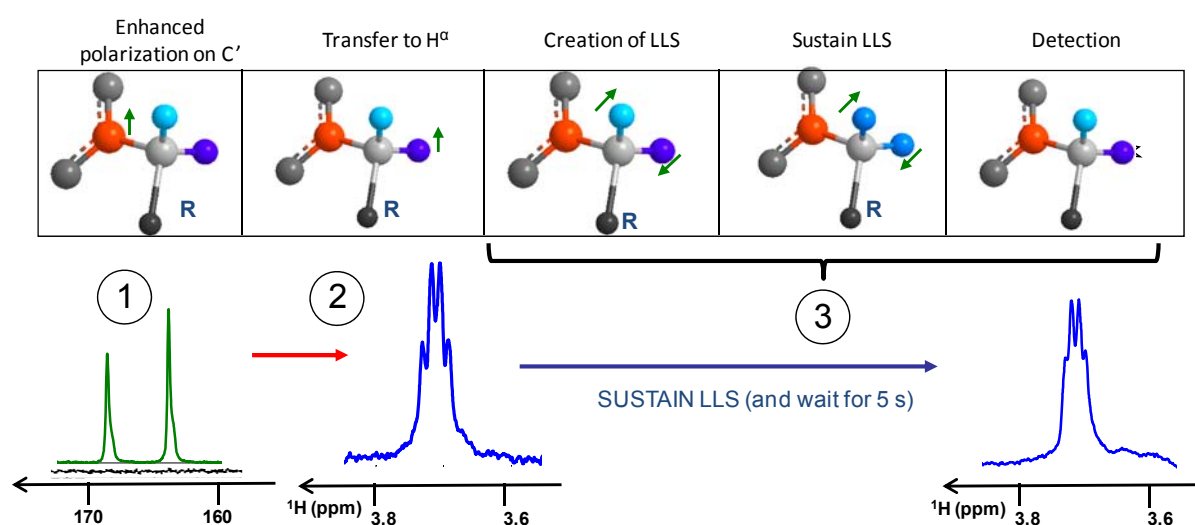


Figure 8.1.1.1. The DNP-LLS experiment: 1) Signal of hyperpolarized carbonyl $^{13}$C spins (highlighted in red) of Ala-Gly detected using a single 10° pulse (green trace) compared to a room-temperature spectrum (black trace) obtained by averaging 128 scans using 90° pulses; 2) Proton signals of the two Gly-H$^{\alpha}$ spins in Ala-Gly, after magnetization transfer from $^{13}$CO of Gly (in light and dark blue); 3) Conversion into an LLS involving inequivalent spins, sustaining of the LLS using WALTZ; detection of LLS: The same proton signals, following an interval $\tau_m = 5$ s where LLS are sustained.

The experiment described above was demonstrated on the dipeptide Ala-Gly. Natural-abundance $^{13}$C nuclei were hyperpolarized as described in ref. 86. The long $T_1$ of $^{13}$CO carbons of Gly allows one to transfer the polarized sample from the polarizer to the NMR magnet in 6 s while retaining a significant amount of polarization. The enhanced $^{13}$CO polarization is converted into antiphase proton magnetization, and then into LLS involving the diastereotopic CH$^{\alpha}_2$ of the Gly residue, sustaining them, and finally transformed back into

detectable magnetization. The pulse sequence is shown in Fig. 8.1.1.2 and consists of mainly two parts: *a) Pumping the polarization from $^{13}CO$ to the α-protons of glycine*, which can be done by using a refocused INEPT sequence for magnetization transfer from $^{13}C$ to $^{1}H$. A spin-echo $\tau_3$-$\pi$-$\tau_3$ is then inserted to evolve the magnetization under homonuclear *J*-coupling so as to have antiphase terms on $H^{\alpha 1}$ and $H^{\alpha 2}$ of glycine. *b) The long-lived states sequence*, which includes the conversion of antiphase terms of $H^{\alpha 1}$ and $H^{\alpha 2}$ to LLS, then sustaining the LLS for a period $\tau_m$ and converting it back to detectable magnetization, as described in detail in section 2.2.
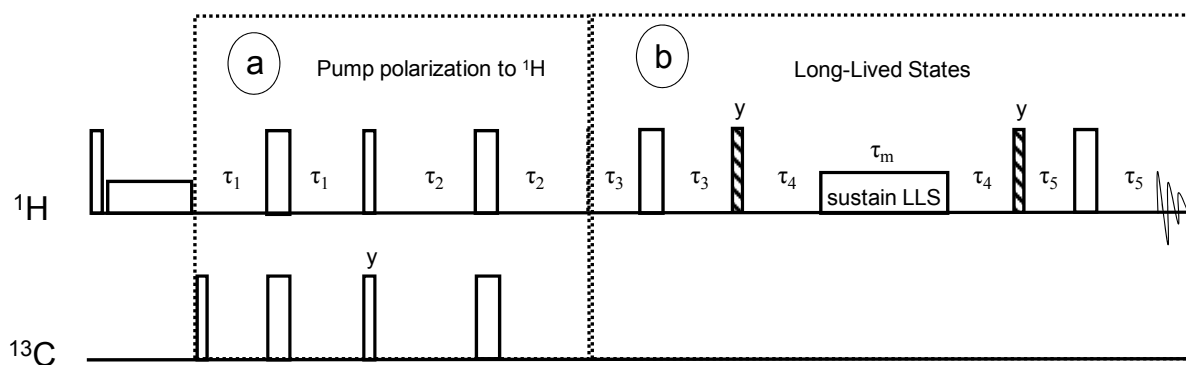


Figure 8.1.1.2. A. Pulse sequence for the DNP-LLS experiment used to transfer hyperpolarized natural abundance $^{13}C$ magnetization to the $CH^{\alpha}_2$ protons of Gly (a), excite and sustain LLS on these spins and transform this into detectable magnetization (b). Hatched, narrow and wide rectangles represent ($\pi$/4), ($\pi$/2), and $\pi$ pulses, respectively. The phases are given only when they differ from x. The delays were: $\tau_1 = 1/(8J_1) = 24$ ms, $\tau_2 = 1/(4J_1) = 48$ ms, $\tau_3 = 5/(4J_2) - \tau_2 = 24.3$ ms, $\tau_4 = 1/(2\Delta v_{IS}) = 13.4$ ms, and $\tau_5 = 1/(4J_2) = 14.5$ ms, where $J_1 = J(C^{'},H^{\alpha 1,2}) = 5.2$ Hz, $J_2 = J(H^{\alpha 1},H^{\alpha 2}) = -17.3$ Hz, and the chemical shift difference between the two diastereotopic protons $\Delta v_{IS} = 0.12$ ppm $= 37.2$ Hz at 7 Ts. The interval $\tau_m$ where LLS are sustained ranged from 4 to 25 s.

## 8.1.2 Results and Discussion

An enhancement factor of at least 7600 has been measured on $^{13}CO$ of Gly in Ala-Gly, which corresponds to a polarization $P = (P_\alpha - P_\beta)/(P_\alpha + P_\beta) \geq 5\%$. This lower limit is a rough estimate because of the poor signal to noise of the RT reference experiment of the same sample, consisting of Ala-Gly with natural abundance of $^{13}C$ isotope.

Each *dissolution*-DNP experiment yielded 2 to 5 mL of hyperpolarized solution. Rather than using the entire amount for one NMR experiment, several experiments with different mixing times, $\tau_m$ were carried out. The remainder of the hyperpolarized solution was stored in a container located immediately above the high-resolution NMR probe. As the polarization level is not identical from one experiment to the next, because of relaxation, the final proton signal intensities were normalized dividing them by the intensity of the enhanced $^{13}$C signal measured by direct $^{13}$C detection after a $10^0$ pulse. The ratio between the proton signal derived from the LLS and the $^{13}$C signal obtained in this manner was fitted to an exponential decay with three parameters.

Relaxation time constants $T_{LLS} = 16 \pm 0.6$ s and $T_1 = 2.3 \pm 0.2$ s were measured at 298 K and 7.05 T, in agreement with the value $T_{LLS} = 15 \pm 2$ s which was measured for a similar sample *without* DNP enhancement with same radical concentration (Fig. 8.1.2.1).

However, in the case of Ala-Gly in degassed $D_2O$, a value $T_{LLS} = 42.2 \pm 0.2$ s has been observed (discussed in section 5.1). Here, $T_{LLS}$ is shortened by dipolar interactions with radicals and paramagnetic species like $O_2$ in solution. Recently, we have found that these paramagnetic species can be quenched using sodium ascorbate.[85] This procedure improves both the polarization enhancement and lifetimes $T_{LLS}$. The $T_1$ of the transporter nucleus may be either shorter or longer than the $T_{LLS}$ of the protons. In the present case, $T_{LLS}(^1H)/T_1(^{13}C) = 0.63$ and $T_{LLS}(^1H)/T_1(^1H) = 7$ while in case of scalar coupled three-spin systems, for instance in serine, the $T_1$ of the transporter nucleus (i.e., $H^\beta$) is shorter by a factor of $\sim 2$ compared to the $T_{LLS}$ of long-lived states on side chain protons, which can be exploited for creating enhanced LLS using $^1H$-polarization. This will be discussed in the next section.
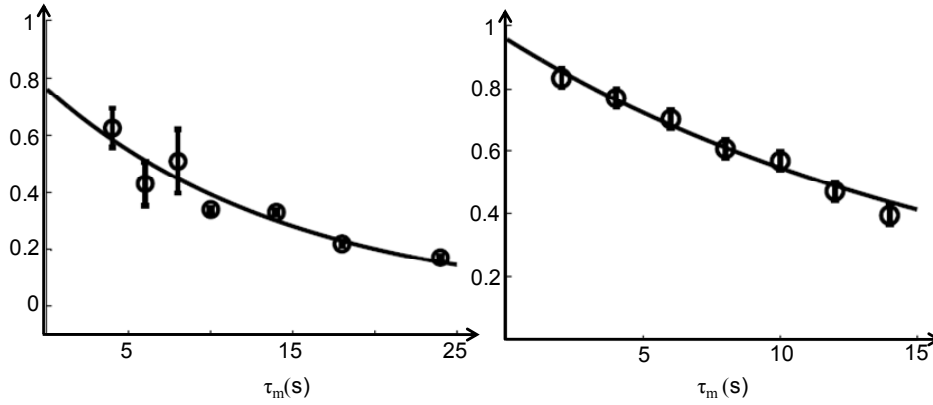
Figure 8.1.2.1. Experimental verification of the lifetimes of enhanced LLS with a room-temperature experiment. Fits of the exponential decay of a DNP-enhanced long-lived state of the two $H^{\alpha}$ protons in Gly yielding $T_{LLS} = 15 \pm 2$ s (left), and LLS decay obtained without DNP enhancement in a similar sample, yielding $T_{LLS} = 16 \pm 0.6$ s (right).

## 8.2 Enhanced long-lived states in multiple-spin systems using proton DNP

The applications of *dissolution* DNP to the most common nuclei, i.e., protons ($^1$H), are still explored to a very limited extent because of the short spin-lattice relaxation times ($T_1$) of these nuclei, irrespective of their fast polarization build up. The transfer from the DNP polarizer to the high-resolution NMR spectrometer (which requires typically 5 s in our laboratory) represents a major source of losses, since the polarization tends to decay during the transfer due to the spin lattice relaxation. This has kept applications of dissolution DNP mostly limited to low-γ nuclei with spin $I = \frac{1}{2}$ such as $^{13}$C,[86] $^{15}$N,[83] $^6$Li[87] and $^{89}$Y[88] because they have comparatively long spin lattice relaxation times $T_1$ in low fields.

The experiment combining both *dissolution* DNP and LLS, where the magnetization is transferred from a polarized carbonyl $^{13}$C (in natural abundance, as described in the previous section), tends to be cumbersome because the build-up of $^{13}$C spin polarization typically requires about an hour to achieve a polarization $P = (P_{\alpha} - P_{\beta})/(P_{\alpha} + P_{\beta}) = 10\%$. A nuclear polarization $P(^{13}\text{C}) = 10\%$ corresponds to an enhancement of about four orders of magnitude in comparison to the room temperature Boltzmann distribution $P(^{13}\text{C}) = 0.6 \times 10^{-5}$ at 300 K in a 300 MHz spectrometer. However, if the transfer of the magnetization to protons starts from

$^{13}$C in natural abundance (ca. 1%), the net enhancement of the protons (compared to 100 % abundant protons with a room temperature Boltzmann polarization P($^1$H) = 2.5×10$^{-5}$ at 300 K and 7.05 T) is only a factor 40. The net enhancement can of course be improved by $^{13}$C isotope labeling of the molecule under investigation, but this short-cut is not always possible. In this section, we show how enhanced long-lived proton states can be excited directly from hyperpolarized protons, without taking recourse to any dilute low-γ 'transporter spins' such as $^{13}$C. We start with a *proton* nuclear spin polarization enhanced to about $P(^1\text{H}) = 40\%$ by DNP, which can be achieved in a time as short as 10 minutes at 1.5 K and 3.35 T. This does not require any isotope labeling and leads to a better enhancement factor for direct proton DNP-LLS experiments, compared to previously reported indirect carbon-13/proton DNP-LLS experiments.

*8.2.1 Results and Discussion*

A challenging system with three scalar-coupled protons was used to illustrate the potential of the new experiments. In acrylic acid (CH$^\text{I}$H$^\text{R}$=CH$^\text{S}$COOH) dissolved in D$_2$O (Fig. 8.2.1.1), long-lived states (LLS) delocalized over the three protons H$^\text{I}$, H$^\text{R}$ and H$^\text{S}$ can have a lifetime $T_{LLS}$ = 52 s with a ratio $T_{LLS}/T_1$ = 2.7, provided paramagnetic species, i.e., stable radicals such as TEMPO and dissolved molecular oxygen are reduced to a significant extent.[43]
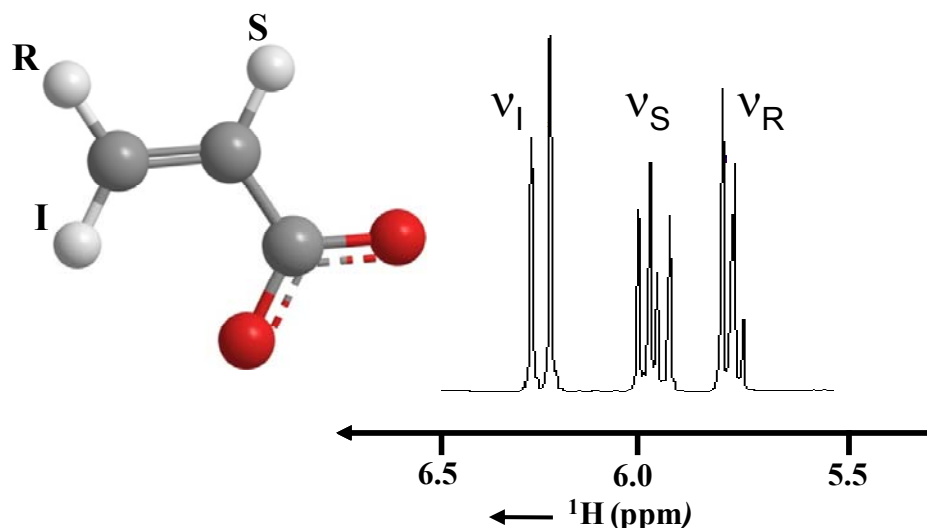
Figure 8.2.1.1. The labeling of the three protons in acrylic acid and the conventional proton spectrum at 500 MHz ($B_0$ = 11.75 T) and 298 K. The three protons $H^I$, $H^S$, and $H^R$ are coupled by $J_{IS}$ = 17.3, $J_{IR}$ = 1.4, and $J_{SR}$ = 10.4 Hz.

To carry out the experiment, frozen beads of acrylic acid mixed with a free-radical such as TEMPOL, are polarized in a home-built polarizer and then rapidly dissolved with hot water vapor, prior to the transfer to NMR spectrometer. Under the present experimental conditions, $T_1(H^S)$ = 12 s is much longer than the other two protons in acrylic acid, $T_1(H^{I,R})$ = 5 s, by virtue of the internuclear distances between the three protons. Therefore, Proton $H^S$ retains maximum polarization as it suffers the least during the voyage, featuring an enhancement factor $\varepsilon$ = 1000 or more compared to room temperature polarization as shown in Fig. 8.2.1.2.

Figure 8.2.1.2. Enhanced spectrum (red) of hyperpolarized acrylic acid obtained immediately after rapid dissolution. The free induction decay was excited with a 10° pulse. The conventional spectrum (blue) obtained at room temperature under similar conditions with a 10° pulse (x 100). An enhancement factor $\varepsilon = 1000$ is observed for H$^S$ in the central region.
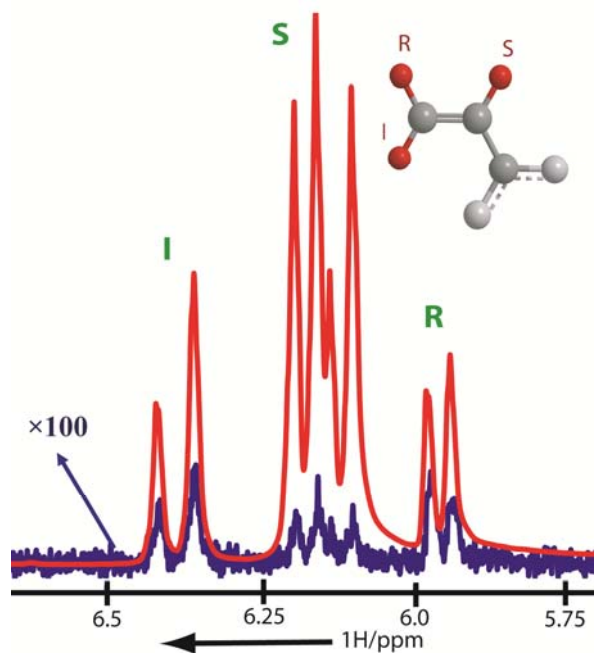
Enhanced H$^S$ magnetization is then stored in the form of LLS by using the pulse sequence shown in Fig. 8.2.1.3. The pulse sequence consists of two parts: *i) A coherence transfer sequence,* which converts the enhanced H$^S$ magnetization to in-phase magnetization of H$^I$ and H$^R$, and *ii) An LLS sequence,* which includes the excitation and sustaining of an operator $Q^{ISR}$, then transforming it back to detectable magnetization.

The delays in the pulse sequence have been optimized numerically to achieve the largest possible coefficient of the delocalized long-lived state described by a linear combination of operator products of the form:

$$Q_l^{ISR} = \frac{1}{\sqrt{3}} \left( \lambda_{IS} \vec{I} \cdot \vec{S} + \lambda_{IR} \vec{I} \cdot \vec{R} + \lambda_{SR} \vec{S} \cdot \vec{R} \right)$$

(8.2.1.1)

where $\lambda_{IS} = -0.23$, $\lambda_{IR} = 0.93$, and $\lambda_{SR} = 0.28$ for acrylic acid.
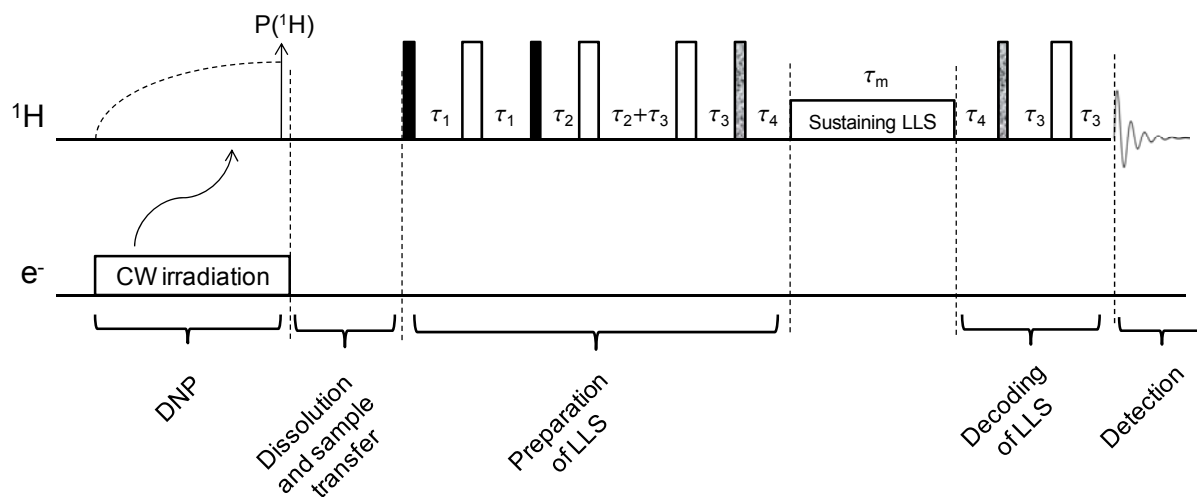
Figure 8.2.1.3. The pulse sequence used for creating delocalized LLS in acrylic acid, starting with a hyperpolarized proton $H^S$, with a transfer of magnetization from $H^S$ to $H^I$ and $H^R$ followed by the excitation of a long-lived state described by Eq. (8.2.1.1).

The delocalized long-lived state in Eq. (8.2.1.1) is sustained for a mixing time $\tau_m$ using a suitable RF scheme. The resultant proton signal intensities from each experiment are normalized by dividing by the signal intensity of enhanced $H^S$, measured in a preliminary experiment with a $10^0$ pulse, so as to account for differences in enhancement in various experiments. Mono-exponential decays were obtained with $T_{LLS} = 51 \pm 4$ s (Fig. 8.2.1.4) when the sum of the normalized intensities were fitted. In the experiments carried out under similar conditions at room temperature *without* DNP, a value $T_{LLS} = 42 \pm 2$ s was obtained (Fig. 8.2.1.4).
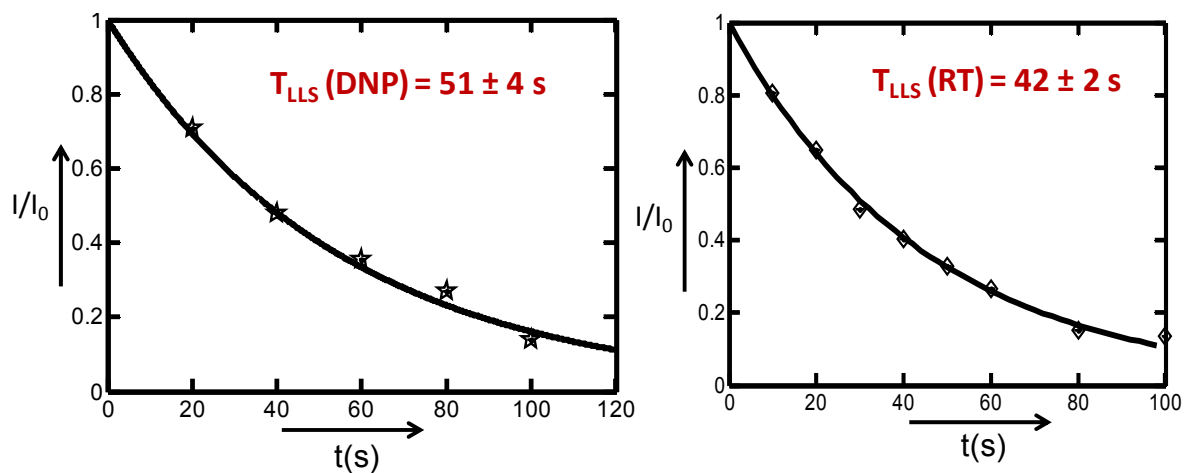
Figure 8.2.1.4. Fits of exponential decays of DNP-enhanced long-lived states on the two protons $H^I$ and $H^R$ in acrylic acid with $T_{LLS}$ (DNP) = 51 ± 4 s (Left). $T_{LLS}$ (RT) = 42 ± 2 s was obtained from the room temperature (RT) experiments under similar conditions (Right).

It is noteworthy that similar enhanced long-lived states can be excited in some common amino acids like serine, cysteine, aspartate, etc. where states with long lifetimes are also described by linear combinations of product operators.[43]  In the case of serine, which has a side-chain $HOC^\beta H_2-HC^\alpha-$, we have observed an enhancement factor $\varepsilon$ = 350 for the isolated proton ($H^\alpha$) because it has a shorter $T_1$ compared to the proton $H^R$ in acrylic acid. Here, TEMPOL was quenched by sodium ascorbate (Vitamin C) by mixing the frozen beads containing serine and TEMPOL, with equal number of frozen beads of 3 M sodium ascorbate prior to polarization.[85]  During the dissolution process, all beads melt rapidly, leading to the mixing of both solutions and rapidly quenching the TEMPOL radical by ascorbate.

In brief, newly designed methods by combining LLS with *dissolution* DNP allows one to store enhanced magnetization for lifetimes $T_{LLS}$ that can be significantly longer than $T_1$.

## 8.3 Experimental Details

The experiments were performed using frozen beads of 0.6 M L-Ala-Gly mixed with 50 mM TEMPO, dissolved in 5 ml 35 % / 65 % v/v glycerol-$d_8$ / $D_2O$ (or 1 M acrylic acid mixed with 50 mM 2, 2, 6, 6-tetramethylpiperidine-1, 4-diol **(**TEMPOL**)** in 50 % / 50 % *v/v* $CD_3OD$ / $D_2O$). The frozen beads were placed in a home-built prepolarizer, and irradiated at 94 GHz and 30 mW for 5 hours for Ala-Gly (or 20 mins for acrylic acid) at 1.2 K and 3.35 T. The sample was dissolved in 5 ml $D_2O$ (preheated to 190 °C at 12 bar) to a final concentration of 50 mM of Ala-Gly (or 8mM for Acrylic acid). The hyperpolarized solution was transferred to 10 mm (or 5mm for Acrylic acid) tubes maintained at a temperature of 25 °C in an inverse broadband probe in a high-resolution $B_0 = 7.05$ T magnet (Bruker 300 WB). The transfer time was 6 s. Two experiments were carried out on each hyperpolarized sample: i) A reference experiment with a $10^0$ pulse. ii) An LLS experiment which includes the transfer of the enhanced magnetization to the relevant protons, excitation of LLS and Detection. A WALTZ sequence with an *rf* amplitude $\nu_l = 2$ kHz was used to sustain LLS.

The room-temperature experiments using nuclear polarization at Boltzmann equilibrium were carried out at 300 MHz and 298 K using ~ 20 mM Ala-Gly (or 8mM for Acrylic acid) solutions in deuterated water. Eight transients were acquired for each LLS experiment using a delay of 30 s between consecutive experiments. Experimental relaxation time constants $T_1$ and $T_{LLS}$ were determined by fitting normalized spectral intensities to mono-exponentially decaying functions.

# Chapter - 9

# Conclusions and Outlook

## 9.1 Conclusions

This thesis discusses various advancements in long-lived states (LLS) spectroscopy and demonstrates applications to biomolecules for exploring slow dynamic processes.

Various methods to excite LLS and sustain them efficiently have been described. Broadband excitation of LLS is made possible by the use of Thrippleton-Keeler filters and 2D spectroscopy. The 2D LLS-EXSY sequence is suitable for studying two- (or multiple-) site chemical exchange, where the involved spins have different chemical shifts and scalar couplings in various sites. The 2D LLS-EXSY method has been applied to monitor the slow ring flip in Tyr-35 of BPTI. LLS can be sustained over a wide range of offsets (as high as 8 kHz at 600 MHz) using various decoupling sequences, thus making the sequences broadband during the sustaining period. 1D broadband sequences can also be designed to excite LLS in samples featuring a distribution of *J*-coupling constants. This allows the simultaneous determination of slow diffusion coefficients of several slowly-diffusing species, or in mixtures where slowly- and rapidly-diffusing species co-exist. These methods can also be used for the simultaneous determination of relaxation rates $R_{LLS} = 1/T_{LLS}$ of LLS in various environments.

Long-lived spin states can be obtained in small molecules of biological interest, e.g., in several amino acids, taurine and glycerol. The structure of these states was discussed to show how they can be excited and sustained. For most of these molecules, an improvement in spin memory $T_{LLS}/T_1^{max} \approx 2$ is obtained. These findings constitute first steps on the way to the study of slow dynamic phenomena by LLS spectroscopy in molecules containing extended networks of coupled spins.

The LLS associated with diastereotopic proton pairs in small peptides and mobile parts of proteins can have long lifetimes, provided that the nuclei involved are isolated to some extent from other spins with high gyromagnetic ratios. This discovery opens the way to measuring diffusion coefficients of macromolecules using NMR with pulsed field gradients (PFG's) with moderate strengths and durations, thus allowing one to study the diffusion of large, unfolded, intrinsically unstructured proteins, or biomolecular complexes, even in the absence of assignment.[89] $T_{LLS}$ values are more sensitive than $T_1$ values to DD interactions with external spins,[60] which make them a good probe for internal motions in natively unstructured or denatured proteins. The discovery of LLS in peptides can be useful to study the dynamics of peptide binding to receptors.[90]

LLS lifetimes, being more sensitive to structural changes than $T_1$ or $T_2$, can be used as a probe to study unfolding of proteins. We investigated the unfolding of Ubiquitin by addition of urea and by pH changes and could detect destabilized conformer whose population is dependent on the urea concentration. This conformer has the H-bonds between β1-β5 sheets destabilized by urea and also has structural similarities with two mutants of Ubiquitin, L69S and L67S.

LLC's offer a means to obtain spectra featuring line-widths $\Delta\nu_{LLC}$ that can be a factor 3 narrower than in spectra of ordinary single-quantum coherences (SQC's) of small molecules. In the slow motion limit (for large molecules), the improvement in line-widths can in principle be a factor 9 in favorable cases. The enhancement in resolution obtained from LLC's may open the way to structural and dynamic NMR studies of macromolecules with a molecular mass that is almost an order of magnitude higher than the current limit.

We introduced a method to enhance LLS in a dipeptide Ala-Gly, using *dissolution* DNP. The novel experiment alleviates one of the major drawbacks of *dissolution* DNP experiments, i.e., the requirement that the enhanced polarization must be used within time interval shorter than $5T_1$. We also demonstrated detection of hyperpolarized protons using *dissolution* DNP with

significant enhancement factors. The use of protons has numerous advantages over the use of low-gamma nuclei such as ^{13}C or [15]N: 100% natural abundance of the detected nuclei, the sensitivity of their Larmor frequency to chemical changes (for studies of metabolic transformations), and the short polarizing time.

**9.2 Outlook**

Applications of long-lived states (LLS) and long-lived coherences (LLC's) have been demonstrated for **Gly-**residues located on the mobile *C*-terminus of **Ubiquitin**. Also, LLS have been observed in a series of amino acids such as **Serine**, **Aspartic Acid**, etc. Though LLS have lifetimes longer than $T_1$ in these favorable sytems, in residues buried inside the core of Ubiquitin they decay with lifetime constants that are similar to the spin-lattice relaxation times ($T_{LLS} \sim T_1$) because of the dipolar interactions with external protons. Having proton pairs of these amino acids inserted in deuterated proteins should make it possible to achieve better LLS lifetimes ($T_{LLS}$).

There are various deuteration techniques available which allow one to attain selective isotope labeling of proteins. For instance, deuterated proteins containing only aromatic protons in **Phe**, **Tyr**, and **Trp** can be expressed by prior addition of the aromatic amino acid precursor **Shikimic Acid** to fully deuterated media.[91] Also, some specific positions in the sidechains of **Isoleucine, Leucine and Valin**e residues can be protonated if the respective isotopomers of the precursors **α-Ketoisovaleric Acid** and **α-Ketobutyric Acid** are added to the media for the expression of deuterated proteins.[92-93] LLS may be excited for protons of these residues, making it possible to investigate slow dynamics in proteins. The excitation of LLC's, which offer significant resolution enhancement for big proteins, can be of use for assignments.

The new DNP-LLS experiments open avenues that can be explored in various contexts. They may find applications for the study of biochemical reactions that are slow on the NMR time

scale. LLS enhanced by DNP in a peptide may find applications in studies of peptides binding to receptors. The use of *enhanced long-lived proton* magnetization circumvents the requirement of isotope labeling, thus making it applicable to common molecules. This method is also applicable to a wide range of systems of *J*-coupled protons and is promising for the study of slow biochemical reactions.

# References

(1)    Boehr, D. D.; Dyson, H. J.; Wright, P. E. *Chem. Rev.* **2006**, *106*, 3055.

(2)    Kay, L. E.; Torchia, D. A.; Bax, A. *Biochemistry* **1989**, *28*, 8972.

(3)    Farrow, N. A.; Muhandiram, R.; Singer, A. U.; Pascal, S. M.; Kay, C. M.; Gish, G.; Shoelson, S. E.; Pawson, T.; Formankay, J. D.; Kay, L. E. *Biochemistry* **1994**, *33*, 5984.

(4)    Lipari, G.; Szabo, A. *J. Am. Chem. Soc.* **1982**, *104*, 4546.

(5)    Carr, H. Y.; Purcell, E. M. *Phys. Rev.* **1952**, *88*, 415.

(6)    Meiboom, S.; Gill, D. *Rev. Sci. Instrum.* **1958**, *29*, 688.

(7)    Deverell, C.; Morgan, R. E.; Strange, J. H. *Mol. Phys.* **1970**, *18*, 553.

(8)    Palmer, A. G. *Chem. Rev.* **2004**, *104*, 3623.

(9)    Cavadini, S.; Dittmer, J.; Antonijevic, S.; Bodenhausen, G. *J. Am. Chem. Soc.* **2005**, *127*, 15744.

(10)    Wenter, P.; Bodenhausen, G.; Dittmer, J.; Pitsch, S. *J. Am. Chem. Soc.* **2006**, *128*, 7579.

(11)    Sarkar, P.; Reichman, C.; Saleh, T.; Birge, R. B.; Kalodimos, C. G. *Mol. Cell* **2007**, *25*, 413.

(12)    Wagner, G.; Bodenhausen, G.; Muller, N.; Rance, M.; Sorensen, O. W.; Ernst, R. R.; Wuthrich, K. *J. Am. Chem. Soc.* **1985**, *107*, 6440.

(13)    Ferrage, F.; Zoonens, M.; Warschawski, D. E.; Popot, J. L.; Bodenhausen, G. *J. Am. Chem. Soc.* **2003**, *125*, 2541.

(14)    Carravetta, M.; Johannessen, O. G.; Levitt, M. H. *Phys. Rev. Lett.* **2004**, *92,* 153003.

(15)    Carravetta, M.; Levitt, M. H. *J. Am. Chem. Soc.* **2004**, *126*, 6228.

(16)    Sarkar, R.; Vasos, P. R.; Bodenhausen, G. *J. Am. Chem. Soc.* **2007**, *129*, 328.

(17)    Pileio, G.; Carravetta, M.; Hughes, E.; Levitt, M. H. *J. Am. Chem. Soc.* **2008**, *130*, 12582.

(18)    Ahuja, P.; Sarkar, R.; Vasos, P. R.; Bodenhausen, G. *J. Chem. Phys.* **2007**, *127,* 134112.

(19)    Gopalakrishnan, K.; Bodenhausen, G. *J. Magn. Reson.* **2006**, *182*, 254.

(20)    Pileio, G.; Levitt, M. H. *J. Chem. Phys.* **2009**, *130*, 214501.

(21)    Carravetta, M.; Levitt, M. H. *J. Chem. Phys.* **2005**, *122*, 164502.

(22)    Thrippleton, M. J.; Keeler, J. *Angew. Chem. Int. Ed.* **2003**, *42*, 3938.

(23)    Sarkar, R.; Ahuia, P.; Moskau, D.; Vasos, P. R.; Bodenhausen, G. *ChemPhysChem* **2007**, *8*, 2652.

(24)    Shaka, A. J.; Keeler, J.; Frenkiel, T.; Freeman, R. *J. Magn. Reson.* **1983**, *52*, 335.

(25)    Temps, A. J.; Brewer, C. F. *J. Magn. Reson.* **1984**, *56*, 355.

(26)    Fu, R.; Bodenhausen, G. *Chem. Phys. Lett.* **1995**, *245*, 415.

(27)    Garwood, M.; Ke, Y. *Journal of Magnetic Resonance* **1991**, *94*, 511.

(28)    Barbara, T. M.; Tycko, R.; Weitekamp, D. P. *J. Magn. Reson.* **1985**, *62*, 54.

(29)    Levitt, M. H.; Freeman, R. *J. Magn. Reson.* **1981**, *43*, 502.

(30)    Levitt, M. H. *J. Magn. Reson.* **1982**, *48*, 234.

(31)    Wimperis, S.; Bodenhausen, G. *J. Magn. Reson.* **1986**, *69*, 264.

(32)    Sarkar, R.; Ahuja, P.; Vasos, P. R.; Bodenhausen, G. *ChemPhysChem* **2008**, *9*, 2414.

(33)    *Prog. Nucl. Magn. Reson. Spectrosc.*Johnson, C. **1998**, *34*, 203.

(34)    Cavanagh, J.; Fairbrother, W. J.; Palmer, A. G.; Skelton, N. J. *Protein NMR Spectroscopy: Principles and Practice, Elsevier Science* **1996**.

(35)    Goldman, M. *Quantum Descrption of High Resolution NMR in Liquids*; Oxford University Press, 1990.

(36)    Smith, S. A.; Levante, T. O.; Meier, B. H.; Ernst, R. R. *J. Magn. Reson. Ser. A* **1994**, *106*, 75.

(37)    Pileio, G.; Concistre, M.; Carravetta, M.; Levitt, M. H. *J. Magn. Reson.* **2006**, *182*, 353.

(38)    Vinogradov, E.; Grant, A. K. *J. Magn. Reson.* **2008**, *194*, 46.

(39)    Grant, A. K.; Vinogradov, E. *J. Magn. Reson.* **2008**, *193*, 177.

(40)    Canet, D.; Bouguet-Bonnet, S.; Aroulanda, C.; Reineri, F. *J. Am. Chem. Soc.* **2007**, *129*, 1445.

(41)    Vinogradov, E.; Grant, A. K. *J. Magn. Reson.* **2007**, *188*, 176.

(42)    Pileio, G.; Levitt, M. H. *J. Magn. Reson.* **2007**, *187*, 141.

(43)    Ahuja, P.; Sarkar, R.; Vasos, P. R.; Bodenhausen, G. *ChemPhysChem* **2009**, *10*, 2217.

(44)    Kumar, A.; Rao, B. D. N. *Mol. Phys.* **1968**, *15*, 377.

(45)    Ahuja, P.; Sarkar, R.; Vasos, P. R.; Bodenhausen, G. *J. Am. Chem. Soc.* **2009**, *131*, 7498.

(46)    Sangappa; Mahesh, S. S.; Somashekar, R. *J. Biosc.* **2005**, *30*, 259.

(47)    Dingley, A. J.; Mackay, J. P.; Shaw, G. L.; Hambly, B. D.; King, G. F. *J. Biomol. NMR* **1997**, *10*, 1.

(48)    Vijaykumar, S.; Bugg, C. E.; Cook, W. J. *J. Mol. Biol.* **1987**, *194*, 531.

(49)    Cavadini, S.; Vasos, P. R. *Conc. Magn. Reson.* **2008**, *32A*, 68.

(50)    Dobson, C. M.; Karplus, M. *Curr. Opin. Struct. Biol.* **1999**, *9*, 92.

(51)    Fersht, A. R.; Daggett, V. *Cell* **2002**, *108*, 573.

(52)    Ibarra-Molero, B.; Loladze, V. V.; Makhatadze, G. I.; Sanchez-Ruiz, J. M. *Biochemistry* **1999**, *38*, 8138.

(53)    Haririnia, A.; Verma, R.; Purohit, N.; Twarog, M. Z.; Deshaies, R. J.; Bolon, D.; Fushman, D. *J. Mol. Biol.* **2008**, *375*, 979.

(54)    Weber, P. L.; Brown, S. C.; Mueller, L. *Biochemistry* **1987**, *26*, 7282.

(55)    Schanda, P.; Forge, V.; Brutscher, B. *Proc. Nat. Acad. Sci. U.S.A.* **2007**, *104*, 11257.

(56)    Brutscher, B.; Bruschweiler, R.; Ernst, R. R. *Biochemistry* **1997**, *36*, 13043.

(57)    Cordier, F.; Grzesiek, S. *J. Am. Chem. Soc.* **1999**, *121*, 1601.

(58)    Krishnan, A.; Giuliani, A.; Zbilut, J. P.; Tomita, M. *Plos One* **2008**, *3*.

(59)    Das, A.; Mukhopadhyay, C. *J. Chem. Phys.* **2007**, *127*.

(60)    Tayler, M. C. D.; Marie, S.; Ganesan, A.; Levitt, M. H. *J. Am. Chem. Soc.* **2010**, *132*, 8225.

(61)    Peti, W.; Smith, L. J.; Redfield, C.; Schwalbe, H. *J. Biomol. NMR* **2001**, *19*, 153.

(62)    Davis, D. G.; Bax, A. *J. Am. Chem. Soc.* **1985**, *107*, 2820.

(63)    Peng, J. W.; Thanabal, V.; Wagner, G. *J. Magn. Reson.* **1991**, *94*, 82.

(64)    Pelupessy, P.; Rennella, E.; Bodenhausen, G. *Science* **2009**, *324*, 1693.

(65)    Goldman, M. *J. Magn. Reson.* **1984**, *60*, 437.

(66)    Shimizu, H. *J. Chem. Phys.* **1964**, *40*, 3357.

(67)    Mackor, E. L.; MacLean, C. *J. Chem. Phys.* **1966**, *44*, 64.

(68)    Wimperis, S.; Bodenhausen, G. *Chem. Phys. Lett.* **1987**, *140*, 41.

(69)    Wimperis, S.; Bodenhausen, G. *Mol. Phys.* **1989**, *66*, 897.

(70)    Wimperis, S.; Bodenhausen, G. *Chem. Phys. Lett.* **1987**, *140*, 41.

(71)    Pervushin, K.; Riek, R.; Wider, G.; Wuthrich, K. *Proc. Natl. Acad. Sci. U. S. A.* **1997**, *94*, 12366.

(72)     Tugarinov, V.; Hwang, P. M.; Ollerenshaw, J. E.; Kay, L. E. *J. Am. Chem. Soc.* **2003**, *125*, 10420.

(73)     Sarkar, R.; Ahuja, P.; Vasos, P. R.; Bodenhausen, G. *Phys. Rev. Lett.* **2010**, *104,* 053001.

(74)     Sarkar, R.; Ahuja, P.; Vasos, P. R.; Bornet, A.; Wagnières, O.; Bodenhausen, G. *Prog. Nucl. Magn. Reson. Spectrosc., Accepted.*

(75)     Pileio, G.; Carravetta, M.; Levitt, M. H. *Phys. Rev. Lett.* **2009**, *103,* 083002.

(76)     Bornet, A.; Sarkar, R.; Bodenhausen, G. *J. Magn. Reson.* **2010,** *206*, 154.

(77)     Goodson, B. M. *J. Magn. Reson.* **2002**, *155*, 157.

(78)     Overhauser, A. W. *Phys. Rev.* **1953**, *92*, 411.

(79)     Bowers, C. R.; Weitekamp, D. P. *J. Am. Chem. Soc.* **1987**, *109*, 5541.

(80)     Carver, T. R.; Slichter, C. P. *Phys. Rev.* **1956**, *102*, 975.

(81)     Becerra, L. R.; Gerfen, G. J.; Temkin, R. J.; Singel, D. J.; Griffin, R. G. *Phys. Rev. Lett.* **1993**, *71*, 3561.

(82)     Ardenkjaer-Larsen, J. H.; Fridlund, B.; Gram, A.; Hansson, G.; Hansson, L.; Lerche, M. H.; Servin, R.; Thaning, M.; Golman, K. *Proc. Natl. Acad. Sci. U. S. A.* **2003**, *100*, 10158.

(83)     Sarkar, R.; Comment, A.; Vasos, P. R.; Jannin, S.; Gruetter, R.; Bodenhausen, G.; Hall, H.; Kirik, D.; Denisov, V. P. *J. Am. Chem. Soc.* **2009**, *131*, 16014.

(84)     Frydman, L.; Scherf, T.; Lupulescu, A. *Proc. Natl. Acad. Sci. U. S. A.* **2002**, *99*, 15858.

(85)     Mieville, P.; Ahuja, P.; Sarkar, R.; Jannin, S.; Vasos, P. R.; Gerber-Lemaire, S.; Mishkovsky, M.; Comment, A.; Gruetter, R.; Ouari, O.; Tordo, P.; Bodenhausen, G. *Angew. Chem. Int. Ed. Engl.* **2010**, *49*, 6182.

(86)     Comment, A.; van den Brandt, B.; Uffmann, K.; Kurdzesau, F.; Jannin, S.; Konter, J. A.; Hautle, P.; Wenckebach, W. T. H.; Gruetter, R.; van der Klink, J. J. *Conc. Magn. Reson. Part B* **2007**, *31B*, 255.

(87)     van Heeswijk, R. B.; Uffmann, K.; Comment, A.; Kurdzesau, F.; Perazzolo, C.; Cudalbu, C.; Jannin, S.; Konter, J. A.; Hautle, P.; van den Brandt, B.; Navon, G.; van der Klink, J. J.; Gruetter, R. *Magn. Reson. Med.* **2009**, *61*, 1489.

(88)     Mieville, P.; Jannin, S.; Helm, L.; Bodenhausen, G. *J. Am. Chem. Soc.* **2010**, *132*, 5006.

(89)     Dyson, H. J.; Wright, P. E. *Nat. Rev. Mol. Cell Biol.* **2005**, *6*, 197.

(90)    Edwards, C. M. B.; Cohen, M. A.; Bloom, S. R. *Qjm-an Int. J. Med.* **1999**, *92*, 1.

(91)    Rajesh, S.; Nietlispach, D.; Nakayama, H.; Takio, K.; Laue, E. D.; Shibata, T.; Ito, Y. *J. Biomol. NMR* **2003**, *27*, 81.

(92)    Lichtenecker, R.; Ludwiczek, M. L.; Schmid, W.; Konrat, R. *J. Am. Chem. Soc.* **2004**, *126*, 5348.

(93)    Sibille, N.; Hanoulle, X.; Bonachera, F.; Verdegem, D.; Landrieu, I.; Wieruszeski, J. M.; Lippens, G. *J. Biomol. NMR* **2009**, *43*, 219.

# *Curriculum Vitae*

## Puneet Ahuja

Date of Birth: 08th September, 1983

Nationality: Indian

Contact: [puneet.ahuja@epfl.ch,](puneet.ahuja@epfl.ch)

[antarnad@gmail.com](antarnad@gmail.com)

| **Professional Address** | **Home Address** |
|---|---|
| Laboratory of Biomolecular Magnetic Resonance | Escalier Du Marche-13 |
| LRMB, BCH-1535, ISIC, EPFL | CH- 1003   Lausanne |
| CH-1015 Lausanne, Switzerland | Switzerland |
| Tel: +41 21 693 9429 | Tel: +41 78 827 3341 |

## *Scientific Career*

**Aug. 2006 - present:**  Ecole Polytechnique Fédérale de Lausanne **(EPFL)** - Doctoral Student **(PhD)** in the group of Prof. Geoffrey Bodenhausen.

**Aug. 2001 - Aug. 2006:** Indian Institute of Technology, Bombay **(IIT B)** – Integrated Masters in Science, in Chemistry **(CPI-7.9/10)**.

### Projects during Masters:

**Study of the Effect of Micellar Environment on 2(2'-pyridyl) Benzimidazole (2PBI) Using Steady-State and Time-Resolved Fluorescence.** (May, 2004 – July, 2004)

**MRI and Brain: A Literature Survey.** (July, 2004 – Dec, 2004)

**Theoretical Approach to Selective Cleavage of Bonds in HOD Molecule Using a Combination of IR and UV Pulses.** (August, 2005 – May, 2006)

# Computer experience

MATLAB, MATHEMATICA, C++ (used with GAMMA libraries for NMR simulations), BRUKER software for NMR spectra acquisition and simulations.

# Languages

**Hindi, English:** fluent in writing and speaking

**Punjabi:** mother tongue

# Hobbies

Indian Classical Music, Yoga, Poetry, Argentine Tango.

# *Scientific Publications*

*(1) ESPT of 2-(2'-Pyridyl)benzimidazole at the Micelle−Water Interface: Selective Enhancement and Slow Dynamics with Sodium Dodecyl Sulfate.* Mukherjee, T. K.; **Ahuja, P.**; Koner, A. L.; Datta, A.; **Journal of Physical Chemistry B** 2005, 109, 12567-12573.

*(2) Molecular Properties Determined from the Relaxation of Long-Lived Spin States.* **Ahuja, P.**; Sarkar, R.; Vasos, P. R.; Bodenhausen, G.; **Journal of Chemical Physics** 2007, 127, 134112.

*(3) Extending the Scope of Singlet-State Spectroscopy.* Sarkar, R.; **Ahuja, P.**; Moskau, D.; Vasos, P. R.; Bodenhausen, G.; **ChemPhysChem** 2007, 8, 2652-2656.

*(4) Measurement of Slow Diffusion Coefficients of Molecules with Arbitrary Scalar Couplings via Long-Lived Spin States.* Sarkar, R; **Ahuja, P.**; Vasos, P. R.; Bodenhausen, G.; **ChemPhysChem** 2008, 9, 2414-2419.

*(5) Diffusion Coefficients of Biomolecules Using Long-Lived Spin States.* **Ahuja, P.**; Sarkar, R.; Vasos, P. R.; Bodenhausen, G. ; **Journal of the American Chemical Society** 2009, 131, 7498-7499.

*(6) Long-Lived States in Multiple-Spin Systems.* **Ahuja, P.**; Sarkar, R.; Vasos, P. R.; Bodenhausen, G.; **ChemPhysChem** 2009,10, 2217-2220.

*(7) Long-lived States to Sustain Hyperpolarized Magnetization.* Vasos, P. R.; Comment, A.; Sarkar, R.; **Ahuja, P.**; Jannin, S.; Ansermet, J.-Ph.; Konter, J.A.; Hautle, P.; Brandt, B. van den and Bodenhausen, G.; 2009, **Proceedings of the National Academy of Sciences of the United States of America** 2009, 106(44), 18469-18473.

*(8) Long-lived Coherences for Homogeneous Line-Narrowing in Spectroscopy.* Sarkar, R.; **Ahuja, P.**; Vasos, P. R.; Bodenhausen, G.; **Physical Review Letters**, 2010, 104, 053001.

*(9) Producing Hyperpolarized Gases via Dynamic Nuclear Polarization and Sublimation.* Comment, A.; Jannin, S.; Hyacinthe, J.-N.; Miéville, P.; Sarkar, R.; **Ahuja, P.**; Vasos, P. R.; Montet, X.; Lazeyras, F.; Vallée, J.-P.; Konter, J. A.; Hautle, P.; van den Brandt, B.; Ansermet, J.-Ph.; Gruetter, R.; Bodenhausen, G.; **Physical Review Letters**, 2010, 105, 018104.

*(10) Scavenging Free Radicals to Extend Longitudinal and Transverse Relaxation Times in NMR using Hyperpolarization by Dissolution Dynamic Nuclear Polarization.* Miéville, P.; **Ahuja, P.**; Sarkar, R.; Jannin, S.; Vasos, P. R.; Gerber, S.; Mishkovski, M.; Comment, A.; Gruetter, R.; Ouari, O.; Tordo, P.; Bodenhausen, G.; **Angewandte Chemie International Edition,** 2010, 49, 6182-6185.

*(11) Long-Lived Coherences for Line-Narrowing in High-Field NMR*. Sarkar, R.; **Ahuja, P.**; Bornet, A.; Wagnières, O.; Vasos , P. R.; Bodenhausen, G.; **Progress in NMR Spectroscopy** (Accepted).

 *(12) Proton Hyperpolarization preserved in Long-Lived States.* **Ahuja, P.**; Sarkar, R.; Jannin, S.; Vasos, P. R.; Bodenhausen, G.; **ChemComm** (Accepted).

*(13) Long-Lived States as a Probe to Study Protein Stability.* **(In Preparation)**

# *EU patent application*